Geologica Acta, Vol.16, Nº 1, March 2018, 1-23, I-XIV
DOI: 10.1344/GeologicaActa2018.16.1.1

geologica acta

1.90-1.88Ga arc magmatism of central Fennoscandia: geochemistry, U-Pb geochronology, Sm-Nd and Lu-Hf isotope systematics of plutonic-volcanic rocks from southern Finland

J. KARA[1] M. VÄISÄNEN[1] Å. JOHANSSON[2] Y. LAHAYE[3] H. O'BRIEN[3] O. EKLUND[4]

[1]Department of Geography and Geology, University of Turku
FI-20014 Turku, Finland. Kara E-mail: jkmkar@utu.fi

[2]Department of Geosciences, Swedish Museum of Natural History
P.O. Box 50007, SE-104 05 Stockholm, Sweden

[3]Geological Survey of Finland
P.O. Box 96, FI-02151 Espoo, Finland

[4]Geology and Mineralogy, Åbo Akademi University
FI-20500 Turku, Finland

ABSTRACT

The earliest Svecofennian magmatism in southern Finland has been dated to 1.90-1.88Ga. As an example of this, the Orijärvi (*ca*. 1.89Ga) and Enklinge (*ca*. 1.88Ga) volcanic centres comprise bimodal plutonic batholiths surrounded by volcanic rocks of comparable ages and chemical compositions. The rock types range from gabbros to granites and indicate a subduction-related continental margin setting. The zircons from the Orijärvi granodiorite define an age of 1892±4Ma whereas the Enklinge granodiorite yields an age of 1882±6Ma. Several inherited ages of 2.25-1.95Ga as well as younger metamorphic ages of 1.86-1.80Ga were found in the Enklinge granodiorite. The initial ε_{Nd} values of the mafic rocks from both locations fall in the range +1.1 to +2.9, whereas the felsic rocks exhibit initial ε_{Nd} values of -0.4 to +1.2. The magmatic zircons from the Orijärvi and Enklinge granodiorites show average initial ε_{Hf} values of -1.1 (at 1892Ma) and zero (at 1882Ma), respectively, both with a spread of about 7 ε-units. The initial ε_{Hf} values for the inherited zircons from Enklinge range from +3.5 to +7.6 with increasing age. The Sm-Nd data indicate that the mafic rocks were derived from a "mildly depleted" mantle source while the felsic rocks show some crustal contribution. Also, the variation in ε_{Hf} values indicates minor mixing between mildly depleted mantle-derived magmas and crustal sources. U-Pb ages and Hf isotopes for inherited zircons from the Enklinge granodiorite suggest the presence of juvenile Svecofennian "proto-crust" at depth.

KEYWORDS | **Fennoscandian shield. Svecofennian orogeny. Lu-Hf. U-Pb. Sm-Nd. Geochemistry.**

INTRODUCTION

Major crust-forming processes occurred in connection with the amalgamation of the supercontinent Columbia *a.k.a.* Nuna during Paleoproterozoic time (*e.g.* Rogers and Santosh, 2002). One of its components, the Svecofennian Orogen (SO) in the Fennoscandian shield (Fig. 1A), was mainly formed between *ca.* 1.96 and 1.77Ga through accretionary (Gorbatschev and Bogdanova, 1993; Hermansson *et al.*, 2008; Stephens and Andersson, 2015) or combined accretionary and collisional (Lahtinen, 1994; Lahtinen *et al.*, 2005) processes. The orogen also forms

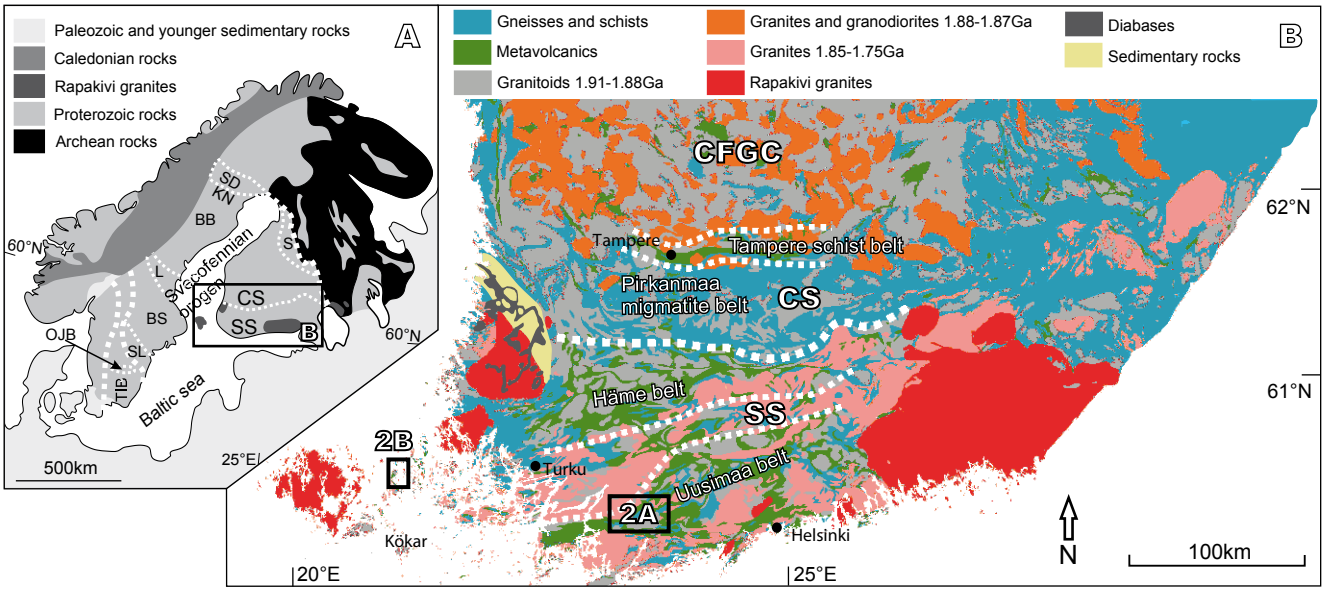

FIGURE 1. A) Geological overview of the Fennoscandian shield and proposed terrane distribution, modified after Koistinen *et al.* (2001). The thick white dashed lines represent the borders of the Svecofennian orogen and Transscandinavian igneous belt, whereas the narrow-dashed lines represent proposed terrane boundaries within the Svecofennian orogen. CS=Central Svecofennia, SS=Southern Svecofennia, S=Savo arc, SD=Skellefte District, KN=Knaften arc, BB=Bothian Basin, L=Ljusdal lithotectonic unit, BS=Bergslagen lithotectonic unit, SL=Småland Lithotectonic unit, TIB=Transscandinavian Igneous Belt, OJB=Oskarshamn-Jönköping Belt. Area of map B) is indicated by a black rectangle. B) General geological map of southern Finland, modified after Kallioperä-Bedrock of Finland 1:200,000. CFGC=Central Finland Granitoid Complex. The white thicker dashed line represents proposed border between Central and Southern Svecofennia (CS and SS, respectively), whereas the white narrower lines represent proposed borders of the other major lithotectonic units. Study areas indicated by black rectangles (2A=Orijärvi, 2B=Enklinge).

a part of the Great Proterozoic Accretionary Orogens, which in places have experienced the longest duration of subduction in the Earth's history, up to 900Ma (Condie, 2013). The SO covers large areas in Finland and Sweden, and smaller areas in Norway and Russia. Much of it is covered by Paleozoic sediments in the South and southeast (Fig. 1A).

The oldest recognised magmatism in the SO is related to subduction which formed almost juvenile volcanic arcs in a continental margin setting (1.96-1.88Ga; *e.g.* Kähkönen, 2005; Stephens *et al.*, 2009 and references therein). The volcanic arcs in the SO are mainly composed of extrusive igneous rocks, but magma chambers or subvolcanic intrusions are also present. Such magma chambers have long been recognised in Sweden (Stephens *et al.*, 2009 and references therein) but only occasionally considered in Finland (Colley and Westra, 1987; Ehlers and Lindroos, 1990; Väisänen and Mänttäri, 2002; Talikka and Mänttäri, 2005). It has been recognised that some parts of the SO have initial ε_{Nd} values close to zero and depleted mantle model ages older than 2.1Ga, indicating an older contribution to the source region (*e.g.* Huhma, 1986; Patchett *et al.*, 1987; Andersson, 1997; Lahtinen and Huhma, 1997). Single zircon U-Pb dating has also revealed inherited older zircons in the oldest plutonic rocks (*e.g.* Ehlers *et al.*, 2004). These findings have evoked models where *ca.* 2.2-2.0Ga small continental fragments, microcratons or pieces of Svecofennian "proto-crust" are hidden under the present crust (Lahtinen *et al.*, 2005; Andersson *et al.*, 2011). However, no direct observations of these microcratons have been made.

In this study, we present whole rock geochemical, U-Pb, Sm-Nd, and Lu-Hf isotope data from two 1.90-1.88Ga magmatic centres in southern Finland: the Orijärvi and Enklinge areas. They comprise plutonic centres surrounded by extrusive volcanic rocks of corresponding ages and chemical compositions. The focus here is on the plutonic and dyke rocks since they have not been previously studied as extensively as their extrusive counterparts. Our aim is to study the magma source/s and the nature of the oldest magmatic rocks of central Fennoscandia. In addition, we evaluate the existence of the proposed proto-crust below the central Fennoscandian bedrock in the light of new Lu-Hf isotope data.

REGIONAL GEOLOGICAL SETTING

The Svecofennian orogen in Finland and Sweden is composed of several large units defined as terranes or lithotectonic units. The oldest volcanic arc-type igneous rocks are found in northern Sweden (1.96-1.92Ga Knaften arc; Wasström, 1993, 2005) and the youngest in southern Sweden (1.83-1.82Ga Oskarshamn-Jönköping Belt; Mansfeld *et al.*, 2005). In the central part, three main terranes are recognised in Finland: the Savo arc (S),

Central Svecofennia (CS) and Southern Svecofennia (SS, Fig. 1A) (Korsman *et al.*, 1997; Kähkönen, 2005).

The Savo arc exposes the oldest Svecofennian igneous rocks in Finland (*ca.* 1.92Ga; Lahtinen, 1994; Vaasjoki *et al.*, 2003) and it is considered an equivalent to the Knaften arc (KN) in Sweden with roughly similar ages (Wasström, 1993; Eliasson *et al.*, 2001; Guitreau *et al.*, 2014). The ages of the volcanic arc-related igneous rocks in central and southern Svecofennia fall between 1.90 and 1.88Ga (*e.g.* Kähkönen, 2005). A few slightly older (1.91Ga; Johansson and Stephens, 2017) and younger (1.85Ga; *e.g.* Stephens and Andersson, 2015) rocks also occur. It is traditionally considered that southern Svecofennia and the Bergslagen area (BS) in South-central Sweden belong to the same unit (*e.g.* Valbracht *et al.*, 1994; Nironen, 1997; Lahtinen *et al.*, 2005), although the presence of large intervening shear zones such as the Singö shear zone along the coast in East-central Sweden and the South Finland shear zone makes such correlations somewhat problematic (*cf.* Torvela and Ehlers, 2010; Bogdanova *et al.*, 2015).

Southern Svecofennia

Southern Svecofennia comprises two parallel volcanic-sedimentary belts: the Häme and Uusimaa belts (Fig. 1B; Kähkönen, 2005 and references therein). The zircon ages in volcanic rocks in both belts are *ca.* 1.90-1.88Ga (*e.g.* Väisänen and Mänttäri, 2002; Ehlers *et al.*, 2004; Skyttä *et al.*, 2005; Väisänen and Kirkland, 2008; Saalmann *et al.*, 2009). Both belts show arc-type geochemical affinities, and the Häme belt is apparently less mature than the bulk of the Uusimaa belt (Lahtinen, 1996; Kähkönen, 2005).

The relationship between the two volcanic belts is ambiguous (*cf.* Kähkönen. 2005). Korja *et al.* (2006) regarded the Häme and Uusimaa belts as separate terranes, whereas Väisänen and Mänttäri (2002) suggested that the belts belonged to the same arc system but were rifted apart. The rift basin was filled with felsic volcanic rocks, tholeiitic mafic/ultramafic lavas with E-MORB affinity (*ca.* 1.88-1.87Ga), sedimentary carbonates (now marbles) and detrital sediments (now mica gneisses; *e.g.* Nironen *et al.*, 2016 and references therein).

The Häme belt includes several mafic/ultramafic plutonic rocks, which often show layered structures. The largest of these is the Hyvinkää layered intrusion, which Peltonen (2005) regarded as synplutonic to the volcanic rocks of the area (see also Eerola, 2002). The interpretation is supported by the U-Pb zircon ages of the gabbro (1880±5Ma, Patchett and Kouvo, 1986) and the plagioclase-phyric mafic volcanic rock (1880±3Ma, Suominen, 1988). Such synvolcanic plutonism is described for central Svecofennia as well (*e.g.* Talikka and Mänttäri, 2005), and it is widespread in the Bergslagen area in Sweden (Lundström *et al.*, 1998; Andersson *et al.*, 2006b; Hermansson *et al.*, 2008; Stephens *et al.*, 2009).

The volcanic rocks in the Uusimaa belt show continental margin and rifting type lithological associations and geochemical affinities (Kähkönen, 2005; Weihed *et al.*, 2005). The belt has indications of an older, *ca.* 2.1-1.91Ga contribution to the magmatism as indicated by initial ε_{Nd} values around zero (Huhma, 1986; Patchett and Kouvo, 1986; Lahtinen and Huhma, 1997; this study) as well as detrital zircons of that age in metasediments and inherited zircons in igneous rocks (*e.g.* Claesson *et al.*, 1993; Lahtinen *et al.*, 2002; Ehlers *et al.*, 2004; Bergman *et al.*, 2008; Lahtinen and Nironen, 2010).

Enklinge and Orijärvi are both well-preserved non-migmatitic mega-enclaves surrounded by higher-grade and more deformed areas. Therefore, Enklinge and Orijärvi make excellent targets to study the earliest events in southern Svecofennia (Ehlers and Lindroos, 1990; Ploegsma and Westra, 1990; Skyttä *et al.*, 2006). The Orijärvi area is situated in the middle of the Uusimaa belt and is a type example of it (*e.g.* Kähkönen, 2005). The Enklinge area, however, is situated in the archipelago to the West of the continuous Häme and Uusimaa belts, and it remains unclear whether it is part of any of them.

Study areas

Orijärvi area

The bedrock in the Orijärvi area (Fig. 2A) in the middle of the Uusimaa belt mainly consists of apparently bimodal volcanic rocks with sedimentary intercalations (Eskola, 1914; Väisänen and Mänttäri, 2002; Kähkönen, 2005; Skyttä *et al.*, 2005). The volcanic rocks are divided into four formations (fms.): the lowermost Orijärvi Formation (Fm.) is a volcanic arc-type bimodal unit with marble and iron formation intercalations as well as Cu-Zn-Pb mineralizations (Eskola, 1914; Latvalahti, 1979; Väisänen and Mänttäri, 2002). The overlying Kisko Fm. is geochemically more evolved, and volcanic rocks range from basalts to rhyolites. The arc rifting started with the Toija Fm. which once again comprises bimodal volcanic rocks. The rifting continued with the Salittu Fm., which mainly consists of E-MORB type basalts and picrites. Age results of the volcanic rocks fall between 1895±3Ma (Orijärvi Fm.) and 1878±4Ma (for both the Kisko and Toija fms.; Väisänen and Mänttäri, 2002; Väisänen and Kirkland, 2008), with the uppermost Salittu Fm. being undated.

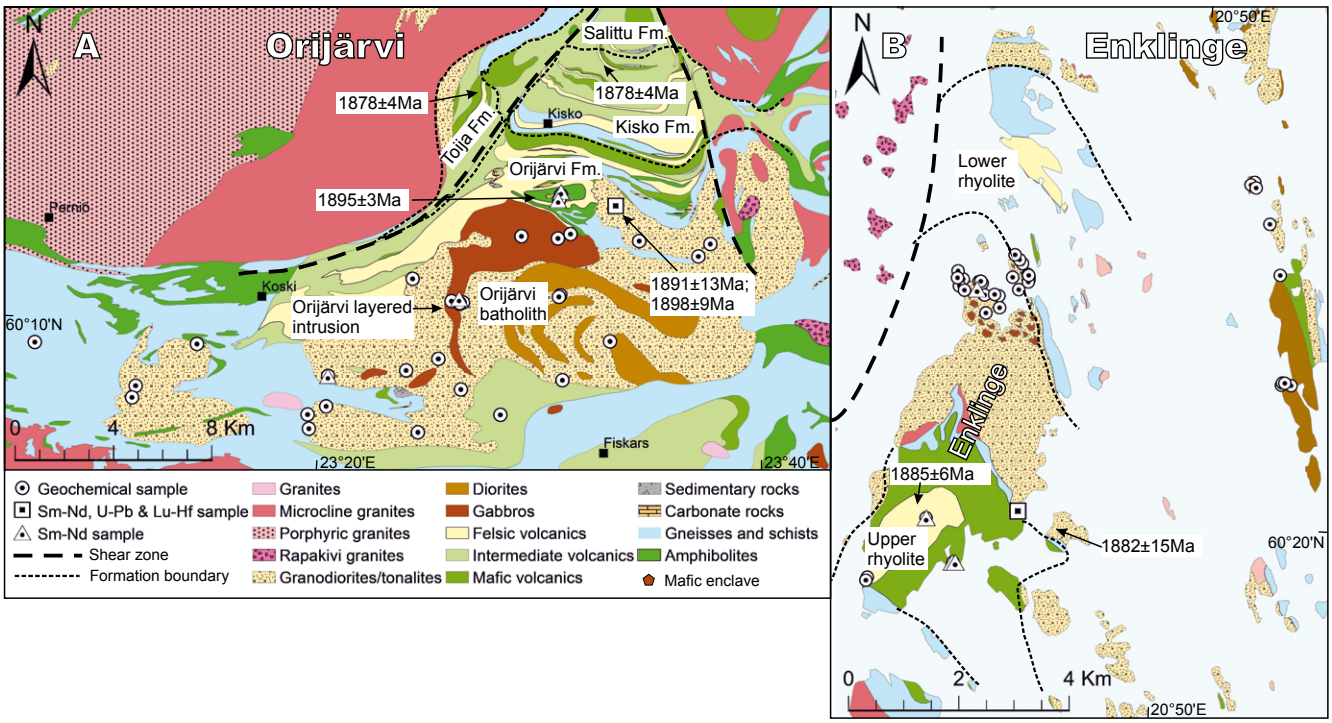

FIGURE 2. Detailed geological map of the A) Orijärvi and B) Enklinge study areas with age determinations, isotope and geochemical sampling sites indicated. Figures are modified after Kallioperä-Bedrock of Finland 1:200,000 (both), Skyttä *et al.* (2006) (Orijärvi) and Ehlers and Lindroos (1990) (Enklinge). For U-Pb ages, see text for references.

The Orijärvi batholith is a composite pluton, where mafic and felsic rocks apparently alternate. Magma mingling between felsic and mafic components is also common (Fig. 3A; B). Mafic rocks are more common in the core, and felsic rocks dominate at the fringes of the pluton. However, a complex structural evolution (Ploegsma and Westra, 1990; Skyttä *et al.*, 2006) might have disrupted the original order of rock types within the pluton. The mafic plutonic rocks show locally a layered structure (Sarapää *et al.*, 2005).

The U-Pb zircon age of the Orijärvi granodiorite (outer border of the batholith) has been determined to 1891±13Ma (Huhma, 1986) and 1898±9Ma (Väisänen *et al.*, 2002; *cf.* this study). Within errors, this is the same as the age of the felsic volcanic rock from the lowest stratigraphic level, and the Orijärvi batholith is regarded as a magma chamber that fed the surrounding volcanic rocks (Colley and Westra, 1987; Väisänen and Mänttäri, 2002).

Enklinge area

The well-preserved Enklinge volcanic-plutonic centre in the Åland archipelago in SW Finland consists of subaqueous felsic and mafic volcanic rocks with sedimentary intercalations (Fig. 2B; Sederholm, 1934; Rancken, 1953; Ehlers, 1976). The bedrock was divided into upper and lower strata (Ehlers and Lindroos, 1990). The lower strata consist of felsic schists, graywackes and the lower rhyolitic series which are capped by thin marble layers. The upper strata are composed of mafic and intermediate volcanics, including pillow lavas and lava flows. The upper series of rhyolites is on top of the stratigraphy.

The lower volcanic rocks are intruded and surrounded by syntectonic granodiorite-tonalite and related dacitic quartz porphyric dykes (Ehlers and Lindroos, 1990). Both granodiorite and dacitic dykes contain mafic enclaves, up to 50% of the volume of the bedrock in the northern side of Enklinge (Fig. 3C; D; Impola, 2004). Most of the dykes are bordered by basalts indicating coeval bimodal magmatism. Chemically, the dykes and the surrounding granodiorite are identical but they both differ slightly from the extrusive rhyolites (Ehlers and Lindroos, 1990).

The upper rhyolite and syntectonic granodiorite have been dated to 1885±6Ma and 1882±15Ma, respectively (Suominen, 1987; Ehlers *et al.*, 2004;). Ehlers *et al.* (2004) also determined ages for three similar gneissic granodiorites a few kilometres North of Enklinge, from Sottunga (30km South from Enklinge) and from Kökar (50km SE from Enklinge), and obtained identical ages of 1884±5Ma for all of them. This supports the coeval nature of the Enklinge rhyolite and surrounding granodiorite, although they are different in geochemistry.

ANALYTICAL METHODS

A total of 75 whole rock samples were studied, of which 34 were from Orijärvi and 41 from Enklinge. The data include plutonic, dyke and volcanic rock samples. Analyses were done by Inductively Coupled Plasma-Optical Emission Spectrometry (ICP-OES) and by Inductively Coupled Plasma-Mass Spectrometry (ICP-MS) at three different laboratories.

Two granodiorite samples, one from each study area, were selected for U-Pb spot analyses on zircon in order to determine their crystallization ages, and to perform Lu-Hf analyses on the same zircon grains. The Orijärvi granodiorite U-Pb dating analyses were performed using a Nu Plasma AttoM single collector ICP-MS, whereas the Enklinge granodiorite zircon U-Pb dating analyses were performed using a Nu Plasma HR multicollector ICP-MS, both at the Geological Survey of Finland in Espoo. With the latter instrument, in-situ zircon Lu-Hf isotope analyses were performed on the same or adjacent domains of the grains on which the U-Pb dating was done.

The Sm-Nd analyses were performed on nine samples, of which four were from Orijärvi and five from Enklinge, by a Finnigan MAT261 multicollector mass spectrometer at the Department of Geosciences, Swedish Museum of Natural History.

The full description of the analytical methods used in this study and the whole rock geochemical data (Table I), U-Pb isotopic data (Table II), Sm-Nd isotopic data (Table III) and Lu-Hf isotopic data (Table IV) are provided in the ELECTRONIC APPENDIX.

RESULTS

Whole rock geochemistry

Major elements

The compositions of the Orijärvi and Enklinge samples range from gabbroic to granitic in the Total Alkali *vs.* Silica (TAS) diagram (Fig. 4A). The classification of the samples (mafic-felsic) was done merely based on silica content of the rocks using 65wt.% of SiO_2 as a threshold value. The plutonic-dyke-volcanic-cumulate division was defined according to field observations. On the K_2O *vs.* SiO_2 diagram (Fig. 5) the mafic rocks from Orijärvi are calc-alkaline but those from Enklinge fall both in the calc-alkaline and tholeiitic fields. One high-K and one shoshonitic outlier can also be found within the Enklinge mafic rocks. The majority of the rocks follow a similar chemical evolution in the major elements in both study areas and the only slight difference can be found in the P_2O_5 contents; most of the Orijärvi mafic rocks are enriched in P_2O_5 compared to the Enklinge ones (Fig. 5). The felsic rocks follow similar trends as the mafic rocks in most of the major element diagrams; only Na_2O content shows a drop towards lower values between mafic and felsic rocks, and K_2O content shows a large spread between 0.24 and 7.7wt.%.

Two subgroups can be distinguished as separate from this 'main trend' based on major element compositions: Orijärvi (six samples) and Enklinge (five samples). The five acumulations of Enklinge are characterized by ferro-magnesian minerals and resulting high MgO and Mg# values, slightly elevated Fe_2O_3 and correspondingly low Na_2O, Al_2O_3 and P_2O_5 contents (Fig. 5). Orijärvi contains five samples of layered intrusions and one separate gabbro (65-MAV-02). The rocks from the Orijärvi layered intrusion are poor in silica (SiO_2 39-54wt.%). Four of the samples, taken from the gabbroic and the hornblende-rich parts, are enriched in TiO_2 and Fe_2O_3 but rather depleted in MgO. One of these samples (45-MAV-02; gabbro) shows anomalously high P_2O_5 content. The sample taken from the plagioclase part (TKJ-13-10-4; anorthosite) shows high Al_2O_3 and Na_2O contents but is depleted in MgO and Fe_2O_3. The

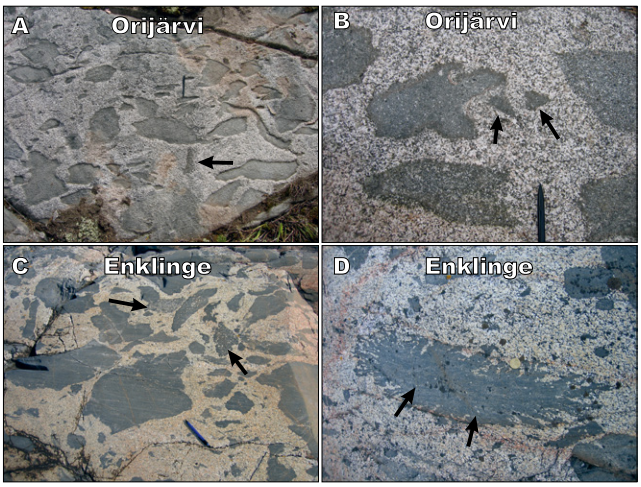

FIGURE 3. Field photos from the study areas. A) Magma mingling and mixing from the Orijärvi batholith. A few mafic enclaves, one of them indicated by a black arrow, show incipient magma mixing between mafic and felsic endmembers resulting in intermediate composition and a blurred boundary between the enclave and the felsic magma. B) Detailed photo from a mafic enclave from Orijärvi. The felsic magma has scavenged two small mafic fragments (black arrows) from the parent enclave on the left. On the left side of the pen there is an enclave with an intermediate composition similar to the one in Fig. 3A. C) Mafic and felsic magma mingling and mixing in the northern part of Enklinge. Black arrows indicate two enclaves with incipient magma mixing. D) The classical mafic enclave from Enklinge, first described by Sederholm (1934) and also found on the front cover of Lithos Vol. 116 (Eklund *et al.*, 2010). The outline of the enclave is resorbed by the surrounding felsic magma and a few feldspar phenocrysts are enclosed in the enclave (black arrows), suggesting coeval mafic and felsic magmas.

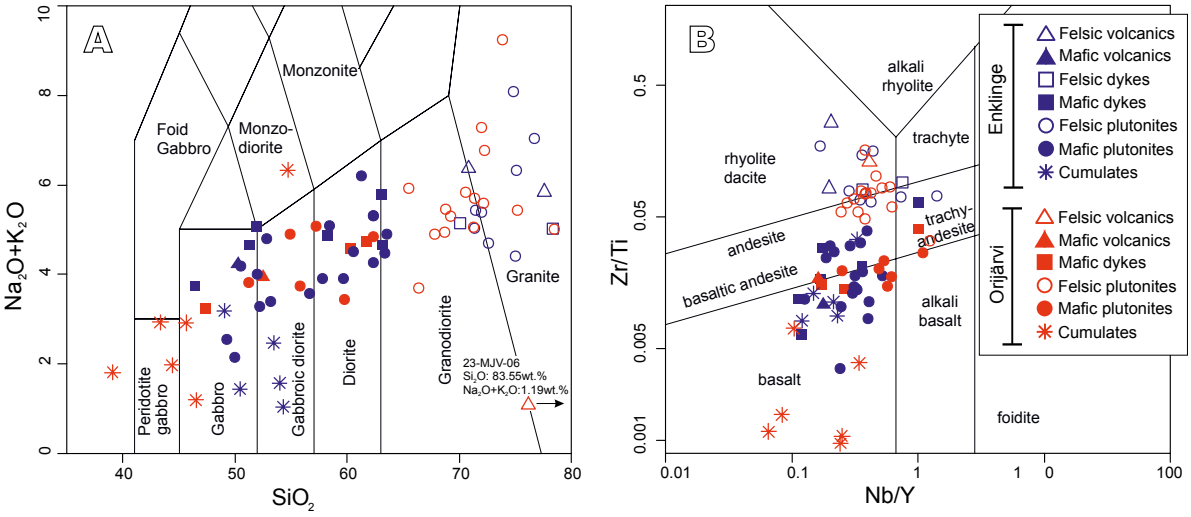

FIGURE 4. A) Total Alkalis *vs.* Silica (TAS) classification diagram (Middlemost, 1985) of the studied rocks. B) Log Zr/Ti *vs.* log Nb/Y classification diagram (Winchester and Floyd, 1977, modified by Pearce, 1996).

contents, high Mg# value and very low Na_2O, TiO_2 and P_2O_5 contents compared to the other mafic rocks from Orijärvi (Fig. 5). One rhyolite sample from Orijärvi (23-MJV-06) is hydrothermally altered, which can be seen in high silica (85wt.% SiO_2), very low alkalis (0.8wt.% Na_2O and 0.4wt.% K_2O) and low mobile trace element concentrations (below), so it was excluded from the major element examination but included in the trace element diagrams. The mafic rocks from both study areas are metaluminous except one peraluminious sample from Enklinge. The felsic rocks are metaluminous to peraluminious with Alumina Saturation Index (ASI, molar A/CNK: (Al_2O_3/CaO+Na_2O+K_2O)) between 0.95 and 1.18 (Fig. 5).

Trace elements

The log Zr/Ti *vs.* log Nb/Y classification diagram (Winchester and Floyd, 1977, modified by Pearce, 1996) was used to study the degree of alteration of the samples (Fig. 4B). All the samples form a rather tight and continuous trend from basalts to rhyolites, as in the TAS diagram (Fig. 4A), which supports their unaltered nature. The altered rhyolite sample from Orijärvi plots in the same group as its plutonic counterparts.

The Orijärvi mafic rocks tend to show higher Ba, Sr and Th concentrations compared to those from Enklinge (Fig. 6). Although the trace element data from the mafic rocks from both localities are a little scattered, the majority exhibit similar trace element characteristics in the multi-element diagram showing elevated (relative enrichment) Rb, Ba, Th, U, K and Pb concentrations and distinct negative anomalies (relative depletion) of Nb, Ta and P (Fig. 7). This trend is shared with mafic dykes and volcanics. All the mafic rocks are enriched in LREEs and depleted in HREEs but the rocks from Orijärvi generally show higher LREE concentrations, whereas the Enklinge mafics exhibit flatter REE spectra with higher HREE (Fig. 7). The samples PENK-25 (gabbro), PENK-46 (gabbro), 6-JPI-00 (gabbro dyke) and 12-JPI-00 (gabbro) from Enklinge show a flat, almost MORB-like REE pattern with a relative HREE enrichment. The gabbro sample 31-MJV-06 from Orijärvi differs from the other mafic rocks by its anomalously low HREE concentration. The majority of the mafic samples have AN Eu/Eu* ratio under 1.3.

The trace element data on all the felsic rocks from both localities show large variation in certain Large Ion Lithophile Elements (LILEs) such as Rb, Ba, Sr, Th and Zr. The Orijärvi felsic rocks exhibit lower Cr concentrations than those from Enklinge (Fig. 6). In the multi-element diagram, the felsic plutonic rocks from both localities show very similar trace element patterns with Rb, Ba, Th, U, K and Pb enrichment and depletion of High Field Strength Elements (HFSE) such as Nb and Ta (Fig. 7). The felsic plutonic rocks from both localities are enriched in LREEs and relatively depleted in HREEs. The rocks show mostly negative Eu anomalies and Eu/Eu* ratios under 1.15, except one tonalite sample from Enklinge (21-JPI-00) and two granodiorite samples from Orijärvi (37.2-MAV-02 and 50-MAV-02) which exhibit more positive Eu peaks. The two felsic dykes from Enklinge show very similar characteristics as the felsic plutonics. The two felsic volcanic rocks from Enklinge exhibit slightly different trace element compositions compared to the other felsic rocks from Enklinge with higher HFSE and REE concentrations but low Cr and Pb concentration (Figs. 6 and 7). The rhyolite sample

from Orijärvi (23-MJV-06) shows a similar composition in HFSEs compared to the other felsic rocks but it is depleted in LILEs due to hydrothermal alteration.

The mafic cumulates from Enklinge also stand out in the trace element data. They show very low LILE values as well as low Th, Sr, Zr and Nb concentrations but very high Cr and Ni concentrations. In the multi-element diagram, the cumulate group has similar pattern as the other mafic rocks but their REE pattern is fairly flat (Fig. 7). The Enklinge cumulates also show small Eu anomalies, with Eu/Eu* ratios varying from 0.8 to 1.52.

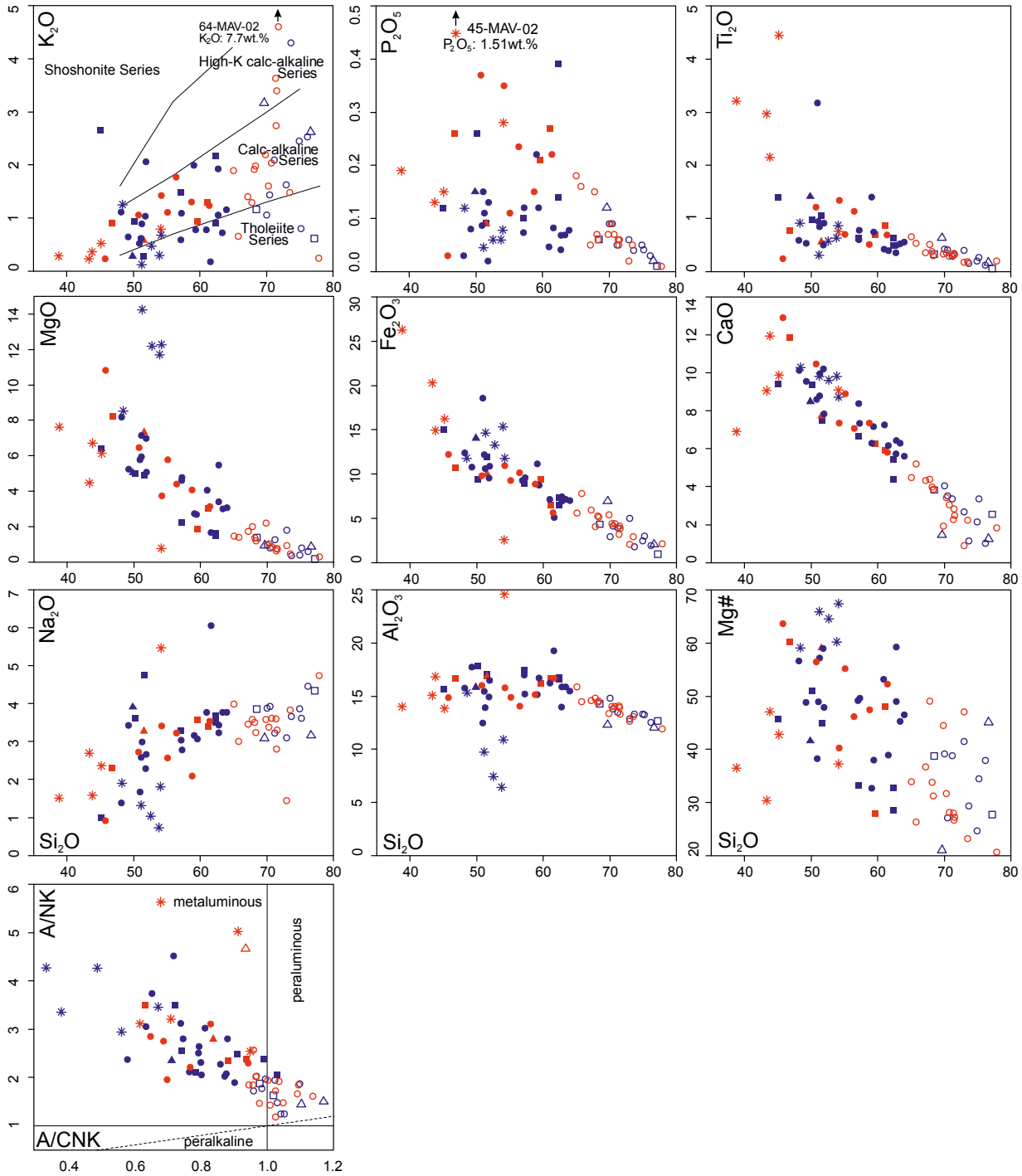

FIGURE 5. Selected major element *vs.* silica diagrams. K_2O *vs.* SiO_2 classification after Peccerillo and Taylor (1976). Mg# (100*MgO/(FeO_t+MgO)), A/NK (Al_2O_3/(Na_2O+K_2O)) and A/CNK (Al_2O_3/(CaO+Na_2O+K_2O)) calculated with GCDkit-software (Janousek *et al.*, 2006). All values in weight% except Mg# and values in the A/CNK diagram. Symbols as in Figure 4.

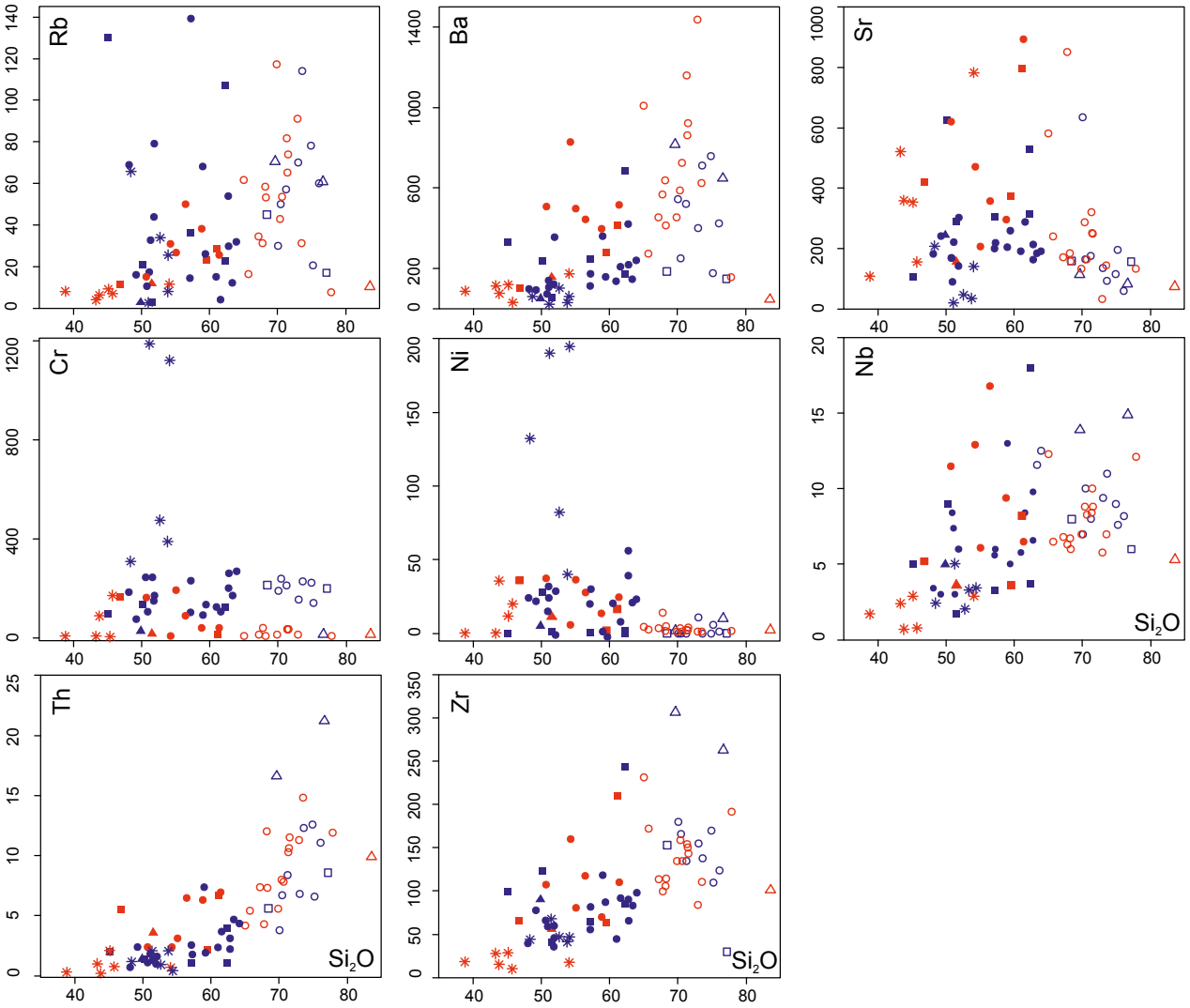

FIGURE 6. Selected trace element diagrams. All values in ppm. Symbols as in Figure 4.

The Orijärvi layered intrusion rocks show very low Rb, Ba, Zr and Nb concentrations, relatively low Ni and Cr concentrations but rather high Sr and P concentration, and in part very high Pb, compared to the other mafic rocks from both localities (Figs. 6 and 7). The REE concentrations are generally low but the rocks are relatively enriched in the LREEs, depleted in the HREEs, with Eu showing a positive peak in the REE diagram (Fig. 7). Eu/Eu* ratios are higher than in other samples, showing values between 1.36 and 3.51. The sample 65-MAV-02 from Orijärvi exhibits similar trace element characteristics as the Orijärvi layered intrusion rocks except it shows negative Eu anomaly.

U-Pb zircon analyses

The zircons from the Orijärvi granodiorite (29a-MJV-06) range from euhedral to more rounded, subhedral grains (Fig. 8A; B) and their colour varies from transparent to light brown. The grains are mainly elongated, 50-150µm in length and 20-100µm in width. The inner structure of the grains is mostly very homogeneous and few crystals show any distinct oscillatory zoning. Cracks and metamict rims are common. The BSE-images show a few cores (Fig. 8B) but they were too small to be analysed with a 25µm spot size so that possible xenocrystic cores were not verified. A total of 12 analyses were performed on 12 grains. Nine of them yielded a concordia age of 1892±4Ma (2σ; MSWD=0.42) and 10 analyses showed an almost identical weighted average $^{207}Pb/^{206}Pb$ age of 1892±5Ma (2σ; MSWD=0.81; Fig. 9A).

The Enklinge granodiorite (3-MJV-06) shows a wide range of zircon shapes but two main types are distinguished based on the degree of metamictization: a group of "euhedral" grains and a group of very heterogeneous

grains. The euhedral grains are also quite metamictic and have cracks, inclusions and inherited cores/domains (Fig. 8C; D). They are only slightly elongated, about 100-200µm in length. The euhedral zircons show oscillatory zoning and metamictization have advanced following the growing pattern of the grain. The "heterogeneous" group includes large, rounded, about 100-300µm-long grains with a wide variety of shapes, which are full of inclusions and almost completely metamicted. All the 42 U-Pb analyses were performed on the euhedral group of zircons. Several different age populations were found (Fig. 9B; C) out of which a group with a concordia age of 1882±6Ma (2σ; MSWD=4.2; n=9/15) and a $^{207}Pb/^{206}Pb$ age of 1880±4 (2σ; MSWD=0.89; n=15/15) are regarded to represent the age of magma crystallisation (Fig. 9C; D). The older zircons probably represent several different inherited populations. The six oldest analyses show $^{207}Pb/^{206}Pb$ ages between 2247Ma and 2049Ma. Two younger inherited populations yielded $^{207}Pb/^{206}Pb$ ages of 1952±16Ma (2σ; MSWD=0.0063; n=3; Fig. 9C) and 1988±13Ma (2σ; MSWD=0.32; n=4; Fig. 9C). The youngest 14 zircons (younger than crystallisation) show a continuous $^{207}Pb/^{206}Pb$ age trend between 1859 and 1802Ma. Nine analyses yielded a concordia age of 1849±9Ma

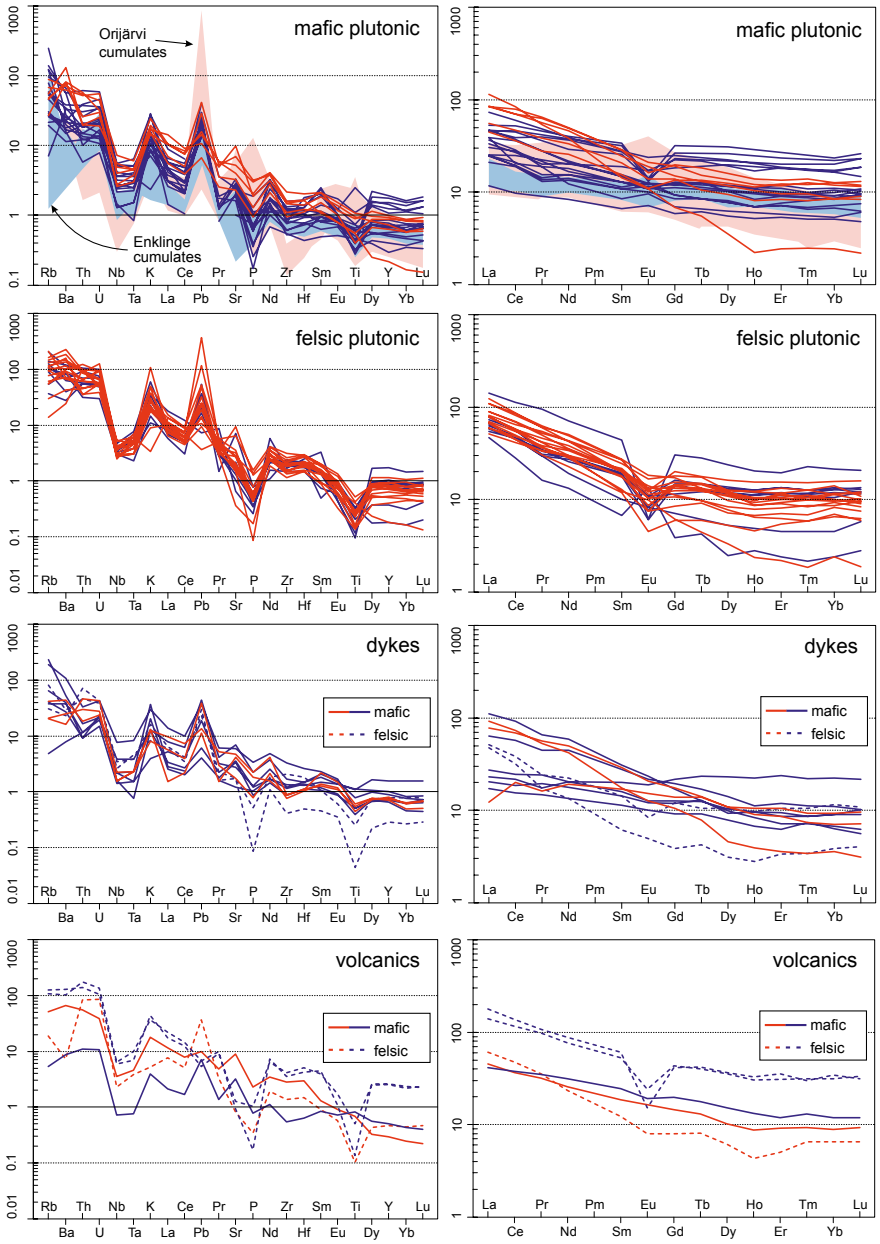

FIGURE 7. N-MORB normalized multi-element diagrams and chondrite normalized REE-diagrams. Normalizing values from Sun and McDonough (1989) and Boynton (1984), respectively. Colours as in Figure 4.

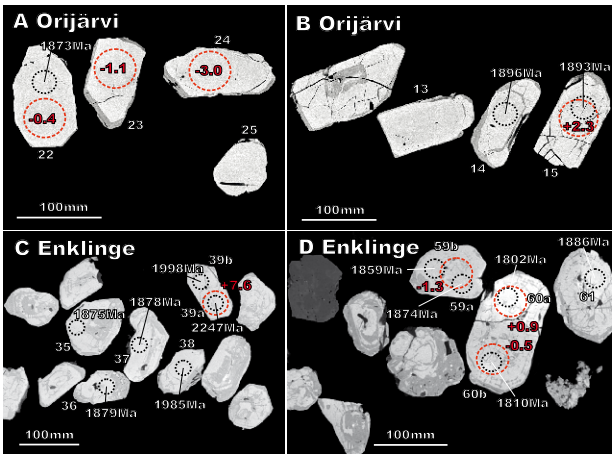

FIGURE 8. Back-Scattered Electron (BSE) images of representative zircons from the Orijärvi granodiorite (A and B) and from the Enklinge granodiorite (C and D). Black dashed circles represent U-Pb spots (25µm) with $^{207}Pb/^{206}Pb$ age; red dashed circles represent Lu-Hf spots (50µm) with initial $\varepsilon_{Hf}(t)$ value. More detailed analysis data available in ELECTRONIC APPENDIX (Tables II and IV).

(95%; MSWD=0.78; n=9/14; Fig. 9E) and a weighted average $^{207}Pb/^{206}Pb$ age of 1848±6Ma (2σ; MSWD=1.14; n=11/14) was obtained on 11 analyses. An upper intercept age of 1850±6Ma (MSWD=0.6) were obtained using 12 analyses. The 1.85Ga age may indicate metamorphic resetting, although the younger zircons or zircon domains do not stand out as texturally different from the magmatic zircon. The three youngest analyses were omitted from the age calculations due to discordancy and/or slightly younger $^{207}Pb/^{206}Pb$ ages between 1818 and 1802Ma.

Sm-Nd whole rock analyses

The mafic rocks from Enklinge have initial ε_{Nd} values (at 1882Ma) from +1.9 to +2.9 whereas the felsic rocks exhibit values of +1.1 and +1.2. The depleted mantle model (T_{DM}) ages for the Enklinge samples fall between 2.15 and 2.12Ga except for the sample 5-MJV06 (gabbro dyke) which shows a T_{DM} age of 2.0Ga. The two mafic samples from Orijärvi have initial ε_{Nd} values (at 1892Ma) of +1.1 and +2.0. The felsic rocks have values of -0.4 and +0.2. The T_{DM} ages for the Orijärvi samples are 2.35 and 2.16Ga for the mafic rocks and 2.21 and 2.16Ga for the felsic rocks. The Sm-Nd isotopic data are compared to previously published Nd-data from central Fennoscandian rocks in Figure 10.

Lu-Hf zircon analyses

In total, 37 analyses were performed on the Orijärvi granodiorite zircons. They show variation in the initial $^{176}Hf/^{177}Hf$ values between 0.28144 and 0.28165 corresponding to ε_{Hf} values between -4.7 and +2.6 with an average of -1.1 (at 1892Ma).

A total of 21 Lu-Hf analyses were performed on the Enklinge granodiorite zircons. Eleven analyses were performed on zircons representing the age of crystallization, five on inherited zircons or inherited domains in zircons and five on zircons representing the younger ages. The magmatic zircons yielded initial $^{176}Hf/^{177}Hf$ values between 0.28150 and 0.28171 corresponding to initial ε_{Hf} values between -3.0 and +4.4 with an average value of 0 (at 1882Ma). The individual $^{207}Pb/^{206}Pb$ age was used for the inherited and young zircon grains (ages varying from 2247 to 1951Ma and 1859 and 1802Ma, respectively) for the calculation of initial ε_{Hf} values. The inherited zircons exhibit initial $^{176}Hf/^{177}Hf$ values between 0.28156 and 0.28164, corresponding to initial ε_{Hf} values between +3.5 and +7.6. The initial $^{176}Hf/^{177}Hf$ values for the young zircons fall in the range 0.28150 to 0.28166, which translates into initial ε_{Hf} of -4.1 to +1.6. The Lu-Hf isotopic data are compared to previously published Hf-data from central Fennoscandian rocks in Figure 11.

DISCUSSION

Whole rock geochemistry

The Enklinge and Orijärvi igneous rocks have formed in a subduction-related volcanic arc environment (*e.g.* Colley and Westra, 1987; Ehlers and Lindroos, 1990; Kähkönen, 2005). The distinct subduction component can be seen in all the samples with pronounced troughs at Nb and Ta, and peaks at the subduction-mobile elements such as Ba, Th, U, Pb and Sr in the multi-element diagrams (Fig. 7). This feature is emphasised by fractionated REE pattern for the mafic rocks, as well as the felsic ones (Fig. 7). On the Th/Yb *vs.* Nb/Yb diagram all the mafic samples plot above the MORB-OIB array (Pearce and Peate, 1995; Pearce, 2008) and show Nb/Yb ratios ≥1.0, suggesting an Active Continental Margin (ACM) setting rather than oceanic arc type magmatism (Fig. 12A). The same feature can be observed on the Th/Ta *vs.* Yb diagram (Schandl and Gorton, 2002), which shows ACM affinity for the felsic rocks (Fig. 12B). The wide range of rocks with intermediate and felsic compositions also support a continental setting as these form more easily from pre-existing continental crust (*e.g.* Tatsumi and Takahashi, 2006). However, part of the intermediate rocks is supposed to result from magma mixing (Fig. 3). The Nb/Zr *vs.* Nb/Ba diagram (Fig. 12C) indicates a SubContinental Lithospheric Mantle (SCLM) source for the mafic magmas.

The Orijärvi and the Enklinge rocks, especially the mafic ones, display some minor differences. The Enklinge rocks are slightly more enriched in HREEs and Cr, and depleted in LILEs, K_2O and P_2O_5. This feature can be explained in different ways, for example: i) mantle

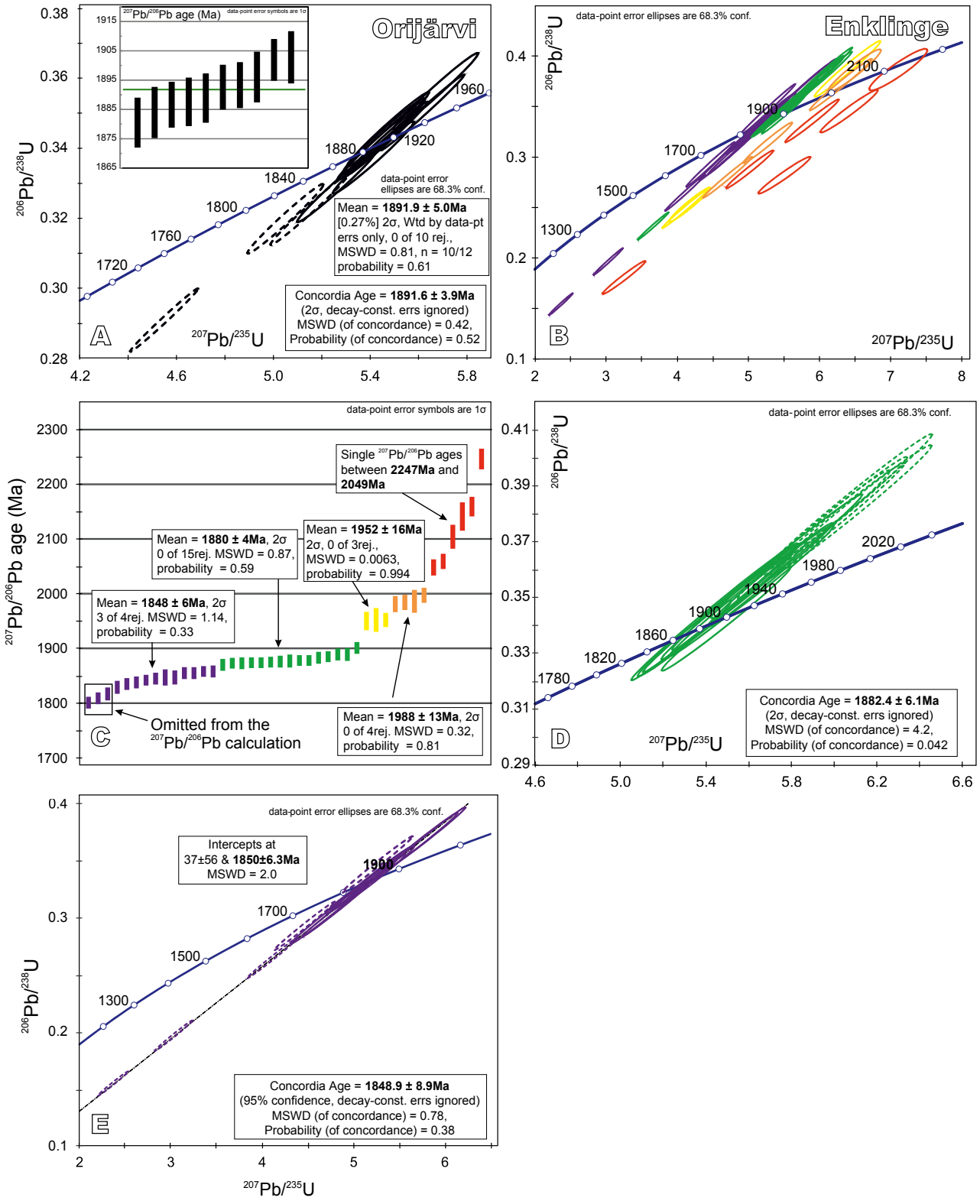

FIGURE 9. U-Pb and $^{207}Pb/^{206}Pb$ age diagrams and regression statistics for the zircon analyses. A) Data from the Orijärvi granodiorite (29a-MJV-06); B), C), D) and E) show data from the Enklinge granodiorite (3-MJV-06). Diagrams B) and C) represent all the Enklinge granodiorite U-Pb analyses. Different colours represent different age groups. See text for explanation.

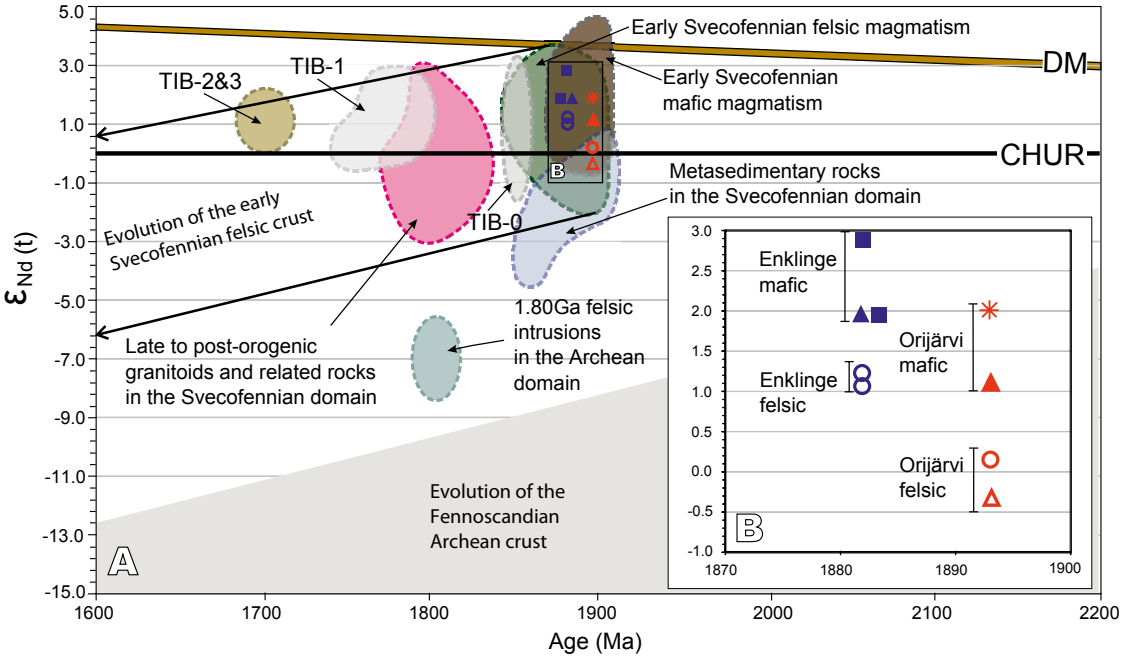

FIGURE 10. A) ε_{Nd} *vs.* Age diagram for the present samples and other relevant data from the Fennoscandian shield. CHUR=Chondritic Uniform Reservoir and DM=Depleted Mantle, after DePaolo (1981); TIB = Transscandinavian Igneous Belt; Evolution of the Fennoscandian Archean crust drawn after Andersson *et al.* (2001); Evolutionary trend for the early Svecofennian felsic crust drawn after Rutanen *et al.* (2011); Early Svecofennian mafic magmatism (Huhma, 1986, 1987; Patchett and Kouvo, 1986; Vaasjoki and Huhma, 1999; Makkonen and Huhma, 2007); Early Svecofennian felsic magmatism (Huhma, 1986; Patchett and Kouvo, 1986; Patchett *et al.*, 1987; Lahtinen and Huhma, 1997; Rämö *et al.*, 2001); Metasedimentary rocks in the Svecofennian domain (Huhma, 1987; Patchett *et al.*, 1987; Kumpulainen *et al.*, 1996; Lahtinen *et al.*, 2002); 1.8Ga felsic intrusions in the Archean domain (Huhma, 1986); Late to post-orogenic granitoids and related rocks in the Svecofennian domain (Huhma, 1986; Patchett and Kouvo, 1986; Patchett *et al.*, 1987; Lahtinen and Huhma, 1997; Kurhila *et al.*, 2005; Andersson *et al.*, 2006a; Rutanen *et al.*, 2011); *ca.* 1.85Ga TIB-0 mafic and felsic rocks (Andersson, 1997; Claeson and Andersson, 2000); *ca.* 1.80Ga TIB-1 mafic and felsic rocks (Wilson *et al.*, 1985; Patchett *et al.*, 1987; Andersson, 1997; Wikström and Andersson, 2004; Andersson *et al.*, 2004, 2007; Johansson *et al.*, 2006; Rutanen and Andersson 2009); *ca.* 1.70Ga TIB-2&3 felsic rocks (Wilson *et al.*, 1985; Patchett *et al.*, 1987; Heim *et al.*, 1996; Nyström 1999; Appelquist *et al.*, 2011). B) Close-up of the current data. Symbols as in Figure 4, same units as in A).

heterogeneity (*i.e.* depleted or enriched magma sources), ii) variations in the materials being contributed by the subducting slab to the mantle wedge, iii) different degrees of partial melting in the mantle wedge, or iv) assimilation of the surrounding crust during magma ascent. These processes are difficult to distinguish from each other. However, different element ratios can give a hint on the petrogenesis of the mafic rocks. A ratio of highly fluid-mobile to less fluid-mobile or fluid-immobile elements (*e.g.* Sr/Ce, Ba/Nb, Ba/Th and U/Th; Carr *et al.*, 1990; Kessel *et al.*, 2005; Pearce *et al.*, 2005; Wehrmann *et al.*, 2014) shows only very limited subduction additions and low degree of fluid flux from the subducting slab to the mantle wedge. Based on the ratio of more incompatible to less incompatible elements (*e.g.* Sm/Lu, La/Yb, La/Sm, Nb/Y; Carr *et al.*, 1990; Yang *et al.*, 2007, Wehrmann *et al.*, 2014), the Enklinge rocks tend to show a higher degree of partial melting (Fig. 13A). Thus, different degrees of partial melting may explain some compositional differences between Orijärvi and Enklinge.

Crustal contamination is estimated through Nb/Th ratio combined with Nb/La ratio (Fig. 13B) which suggests that some of the Orijärvi rocks are more affected by such a process. Part of this is the result of magma mixing between mafic and felsic magmas, something which is also supported by field observations (Fig. 3) and visible in the rather high SiO_2 content of a few contaminated mafic rocks. We suggest that the small differences in the mafic rocks in the study areas are due to higher degree of partial melting in Enklinge and slightly more intense magma mixing between mafic and felsic magma in Orijärvi. However, scattered and partly overlapping data between the study areas hinders further interpretations.

The felsic rocks of both study areas are similar which indicate similar petrogenesis. The ASI mostly below 1.1, Na_2O over 3.2wt.% with a few exceptions, low K_2O/Na_2O ratios and abundant mafic magmatic enclaves suggest that the felsic rocks are I-type (Fig. 5; Table I; *e.g.* Chappell and White, 1974) with an amphibolitic source in the granite source diagram (Patiño Douce, 1999; Fig. 14). This suggests that the felsic rocks have formed by partial melting of mafic lithosphere and that no large scale sedimentary components have been involved in the magma generation.

The cumulate rocks from Enklinge and Orijärvi share the same ACM signature as the major group of the mafic rocks

(Fig. 12A). However, they show very different geochemical features. The likely cause for the primitive signature of the Enklinge cumulates is accumulation of MgO-rich minerals like hornblende and pyroxene (±olivine). This is supported by low Na_2O and Al_2O_3, and moderate CaO contents. The characteristic geochemical signature of the Orijärvi layered intrusion rocks can be explained by mineral accumulation processes in a magma chamber. Different types of cumulates can be found within the layered intrusion (Sarapää *et al.*, 2005) ranging from hornblendites to garnet-bearing gabbro and anorthosite, the latter being absent in Enklinge. In addition, the Orijärvi samples show much higher Eu/Eu* ratios compared to the Enklinge cumulates suggesting overall plagioclase accumulation within the layered intrusion. The Orijärvi sample 45-MAV-02 is extremely rich in P_2O_5 which can be explained by accumulation of apatite, whereas the sample 22-MJV-06 is high in TiO_2 due to titanite enrichment. Johansson *et al.* (2012) have studied arc cumulates of similar age from the Roslagen area of East-central Sweden, which show some similar features. For example, the Enklinge primitive cumulates are comparable to the olivine and pyroxene cumulates whereas the Orijärvi layered intrusion resembles the plagioclase cumulates of the Roslagen area. Moreover, the Enklinge cumulates might represent a low intersection of a magma chamber (*i.e.* early fractionates and/or bottom cumulates of a magma chamber) whereas the Orijärvi cumulates suggest later fractionation processes and a higher intersection.

In summary, the co-genetic relation between intrusive and extrusive rocks is supported by their similar whole rock compositions. In addition, the coeval relation between mafic and felsic magmatism is supported by field observations.

Age data

The crystallization age of 1892±4Ma for the Orijärvi granodiorite is supported by the previously obtained TIMS and SIMS ages of 1891±13Ma (Huhma, 1986) and

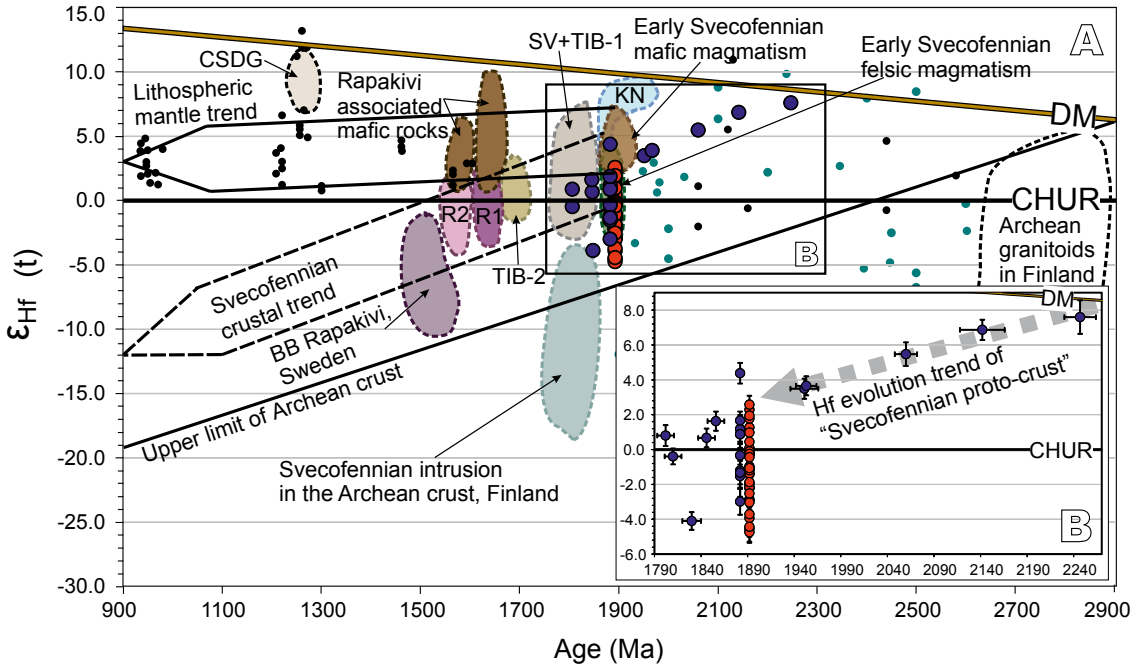

FIGURE 11. A) ε_{Hf} *vs.* Age diagram for the present samples and other relevant data from the Fennoscandian shield. Orijärvi granodiorite Hf data are represented by red dots and Enklinge granodiorite Hf data by blue dots. CHUR=chondritic uniform reservoir (Bouvier *et al.*, 2008); DM=Depleted Mantle (Griffin *et al.*, 2000); The Hf evolution trend for Paleoproterozoic Fennoscandian lithospheric mantle ($\varepsilon_{Hf}(1.90)$=+4.5±2.5 and $^{176}Lu/^{177}Hf$≈0.0315) drawn after Andersen *et al.* (2009), modified by Andersson *et al.* (2011); The Hf evolution trend for the Svecofennian crust $\varepsilon_{Hf}(1.90)$=+2±3 and $^{176}Lu/^{177}Hf$≈0.015 (Andersen *et al.*, 2009); Upper limit of Fennoscandian Archean crust (Andersen *et al.*, 2009); Archean granitoids in Finland (Patchett *et al.*, 1981; Lauri *et al.*, 2011); Knaften arc (KN; Guitreau *et al.*, 2014); Early Svecofennian mafic intrusion (Patchett *et al.*, 1981; Andersson *et al.*, 2011); Early Svecofennian felsic magmatism (Andersen *et al.*, 2009; Heinonen *et al.*, 2010; Andersson *et al.*, 2011; this study); Syn to late Svecofennian granitoids and Transscandinavian Igneous Belt generation 1 (SV+TIB1; Patchett *et al.*, 1981; Vervoort and Patchett, 1996; Andersen *et al.*, 2009; Andersson *et al.*, 2011; Johansson *et al.*, 2015); Transscandinavian Igneous Belt generation 2 (TIB2; Andersen *et al.*, 2009); Rapakivi granites from South-East Finland (R1), South-West Finland (R2) and associated mafic rocks (Heinonen *et al.*, 2010); Rapakivi granites from Bothian Basin (BB), Sweden (Andersson *et al.*, 2011); Central Scandinavian Dolerite Group (CSDG; Patchett *et al.*, 1981; Söderlund *et al.*, 2006); Black dots represent mafic intrusions in the Fennoscandian shield (Patchett *et al.*, 1981; Söderlund *et al.*, 2005); Turquoise dots represent inherited zircons/cores from Svecofennian felsic rocks (Andersen *et al.*, 2009; Kurhila *et al.*, 2010; Andersson *et al.*, 2011). B) Close-up of the present data. The grey arrow indicates an extension for the Svecofennian crustal Hf trend and a possible Hf evolution for the juvenile "Svecofennian proto-crust" based on a linear regression of the inherited zircon data from the Enklinge granodiorite ($\varepsilon_{Hf}(2.25)$=+8±3 and $^{176}Lu/^{177}Hf$≈0.012). The error bars are 2σ for ε_{Hf} values and for concordia ages (magmatic ages), and 1σ for individual $^{207}Pb/^{206}Pb$ ages.

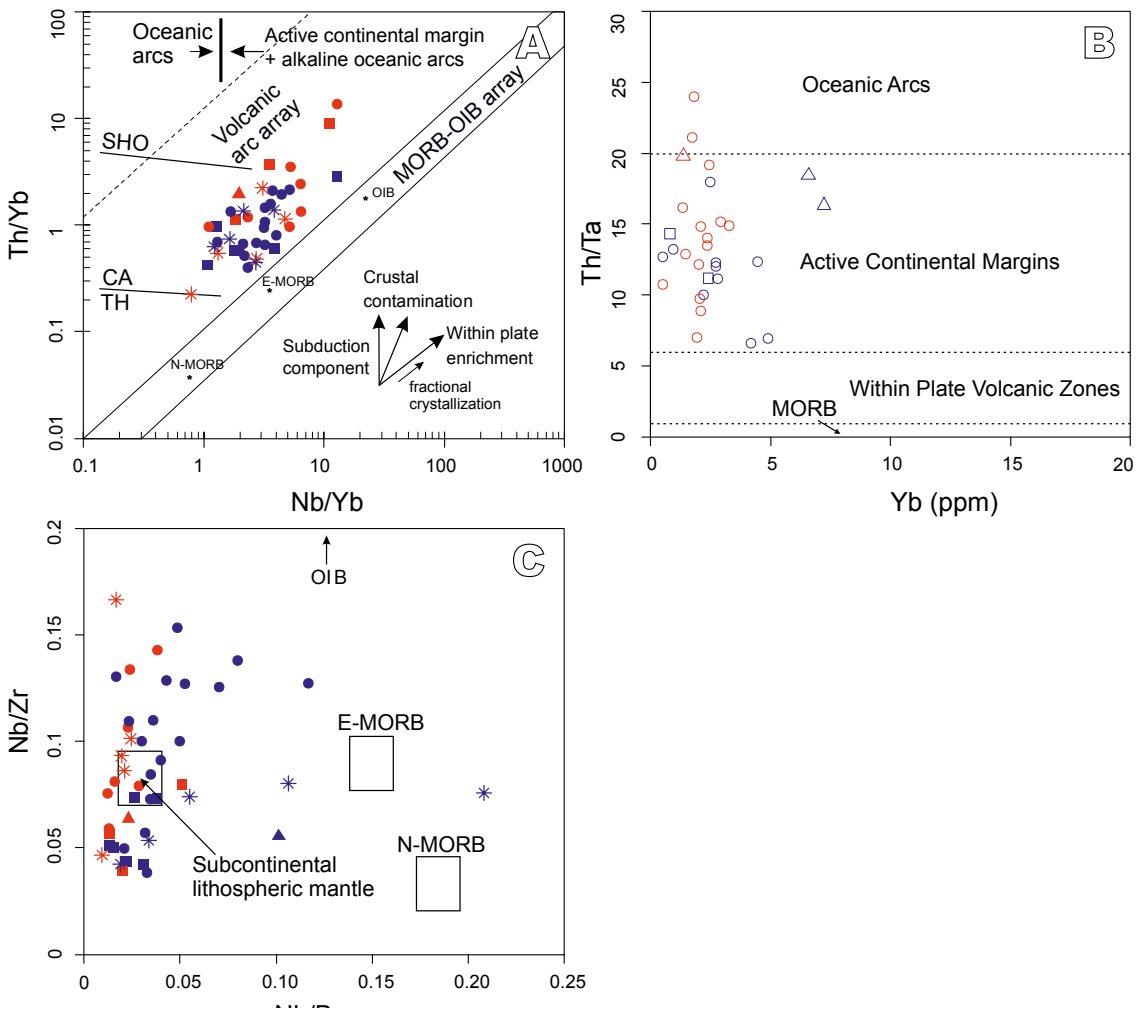

FIGURE 12. Geotectonic setting of A) the mafic rocks (Pearce, 2008) and B) the felsic rocks (Schandl and Gorton, 2002). C) Source of the mafic rocks (Hooper and Hawkesworth, 1993). OIB=Ocean Island Basalt (Sun and McDonough, 1989), E-MORB=Enriched Mid-Ocean Ridge Basalts (Sun and McDonough, 1989), N-MORB=Normal Mid-Ocean Ridge Basalts (Sun and McDonough, 1989), subcontinental lithospheric mantle (Hooper and Hawkesworth, 1993; Albarède, 2005). Symbols as in Figure 4.

1898±9Ma (Väisänen *et al.*, 2002), as well as the previous TIMS age for the adjacent Orijärvi rhyolite (1895±3Ma; Väisänen and Mänttäri, 2002). In contrast, several zircon populations were identified in the Enklinge granodiorite. The age 1882±6Ma for the crystallization is the same as the previous TIMS age 1882±15Ma (Suominen, 1987) and the SIMS age 1885±6Ma for the adjacent Enklinge rhyolite (Ehlers *et al.*, 2004). The inherited zircons have several different ages between 2.25 and 1.95Ga. The oldest grains, with ages between 2.25 and 2.05Ga, probably do not belong to same population but are derived from different sources. The younger inherited zircons might represent two different magmatic source rocks with ages of 1988±13Ma and 1952±16Ma.

The origin of the inherited zircons in the Enklinge granodiorite is unclear but the age range is similar to that of the inherited zircon populations discovered from central Fennoscandian meta-sedimentary rocks (Huhma *et al.*, 1991; Claesson *et al.*, 1993; Lahtinen *et al.*, 2002). Ehlers *et al.*, (2004) found similar zircon ages, *ca.* 2040Ma, for the Kökar granodiorite (Fig. 1B), including the oldest xenocrystic core of 3136Ma. The Sarmatian segment, the southernmost crustal segment of the East European craton, has been proposed to be the provenance for the 2.10-1.95Ga zircon populations (Lahtinen *et al.*, 2002). Recently, Samsonov *et al.* (2016) reported *ca.* 2.0Ga ages on juvenile volcanic rocks and granitoids from the southern part of the Central Russian Fold Belt, in the central part of the East European craton, now covered by platform sediments, which could also be a source. Another explanation is the possible presence of juvenile, *ca.* 2.20-1.93Ga "proto-Svecofennian" crust at depth, predating the early Svecofennian (1.90-1.86Ga) magmatism (*e.g.* Lahtinen and Huhma, 1997; Andersson *et al.*, 2006b, 2011). This proto-crust is not exposed at the present erosion level but it could have been a source for the granodioritic melts.

The interpretation of the youngest zircon ages is somewhat ambiguous due to the heterogeneous zircon morphologies. The youngest zircons, with $^{207}Pb/^{206}Pb$ ages between 1859 and 1802Ma, are considered to represent a metamorphic event. The concordia age of 1849±9Ma is similar to the $^{207}Pb/^{206}Pb$ age of 1848±6Ma and the upper intercept age of 1850±6Ma which suggest a metamorphic phase at *ca.* 1850Ma in the Enklinge area. The three youngest analyses were omitted from the age calculations but they show $^{207}Pb/^{206}Pb$ ages around 1810Ma, and may indicate a second metamorphic event. Alternatively, since the $^{207}Pb/^{206}Pb$ ages for all the metamorphic zircons form a continuous trend between 1859 and 1802Ma they could indicate incomplete resetting of the "U-Pb clock" during a single metamorphic event at around 1800Ma, or even later. A third alternative, which does not exclude the two previous options, would be a continuous Pb loss after 1.86Ga due to late geological event(s) or long-term diffusive radiogenic Pb loss (*cf.* Whitehouse *et al.*, 1999; Kusiak *et al.*, 2013).

Metamorphic ages around 1.85Ga from southern Svecofennia are scarce as the metamorphic peak is usually dated at between 1.83 and 1.81Ga (Korsman *et al.*, 1999; Väisänen *et al.*, 2002; Mouri *et al.*, 2005; Andersson *et al.*, 2006b; Högdahl *et al.*, 2008). However, Torvela *et al.* (2008) obtained a SIMS zircon age of 1850±12Ma for the metamorphic rims from a granodioritic gneiss, and a TIMS titanite age of 1842±8Ma for a wide mylonite zone at Kökar in the SW Finnish archipelago (Fig. 1B). This gives a strong evidence for a *ca.* 1.85Ga metamorphic phase in the study area. In addition, *ca.* 1.86-1.84Ga, intraorogenic mafic magmatism has been described from southern Finland (Pajunen *et al.*, 2008; Väisänen *et al.*, 2012a; Nevalainen *et al.*, 2014), which suggests that high heat flux had already started at *ca.* 1.85Ga (Skyttä and Mänttäri, 2008; Kurhila *et al.*, 2010; Väisänen *et al.*, 2012a, 2012b). Magmatic activity and a metamorphic phase at 1.87-1.85Ga have also been recognized in Bergslagen, Sweden (*e.g.* Stephens and Andersson, 2015; Johansson and Stephens, 2017). The nearest described *ca.* 1.85Ga coeval mafic and felsic magmatism is from Korppoo, 50km East of Enklinge (Väisänen *et al.*, 2012a). The possible late metamorphic age of *ca.* 1.81-1.80Ga is based on only three analyses from two zircons. However, Torvela *et al.* (2008) found evidence for a *ca.* 1.80-1.79Ga metamorphic phase in the same area, and Stephens and Andersson (2015) have described such a late metamorphic pulse in Sweden. These observations could justify a late metamorphic event at *ca.* 1.81-1.80Ga in the Enklinge area. Based on present and previous studies, we thus suggest that two metamorphic events, at *ca.* 1.85Ga and *ca.* 1.80Ga, occurred in the Enklinge region.

The lack of inherited zircons and xenocrystic cores is the most obvious feature in the Orijärvi granodiorite (*cf.* Väisänen *et al.*, 2002), although 2.12-1.93Ga zircons have been found in the Orijärvi meta-greywacke lying stratigraphically above the Orijärvi granodiorite (Claesson *et al.*, 1993). The BSE-images reveal a few cores or core-like structures in zircons but they were too small to be analysed with a 25µm spot size. In any case, the inherited zircon material in the Orijärvi granodiorite is scarce. The new and the previously published age data

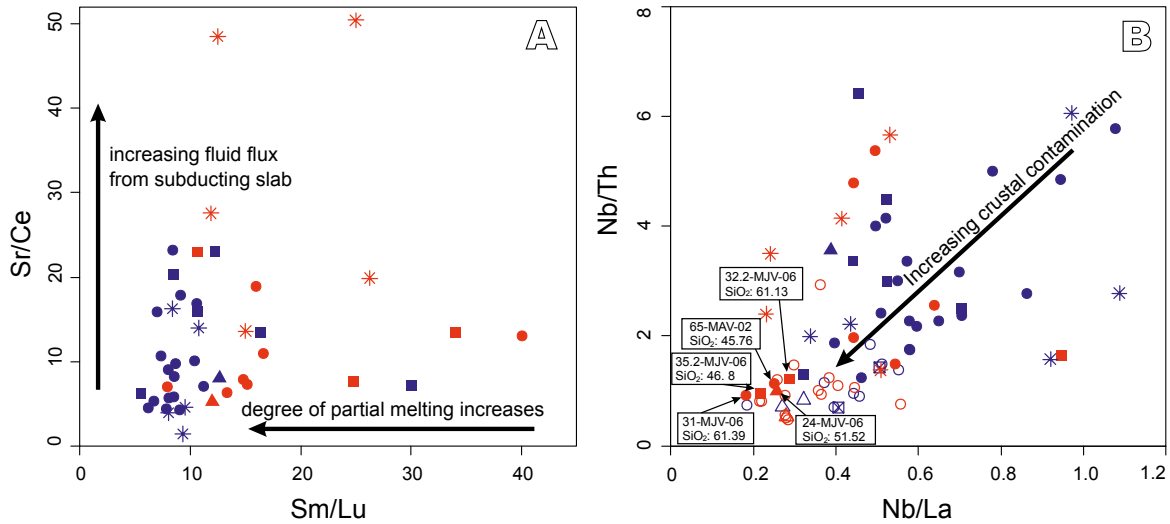

FIGURE 13. A) Partial melting and subducting slab fluid signal in the mafic rocks. Sm/Lu ratio decreases with increasing partial melting, while Sr/Ce ratio increases with increasing amount of fluids derived from subducting slab. B) Nb/Th *vs.* Nb/La diagram suggesting crustal contamination in samples with low values in both ratios. The felsic rocks and SiO_2 content of selected mafic samples are included in the diagram to visualise magma mixing between mafic and felsic magmas. Symbols as in Figure 4.

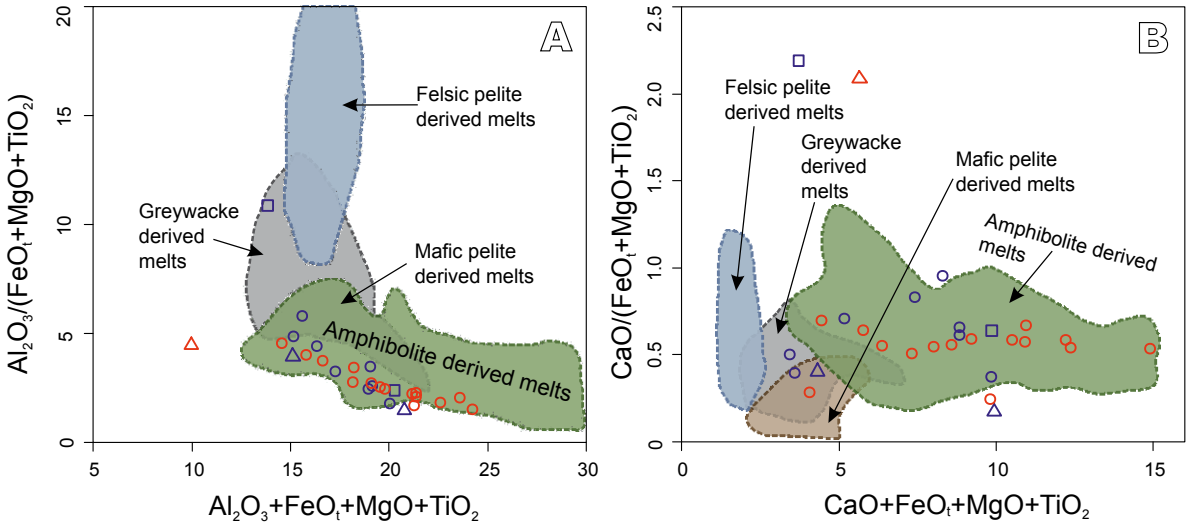

FIGURE 14. Sources for felsic rocks after Patiño Douce (1999). The "Mafic pelite derived melts" in diagram A) is exactly at the cross section of the "Greywacke derived melts" and the "Amphibolite derived melts" areas. Symbols as in Figure 4.

support a co-genetic relationship between the volcanic and plutonic rocks in both localities.

Sm-Nd and Lu-Hf data

A rather homogeneous and geographically extensive "mildly depleted" mantle reservoir has been proposed as a source for the juvenile (2.10-) 1.90-1.86Ga Svecofennian crust based on both the whole rock Nd- (*e.g.* Lahtinen and Huhma, 1997; Andersson *et al.*, 2007; Rutanen and Andersson, 2009; Rutanen *et al.*, 2011) and the single grain zircon Hf-isotope data (*e.g.* Andersen *et al.*, 2009; Andersson *et al.*, 2011; Rutanen *et al.*, 2011; Johansson *et al.*, 2015). The characteristic mild depletion might be a result of prolonged depletion followed by subduction-related enrichment but the extent of this mantle source, both spatial and temporal, is poorly known.

The initial ε_{Nd} values between +1.1 to +2.9 suggest that the mafic rocks from both localities are rather juvenile and have been derived from the mildly depleted mantle source (Fig. 9). The sample 36-MJV-06 (basalt) from Orijärvi shows initial ε_{Nd} value of +1.1, which is slightly lower compared to that of the other mafic rocks. This small discrepancy could be attributed to small scale variations in the mantle source (*cf.* Rutanen *et al.*, 2011; Dahlin *et al.*, 2014) or magma mixing/crustal contamination. The sample 22-MJV-06 is from the Orijärvi layered intrusion and, although it has a different geochemical composition compared to the other mafic rocks, its Nd isotopic composition proves that it has been derived from a similar magma source. The Orijärvi mafic rocks show slightly older T_{DM} ages compared to the Enklinge rocks.

Somewhat more enriched (near-chondritic) initial ε_{Nd} values for the felsic rocks from both localities suggest involvement of crustal material in their magma genesis. This is best explained by the formation of the felsic rocks by partial melting of the juvenile Svecofennian proto-crust whereas the mafic rocks are derived from the mildly depleted upper mantle. It is unlikely that the near-chondritic ε_{Nd} values for the felsic rocks are due to subducted hydrous sediments because lowering the ε_{Nd} from depleted values to values around zero would require a huge sediment input via subduction (*cf.* Hawkesworth *et al.*, 1991), which is not supported by the whole rock geochemical data. In addition, Lahtinen and Huhma (1997) considered only a minor part of the Nd in central Svecofennia to be derived from subducted sediments with the major contribution coming from subducted altered MORB. The small but systematic difference in initial ε_{Nd} between felsic and mafic rocks does not support the evolution of felsic rocks via differentiation from the mafic magmas.

The Enklinge mafic rocks show slightly higher initial ε_{Nd} values than the Orijärvi mafic rocks which suggests a slightly more primitive signature of the former. This is supported also by the initial ε_{Nd} values: around +1 in the felsic rocks from Enklinge and around zero from Orijärvi.

The Hf isotopic data from the two granodiorites are in accordance with the Nd isotopic data. However, the Hf isotopes yield a more detailed view of the magma generation. The average initial ε_{Hf} values for the magmatic zircons are -1.1 and 0 in the Orijärvi and Enklinge granodiorites, respectively, which suggests that both granodiorites are derived mainly from crustal sources (Fig. 10). The zircons have captured some variation in the initial ε_{Hf} values; the

Orijärvi granodiorite shows a range of 7.3 ε-units (at 1892Ma) and the Enklinge shows a range of 7.4 ε-units (at 1882Ma). The variation exceeds the external precision of our Hf isotope analyses. This suggests a minor mixing in the magma genesis between mildly depleted parental magma (slightly positive ε_{Hf} values) and a partial melt from crustal sources (slightly negative ε_{Hf} values), which is considered the major source for the felsic rocks. The mafic parental magmas have probably mostly provided the heat and only small fractions of material to the formation of the felsic rocks.

Andersen *et al.* (2009) defined the Hf evolution trend for the Svecofennian crustal rocks ($\varepsilon_{Hf}(1.90)$=+2±3 and $^{176}Lu/^{177}Hf$≈0.015) and for the mildly depleted mantle source ($\varepsilon_{Hf}(1.90)$=+3±3 and $^{176}Lu/^{177}Hf$≈0.033). These trends were slightly modified by Andersson *et al.* (2011). The inherited zircons from Enklinge define a trend towards a more depleted source with increasing age between 1.95 and 2.25Ga which suggests their juvenile origin and support the presence of Svecofennian juvenile proto-crust. Linear regression of the data suggest an evolutionary trend of $\varepsilon_{Hf}(2.25)$=+8±3 and $^{176}Lu/^{177}Hf$≈0.012 similar to that obtained by Andersen *et al.* (2009) for Svecofennian crust, and by Taylor and McLennan (1995) and Wedepohl (1995) for average continental crust ($^{176}Lu/^{177}Hf$≈0.0113). No clear Archean "contamination" can be identified in the inherited zircons based on the Hf isotope composition. However, it remains uncertain why the proto-crust trend intercepts the magmatic zircons at the upper end of their compositional range. It may suggest that the inherited zircons (and the upper end of the magmatic zircons) represent relatively juvenile lower proto-crust or oceanic crust while a more evolved continental proto-crust would have contributed to the lower end of the magmatic zircon spectrum. The linear trend of the inherited zircons is continued by metamorphic zircons, which have captured a continuum of the Hf-isotope evolution.

Implications for the early Svecofennian crustal growth

During the opening of the proposed pre-Svecofennian sea at *ca.* 2.2-2.0Ga (*cf.* Nironen 1997, Lahtinen *et al.*, 2005; Hermansson *et al.*, 2008; Guitreau *et al.*, 2014) the rift-related mafic magmatism (Vuollo and Huhma, 2005) and/or ocean floor generation (Guitreau *et al.*, 2014) resulted in depletion of the subcontinental lithospheric mantle beneath the Svecofennian domain (Andersson *et al.*, 2006a, 2007, 2011). The depletion was followed by a subduction-related enrichment and an early arc (proto-crust) formation at *ca.* 2.1-1.91Ga, which resulted in characteristic mildly depleted values in the SCLM (*e.g.* initial ε_{Nd} values chondritic to mildly positive, LILE and LREE enrichment, HFSE depletion; Lahtinen and Huhma, 1997; Andersson *et al.*, 2006a, 2011; Andersen *et al.*, 2009; Rutanen *et al.*, 2011; Johansson *et al.*, 2012; Johansson and Hålenius, 2013).

The initial ε_{Nd} values and average initial ε_{Hf} values from both studied granodiorites match previously published data on Svecofennian rocks, and support the model with an extensive mildly depleted mantle source beneath central Fennoscandia at 1.89-1.88Ga. In addition, the Enklinge inherited zircons U-Pb and Hf isotope data suggest the presence of unexposed Svecofennian juvenile proto-crust. The proto-crust hypothesis is also supported by the whole rock geochemical data, which show clear continental arc affinities for all the samples as well as by the bimodal nature of the magmatism.

CONCLUSIONS

i) The Enklinge and Orijärvi volcanic rocks have formed in a continental volcanic arc environment. The intrusive and extrusive rocks are co-genetic, and the felsic and mafic rocks are coeval but not co-magmatic based on field observations, geochemical, age and isotopic data in both study areas. The differences between the Orijärvi and Enklinge mafic rocks are most likely due to a more extensive partial melting in the Enklinge area or a larger crustal contamination in the Orijärvi area.

ii) The age of the Orijärvi granodiorite was determined to be 1892±4Ma, and the age of the Enklinge granodiorite to be 1882±6Ma. Several inherited zircons were found from the Enklinge granodiorite ranging from 2.25 to 1.95Ga. Especially, the 1.99 and 1.95Ga populations are assumed to represent ages within the proposed Svecofennian proto-crust. A metamorphic phase occurred at *ca.* 1.85Ga in the Enklinge area, while the last metamorphic activity in the same area probably occurred at *ca.* 1.80Ga.

iii) The mafic rocks from both localities show mildly depleted mantle signatures with initial ε_{Nd} values between +1.1 and +2.9, and exhibit T_{DM} ages between 2.35 and 2.0Ga. The felsic rocks exhibit initial ε_{Nd} values of -0.4 and +0.2 for Orijärvi, and +1.1 and +1.2 for Enklinge with T_{DM} ages between 2.2–2.1Ga for both localities, which suggests larger crustal contribution in their petrogenesis.

iv) The Lu-Hf data from the Orijärvi granodiorite (average initial ε_{Hf} -1.1 at 1892Ma) and the Enklinge granodiorite (average initial ε_{Hf} 0 at 1882Ma) are in accordance with the Nd data from the same rocks. The variation in the ε_{Hf} (*ca.* 7ε units for both samples) is assumed to result from mixing between depleted parental mantle magmas and partial melts from crustal sources.

v) The evolutionary trend for the Enklinge inherited zircons, $\varepsilon_{Hf}(2.25)$=+8±3 and $^{176}Lu/^{177}Hf$≈0.012, adds more evidence to the presence of Svecofennian proto-crust. The data suggest that the proto-crust originated from a juvenile mantle source.

ACKNOWLEDGMENTS

J. Kara was funded by the Turku University Foundation and the Finnish Cultural Foundation. The Laboratory for Isotope Geology at the Swedish Museum of Natural History provided funding, facilities and guidance for Sm-Nd analyses via SYNTHESYS (project SE TAF 2050), organized by the European Community–Research Infrastructure Action (FP6 programme: Structuring the European Research Area) to M.Väisänen. Maria Fischerström, Kjell Billström and Hans Schöberg helped in numerous ways with analyses. Pietari Skyttä and Karin Högdahl are thanked for their ideas in improving the manuscript and Arto Peltola is thanked for making the zircon mounts. W.L. Griffin and an anonymous reviewer are thanked for their constructive comments. This is a Finnish Geosciences Research Laboratory contribution.

REFERENCES

Albarède, F., 2005. The survival of mantle geochemical heterogeneities. In: van der Hilst, R.D., Bass, J.D., Matas, J., Trampert, J., (eds.). Earth's Deep Mantle: Structure, Composition, and Evolution. American Geophysical Union, 27-46.

Andersen, T., Griffin, W.L., Jackson, S.E., Knudsen, T.-L., Pearson, N.J., 2004. Mid-Proterozoic magmatic arc evolution at the southwest margin of the Baltic Shield. Lithos, 73, 289-318.

Andersen, T., Andersson, U.B., Graham, S., Åberg, G., Simonsen, S.L., 2009. Granitic magmatism by melting of juvenile continental crust: new constraints on the source of Palaeoproterozoic granitoids in Fennoscandia from Hf isotopes in zircon. Journal of the Geological Society, 166, 233-247.

Andersson, U.B., 1997. Petrogenesis of Some Proterozoic Granitoid Suites and Associated Basic Rocks in Sweden: geochemistry and isotope geology. Sveriges Geologiska Undersökning, 91, 1-216.

Andersson, U.B., Neymark, L.A., Billström, K., 2001. Petrogenesis of Mesoproterozoic (Subjotnian) rapakivi complexes of central Sweden: implications from U-Pb zircon ages, Nd, Sr and Pb isotopes. Earth and Environmental Science Transactions of the Royal Society of Edinburgh, 92, 201-228.

Andersson, U.B., Claeson, D.T., Högdahl, K., Sjöström, H., 2004. Geological features of the Småland-Värmland Belt along the Svecofennian margin. Part II: the Nygården, Karlskoga, and Filipstad areas. In: Högdahl, K., Andersson, U.B., Eklund, O., (eds). The Transscandinavian Igneous Belt (TIB) in Sweden: A Review of Its Character. Geological Survey of Finland, Special Paper, 37, 39-47.

Andersson, U.B., Eklund, O., Fröjdö, S., Konopelko, D., 2006a. 1.8Ga magmatism in the Fennoscandian Shield; lateral variations in subcontinental mantle enrichment. Lithos, 86, 110-136.

Andersson, U.B., Högdahl, K., Sjöström, H., Bergman, S., 2006b. Multistage growth and reworking of the Palaeoproterozoic crust in the Bergslagen area, southern Sweden; evidence from U-Pb geochronology. Geological Magazine, 143, 679-697.

Andersson, U.B., Rutanen, H., Johansson, Å., Mansfeld, J., Rimša, A., 2007. Characterization of the Paleoproterozoic mantle beneath the Fennoscandian Shield: Geochemistry and isotope geology (Nd, Sr) of ~1.8Ga mafic plutonic rocks from the Transscandinavian Igneous Belt in Southeast Sweden. International Geology Review, 49, 587-625.

Andersson, U.B., Begg, G.C., Griffin, W.L., Högdahl, K., 2011. Ancient and juvenile components in the continental crust and mantle: Hf isotopes in zircon from Svecofennian magmatic rocks and rapakivi granites in Sweden. Lithosphere, 3, 409-419.

Appelquist, K., Brander, L., Johansson, Å., Andersson, U.B., Cornell, D., 2011. Character and origin of variably deformed granitoids in central southern Sweden: Implications from geochemistry and Nd isotopes. Geological Journal, 46, 597-618.

Belousova, E.A., Griffin, W.L., O'Reilly, S.Y., 2006. Zircon crystal morphology, trace element signatures and Hf isotope composition as a tool for petrogenetic modelling: examples from Eastern Australian granitoids. Journal of Petrology, 47, 329-353.

Bergman, S., Högdahl, K., Nironen, M., Ogenhall, E., Sjöström, H., Lundqvist, L., Lahtinen R., 2008. Timing of Palaeoproterozoic intra-orogenic sedimentation in the central Fennoscandian Shield; evidence from detrital zircon in metasandstone. Precambrian Research, 161, 231-249.

Bogdanova, S., Gorbatschev, R., Skridlaite, G., Soesoo, A., Taran, L., Kurlovich, D., 2015. Trans-Baltic Palaeoproterozoic correlations towards the reconstruction of supercontinent Columbia/Nuna. Precambrian Research, 259, 5-33.

Bouvier, A., Vervoort, J.D., Patchett, P.J., 2008. The Lu-Hf and Sm-Nd isotopic composition of CHUR: constraints from unequilibrated chondrites and implications for the bulk composition of terrestrial planets. Earth and Planetary Science Letters, 273, 48-57.

Boynton, W.V., 1984. Cosmochemistry of the rare earth elements: meteorite studies. In: Henderson, R., (ed.). Rare Earth Element Geochemistry-Developments in Geochemistry 2. Elsevier Science, 63-114.

Carr, M.J., Feigenson, M.D., Bennett, E.A., 1990. Incompatible element and isotopic evidence for tectonic control of source mixing and melt extraction along the Central American arc. Contributions to Mineralogy and Petrology, 105, 369-380.

Chappell, B., White, A., 1974. Two contrasting granite types. Pacific Geology, 8, 173-174.

Chu, N.C., Taylor, R.N., Chavagnac, V., Nesbitt, R.W., Boella, R.M., Milton, J.A., German, C.R., Germain, B., Burton, K., 2002. Hf isotope ratio analysis using multi-collector inductively coupled plasma mass spectrometry: an evaluation of isobaric interference corrections. Journal of Analytical Atomic Spectrometry, 17, 1567-1574.

Claeson, D.T., Andersson, U.B., 2000. The 1.85Ga Nygård pluton, central southern Sweden: An example of early Transscandinavian Igneous Belt (TIB) noritic magmatism. Abstract, The 24th Nordic Geological Winter Meeting in Trondheim, Norway, 6-9.1.2000. Geonytt 1, p.50.

Claesson, S., Huhma, H., Kinny, P.D., Williams, I.S., 1993. Svecofennian detrital zircon ages implications for the Precambrian evolution of the Baltic Shield. Precambrian Research, 64, 109-130.

Colley, H., Westra, L., 1987. The volcano-tectonic setting and mineralization of the early Proterozoic Kemiö-Orijärvi-Lohja belt, SW Finland. Geological Society, London, Special Publication, 33, 95-107.

Condie, K.C., 2013. Preservation and recycling of crust during accretionary and collisional phases of Proterozoic orogens: A bumpy road from Nuna to Rodinia. Geosciences, 3, 240-261.

Dahlin, P., Johansson, Å., Andersson, U.B., 2014. Source character, mixing, fractionation and alkali metasomatism in Palaeoproterozoic greenstone dykes, Dannemora area, NE Bergslagen region, Sweden. Geological Magazine, 151, 573-590.

DePaolo, D.J., 1981. Neodymium isotopes in the Colorado Front Range and crust-mantle evolution in the Proterozoic. Nature, 291, 193-196.

Eerola, T.T., 2002. Mafic-silicic magma interaction in the layered 1.87Ga Soukkio Complex in Mäntsälä, southern Finland. Bulletin of the Geological Society of Finland, 74, 159-183.

Ehlers, C., 1976. Homogenous deformation in Precambrian supracrustal rocks of Kumlinge area, southwest Finland. Precambrian Research, 3, 481-504.

Ehlers, C., Lindroos, A., 1990. Early Proterozoic Svecofennian volcanism and associated plutonism in Enklinge, SW Finland. Precambrian Research, 47, 307-318.

Ehlers, C., Skiöld, T., Vaasjoki, M., 2004. Timing of Svecofennian crustal growth and collisional tectonics in Åland, SW Finland. Bulletin of the Geological Society of Finland, 76, 63-91.

Eklund, O., Korsman, K., Scheinin, B., 2010. Jakob Johannes Sederholm. Lithos, 116, 203-208.

Eliasson, T., Greiling, R., Sträng, T., Triumf, C., 2001. Bedrock map 23H Stensele NV, scale 1:50,000. Geological Survey of Sweden, Uppsala, Ai126.

Eskola, P., 1914. On the petrology of the Orijärvi region in southwestern Finland. Bulletin de la Commission Géologique de Finlande, 40, 277pp.

Gerdes, A., Zeh, A., 2006. Combined U-Pb and Hf isotope LA-(MC-) ICPMS analyses of detrital zircons: Comparison with SHRIMP and new constraints for the provenance and age of an Armorican metasediment in Central Germany. Earth and Planetary Science Letters, 249, 47-61.

Gorbatschev, R., Bogdanova, S., 1993. Frontiers in the Baltic shield. Precambrian Research, 64, 3-21.

Griffin, W.L., Pearson, N.J., Belousova, E., Jackson, S.E., Van Achterbergh, E., O'Reilly, S.Y., Shee, S.R., 2000. The Hf isotope composition of cratonic mantle: LAM-MC-ICPMS analysis of zircon megacrysts in kimberlites. Geochimica et Cosmochimica Acta, 64, 133-147.

Guitreau, M., Blichert-Toft, J., Billström, K., 2014. Hafnium isotope evidence for early-Proterozoic volcanic arc reworking in the Skellefte district (northern Sweden) and implications for the Svecofennian orogen. Precambrian Research, 252, 39-52.

Hawkesworth, C.J., Hergt, J.M., Ellam, R.M., McDermott, F., 1991. Element fluxes associated with subduction related magmatism. Philosophical Transactions of the Royal Society of London A: Mathematical, Physical and Engineering Sciences, 335, 393-405.

Heinonen, A.P., Andersen, T., Rämö, O.T., 2010. Re-evaluation of rapakivi petrogenesis: Source constraints from the Hf isotope composition of zircon in the rapakivi granites and associated mafic rocks of southern Finland. Journal of Petrology, 51, 1687-1709.

Heim, M., Skiöld, T., Wolff, F.C., 1996. Geology, geochemistry and age of the 'Tricolor' granite and some other Proterozoic (TIB) granitoids at Trysil, southeast Norway. Norsk Geologisk Tidsskrift, 76, 45-54.

Hermansson, T., Stephens, M.B., Corfu, F., Page, L.M., Andersson, J., 2008. Migratory tectonic switching, western Svecofennian orogen, central Sweden: Constraints from U/Pb zircon and titanite geochronology. Precambrian Research, 161, 250-278.

Hooper, P.R., Hawkesworth, C.J., 1993. Isotopic and geochemical constraints on the origin and evolution of the Columbia River Basalt. Journal of Petrology, 34, 1203-1246.

Huhma, H., 1986. Sm-Nd, U-Pb and Pb-Pb isotopic evidence for the origin of the Early Proterozoic Svecokarelian crust in Finland. Geological Survey of Finland, Bulletin 337, 48pp.

Huhma, H., 1987. Provenance of Early Proterozoic and Archaean metasediments in Finland: a Sm-Nd isotopic study. Precambrian Research, 35, 127-143.

Huhma, H., Claesson, S., Kinny, P.D., Williams, I.S., 1991. The growth of Early Proterozoic crust: new evidence from Svecofennian detrital zircons. Terra Nova, 3, 175-178.

Huhma, H., Mänttäri, I., Peltonen, P., Kontinen, A., Halkoaho, T., Hanski, E., Hokkanen, T., Hölttä, P., Juopperi, H., Konnunaho, J., Layahe, Y., Luukkonen. E., Pietikäinen. K., Pulkkinen, A., Sorjonen-Ward, P., Vaasjoki, M., Whitehouse, M., 2012. The age of the Archaean greenstone belts in Finland. Geological Survey of Finland, Special Paper, 54, 74-175.

Högdahl, K., Sjöström, H., Andersson, U.B., Ahl, M., 2008. Continental margin magmatism and migmatisation in the west-central Fennoscandian Shield. Lithos, 102, 435-459.

Impola, J., 2004. Samanaikainen hapan–emäksinen magmatismi Enklingen tonaliitti-intruusiossa Ahvenanmaalla. Master Thesis, Department of Geology, University of Turku, 63pp. [In Finnish]

Jackson, S.E., Pearson, N.J., Griffin, W.L., Belousova, E.A., 2004. The application of laser ablation-inductively coupled plasma-mass spectrometry to in-situ U-Pb zircon geochronology. Chemical Geology, 211, 47-69.

Jacobsen, S.B., Wasserburg, G.J., 1984. Sm-Nd isotopic evolution of chondrites and achondrites, II. Earth and Planetary Science Letters, 67, 137-150.

Janousek, V., Farrow, C.M., Erban, V., 2006. Interpretation of whole-rock geochemical data in igneous geochemistry: introducing Geochemical Data Toolkit (GCDkit). Journal of Petrology, 47, 1255-1259.

Johansson, Å., Hålenius, U., 2013: Palaeoproterozoic mafic intrusions along the Avesta-Östhammar belt, east-central Sweden: mineralogy, geochemistry and magmatic evolution. International Geology Review, 55, 131-157.

Johansson, Å., Stephens, M.B., 2017. Timing of magmatism and migmatization in the 2.0-1.8Ga accretionary Svecokarelian orogen, south-central Sweden. International Journal of Earth Sciences, 106, 783-810.

Johansson, Å., Bogdanova, S., Čečys, A., 2006. A revised geochronology for the Blekinge Province, southern Sweden. GFF, 128, 287-302.

Johansson, Å., Andersson, U.B., Hålenius, U., 2012. Petrogenesis and geotectonic setting of early Svecofennian arc cumulates in the Roslagen area, east-central Sweden. Geological Journal, 47, 557-593.

Johansson, Å., Andersen, T., Simonsen, S.L., 2015. Hafnium isotope characteristics of late Palaeoproterozoic magmatic rocks from Blekinge, southeast Sweden: possible correlation of small-scale Hf and Nd isotope variations in zircon and whole rocks. GFF, 137, 74-82.

Kallioperä - Bedrock of Finland 1:200 000 [Electronic resource, first published 17.8.2016]. Geological Survey of Finland, Espoo, Finland. Version 1.0 [Referred 20.9.2016]

Kessel, R., Schmidt, M.W., Ulmer, P., Pettke, T., 2005. Trace element signature of subduction-zone fluids, melts and supercritical liquids at 120–180km depth. Nature, 437, 724-727.

Koistinen, T., Stephens, M.B., Bogatchev, V., Nordgulen, Ø., Wennerström, M., Korhonen, J.(compilation), 2001. Geological map of the Fennoscandian Shield. Scale 1:2,000,000. Geological Survey of Norway, Trondheim, Geological Survey of Sweden, Uppsala, Ministry of Natural Resources of Russia, Moscow, Geological Survey of Finland, Espoo.

Korja, A., Lahtinen, R., Nironen, M., 2006. The Svecofennian orogen: a collage of microcontinents and island arcs. Geological Society of London, Memoirs, 32, 561-578.

Korsman, K., Koistinen, T., Kohonen, J., Wennerström, M., Ekdahl, E., Honkamo, M., Idman, H., Pekkala, Y., (eds.), 1997. Bedrock map of Finland. Scale 1:1,000,000. Geological Survey of Finland, Espoo.

Korsman, K., Korja, T., Pajunen, M., Virransalo, P. GGT/SVEKA Working group, 1999. The GGT/SVEKA transect: structure and evolution of the continental crust in the Paleoproterozoic Svecofennian orogen in Finland. International Geology Review, 41, 287-333.

Kumpulainen, R.A., Mansfeld, J., Sundblad, K., Neymark, L., Bergman, T., 1996. Stratigraphy, age, and Sm-Nd isotope systematics of the country rocks to Zn-Pb sulfide deposits, Ammeberg District, Sweden. Economic Geology, 91, 1009-1021.

Kurhila, M., Vaasjoki, M., Mänttäri, I., Rämö, T., Nironen, M., 2005. U-Pb ages and Nd isotope characteristics of the lateorogenic, migmatizing microcline granites in southwestern Finland. Bulletin of the Geological Society of Finland, 77, 105-128.

Kurhila, M., Andersen, T., Rämö, O.T., 2010. Diverse sources of crustal granitic magma: Lu-Hf isotope data on zircon in three Paleoproterozoic leucogranites of southern Finland. Lithos, 115, 263-271.

Kusiak, M.A., Whitehouse, M.J., Wilde, S.A., Nemchin, A.A., Clark, C., 2013. Mobilization of radiogenic Pb in zircon revealed by ion imaging: Implications for early Earth geochronology. Geology, 41, 291-294.

Kähkönen, Y., 2005. Svecofennian supracrustal rocks. In: Lehtinen, M., Nurmi, P.A., Rämö, O.T., (eds.). Precambrian Geology of Finland–Key to the Evolution of the Fennoscandian Shield. Elsevier, Amsterdam, Developments in Precambrian Geology, 14, 343-405.

Lahtinen, R., 1994. Crustal evolution of the Svecofennian and Karelian domains during 2.1–1.79Ga, with special emphasis on the geochemistry and origin of 1.93–1.91Ga gneissic tonalites and associated supracrustal rocks in the Rautalampi area, Central Finland. Geological Survey of Finland, Bulletin 378, 128pp.

Lahtinen, R., 1996. Geochemistry of Palaeoproterozoic supracrustal and plutonic rocks in the Tampere–Hämeenlinna area, southern Finland. Geological Survey of Finland, Bulletin 389, 113pp.

Lahtinen, R., Huhma, H., 1997. Isotopic and geochemical constraints on the evolution of the 1.93-1.79Ga Svecofennian crust and mantle in Finland. Precambrian Research, 82, 13-34.

Lahtinen, R., Nironen, M., 2010. Paleoproterozoic lateritic paleosol–ultra-mature/mature quartzite–meta-arkose successions in southern Fennoscandia–intra-orogenic stage during the Svecofennian orogeny. Precambrian Research, 183, 770-790.

Lahtinen, R., Huhma, H., Kousa, J., 2002. Contrasting source components of the Paleoproterozoic Svecofennian metasediments: detrital zircon U-Pb, Sm-Nd and geochemical data. Precambrian Research, 116, 81-109.

Lahtinen, R., Korja, A., Nironen, M., 2005. Paleoproterozoic tectonic evolution. In: Lehtinen, M., Nurmi, P.A., Rämö, O.T., (eds.). Precambrian Geology of Finland-Key to the Evolution of the Fennoscandian Shield. Elsevier, Amsterdam, Developments in Precambrian Geology, 14, 481-532.

Latvalahti, U., 1979. Cu-Zn-Pb ores in the Aijala-Orijärvi area, Southwest Finland. Economic Geology, 74, 1035-1068.

Lauri, L.S., Andersen, T., Hölttä, P., Huhma, H., Graham, S., 2011. Evolution of the Archaean Karelian Province in the Fennoscandian Shield in the light of U-Pb zircon ages and Sm-Nd and Lu-Hf isotope systematics. Journal of the Geological Society, 168, 201-218.

Ludwig, K.R., 2003. User's manual for Isoplot/Ex, Version 3.00. A geochronological toolkit for Microsoft Excel. Berkeley Geochronology Center, Special Publication No.4, 75pp.

Lundström, I., Allen, R.L., Persson, P.-O., Ripa, M., 1998. Stratigraphies and depositional ages of Svecofennian, Palaeoproterozoic metavolcanic rocks in E. Svealand and Bergslagen, South central Sweden. GFF, 120, 315-320.

Makkonen, H.V., Huhma, H., 2007. Sm-Nd data for mafic-ultramafic intrusions in the Svecofennian (1.88Ga) Kotalahti Nickel Belt, Finland–implications for crustal contamination at the Archaean/Proterozoic boundary. Bulletin of the Geological Society of Finland, 79, 175-201.

Mansfeld, J., Beunk, F.F., Barling, J., 2005. 1.83-1.82Ga formation of a juvenile volcanic arc–implications from U-Pb and Sm-Nd analyses of the Oskarshamn-Jönköping Belt, southeastern Sweden. GFF, 127, 149-157.

Middlemost, E.A.K., 1985. Magmas and Magmatic Rocks. London, Longman, 266pp.

Morel, M.L.A., Nebel O., Nebel-Jacobsen Y.J., Miller J.S., Vroon P.Z., 2008. Hafnium isotope characterization of the GJ-1 zircon reference material by solution and laser-ablation MC-ICPMS. Chemical Geology, 255, 231-235.

Mouri, H., Väisänen, M., Huhma, H., Korsman, K., 2005. Sm-Nd garnet and U-Pb monazite dating of high-grade metamorphism and crustal melting in the West Uusimaa area, southern Finland. GFF, 127, 123-128.

Müller, W., Shelley, M., Miller, P., Broude, S., 2009. Initial performance metrics of a new custom-designed ArF excimer LA-ICPMS system coupled to a two-volume laser-ablation cell. Journal of Analytical Atomic Spectrometry, 24, 209-214.

Nevalainen, J., Väisänen, M., Lahaye, Y., Heilimo, E., Fröjdö, S., 2014. Svecofennian intra-orogenic gabbroic magmatism: a case study from Turku, southwestern Finland. Bulletin of the Geological Society of Finland, 86, 93-112.

Nironen, M., 1997. The Svecofennian Orogen: a tectonic model. Precambrian Research, 86, 21-44.

Nironen, M., Mänttäri, I., Väisänen, M., 2016. The Salittu Formation in southwestern Finland, part I: Structure, age and stratigraphy. Bulletin of the Geological Society of Finland, 88, 85-10.

Nyström, J.O., 1999. Origin and tectonic setting of the Dala volcanites. Sveriges Geologiska Undersökning, project 03-889/96, Final report, 41pp.

Pajunen, M., Airo, M.L., Elminen, T., Mänttäri, I., Niemelä, R., Vaarma, M., Wennerström, M., 2008. Tectonic evolution of the Svecofennian crust in southern Finland. Geological Survey of Finland, Special Paper, 47, 15-160.

Patchett, J., Kouvo, O., 1986. Origin of continental crust of 1.9-1.7Ga age: Nd isotopes and U-Pb zircon ages in the Svecokarelian terrain of South Finland. Contributions to Mineralogy and Petrology, 92, 1-12.

Patchett, P.J., Kouvo, O., Hedge, C.E., Tatsumoto, M., 1981. Evolution of continental crust and mantle heterogeneity: evidence from Hf isotopes. Contributions to Mineralogy and Petrology, 78, 279-297.

Patchett, P.J., Todt, W., Gorbatschev, R., 1987. Origin of continental crust of 1.9-1.7Ga age: Nd isotopes in the Svecofennian orogenic terrains of Sweden. Precambrian Research, 35, 145-160.

Patiño Douce, A.E., 1999. What do experiments tell us about the relative contributions of crust and mantle to the origin of granitic magmas? Geological Society, London, Special Publications, 168, 55-75.

Pearce, J.A., 1996. A user's guide to basalt discrimination diagrams. In: Wyman, D.A., (ed.). Trace Element Geochemistry of Volcanic Rocks: Applications for Massive Sulphide Exploration. Geological Association of Canada, Short Course Notes, 12, 79-113.

Pearce, J.A., 2008. Geochemical fingerprinting of oceanic basalts with applications to ophiolite classification and the search for Archean oceanic crust. Lithos, 100, 14-48.

Pearce, J.A., Peate, D.W., 1995. Tectonic implications of the composition of volcanic arc magmas. Annual Review of Earth and Planetary Sciences, 23, 251-286.

Pearce, J.A., Stern, R.J., Bloomer, S.H., Fryer, P., 2005. Geochemical mapping of the Mariana arc-basin system: Implications for the nature and distribution of subduction components. Geochemistry, Geophysics, Geosystems, 6, 27pp.

Peccerillo, A., Taylor, S.R., 1976. Geochemistry of Eocene calc-alkaline volcanic rocks from the Kastamonu area, northern Turkey. Contributions to Mineralogy and Petrology, 58, 63-81.

Peltonen, P., 2005. Svecofennian mafic-ultramafic intrusions. In: Lehtinen, M., Nurmi, P.A., Rämö, O.T., (eds.). Precambrian Geology of Finland–Key to the Evolution of the Fennoscandian Shield. Elsevier, Amsterdam, Developments in Precambrian Geology, 14, 407-441.

Pin, C., Zalduegui, J.S., 1997. Sequential separation of light rare-earth elements, thorium and uranium by miniaturized extraction chromatography: application to isotopic analyses of silicate rocks. Analytica Chimica Acta, 339, 79-89.

Ploegsma, M., Westra, L., 1990. The Early Proterozoic Orijärvi triangle (southwest Finland): a key area on the tectonic evolution of the Svecofennides. Precambrian Research, 47, 51-69.

Rancken, R., 1953. Uber eine Archäishce Superkrustale Formation im Schärenhof von Kumlinge, Ålandsgebiet, SW-Finnland. Åbo Akademi Meddelande, Geologi Och Mineralogi Institut, 35, 1-38.

Rogers, J.J., Santosh, M., 2002. Configuration of Columbia, a Mesoproterozoic supercontinent. Gondwana Research, 5, 5-22.

Rosa, D.R.N., Finch, A.A., Andersen, T., Inverno, C.M.C., 2009. U-Pb geochronology and Hf isotope ratios of magmatic zircons from the Iberian pyrite belt. Mineralogy and Petrology, 95, 47-69.

Rutanen, H., Andersson, U.B., 2009. Mafic plutonic rocks in a continental-arc setting: Geochemistry of 1.87–1.78Ga rocks from south-central Sweden and models of their palaeotectonic setting. Geological Journal, 44, 241-279.

Rutanen, H., Andersson, U.B., Väisänen, M., Johansson, Å., Fröjdö, S., Lahaye, Y., Eklund, O., 2011. 1.8Ga magmatism in southern Finland: strongly enriched mantle and juvenile crustal sources in a post-collisional setting. International Geology Review, 53, 1622-1683.

Rämö, O.T., Vaasjoki, M., Mänttäri, I., Elliott, B.A., Nironen, M., 2001. Petrogenesis of the post-kinematic magmatism of the Central Finland Granitoid Complex I; radiogenic isotope constraints and implications for crustal evolution. Journal of Petrology, 42, 1971-1993.

Saalmann, K., Mänttäri, I., Ruffet, G., Whitehouse, M.J., 2009. Age and tectonic framework of structurally controlled Palaeoproterozoic gold mineralization in the Häme belt of southern Finland. Precambrian Research, 174, 53-77.

Samsonov, A.V., Spiridonov, V.A., Larionova, Y.O., Larionov, A.N., 2016. The Central Russian fold belt: Paleoproterozoic boundary of Fennoscandia and Volgo-Sarmatia, the East European Craton. The 32nd Nordic Geological Winter Meeting in Helsinki, 2016. Bulletin of the geological Society of Finland, Special Volume, Abstracts, p. 162.

Sarapää, O., Ahtola, T., Lohva, J., Hagelberg, K., Karimerto, P., 2005. Tutkimustyöselostus Kiskon kunnassa valtausalueella Iso-Kisko (kaivosrekisterinumero 7495/1) tehdyistä ilmeniittitutkimuksista vuosina 2001-2003. Geologian Tutkimuskeskus, AGrkistoraportti, M 06/2014/2005/1/10, 17pp. [In Finnish]

Schandl, E.S., Gorton, M.P., 2002. Application of high field strength elements to discriminate tectonic settings in VMS environments. Economic Geology, 97, 629-642.

Scherer, E.E., Münker, C., Mezger, K., 2001. Calibration of the lutetium hafnium clock. Science, 293, 683-687.

Scherer, E.E., Münker, C., Mezger, K., 2007. The Lu-Hf systematics of meteorites: Consistent or not. Goldschmidt Conference Abstracts 2007. Geochimica et Cosmochimica Acta, 71:A888

Sederholm, J.J., 1934. On migmatites and associated Pre-Cambrian rocks of southwestern Finland, Part III. The Åland Islands. Bulletin de la Commission Géologique de Finlande, 107, 68pp.

Skyttä, P., Mänttäri, I., 2008. Structural setting of late Svecofennian granites and pegmatites in Uusimaa Belt, SW Finland: Age constraints and implications for crustal evolution. Precambrian Research, 164, 86-109.

Skyttä, P., Käpyaho, A., Mänttäri, I., 2005. Supracrustal rocks in the Kuovila area, southern Finland: structural evolution, geochemical characteristics and the age of volcanism. Bulletin of the Geological Society of Finland, 77, 129-150.

Skyttä, P., Väisänen, M., Mänttäri, I., 2006. Preservation of Palaeoproterozoic early Svecofennian structures in the Orijärvi area, SW Finland–Evidence for polyphase strain partitioning. Precambrian Research, 150, 153-172.

Stacey, J.S., Kramers, J.D., 1975. Approximation of terrestrial lead isotope evolution by a two-stage model. Earth and Planetary Science Letters, 26, 207-221.

Stephens, M.B., Andersson, J., 2015. Migmatization related to mafic underplating and intra-or back-arc spreading above a subduction boundary in a 2.0–1.8Ga accretionary orogen, Sweden. Precambrian Research, 264, 235-257.

Stephens, M.B., Ripa, M., Lundström, I., Persson, L., Bergman, T., Ahl, M., Wahlgren, C.H., Persson, P.O., Wickström, L., 2009. Synthesis of the bedrock geology in the Bergslagen region, Fennoscandian Shield, south-central Sweden. Sveriges Geologiska Undersökning (SGU), 58, 260pp.

Suominen, V., 1987. Lounais-Suomen mafiset juonikivet. In: Aro, K., Laitakari I., (eds.). Suomen Diabaasit ja muut mafiset juonikivilajit. Geological Survey of Finland, Report of Investigation, 76, 151-172.

Suominen, V., 1988. Radiometric ages on zircons from a cogenetic gabbro and plagioclase porphyrite suite in Hyvinkää, southern Finland. Bulletin of the Geological Society of Finland, 60, 135-140.

Sun, S.S., McDonough, W.F., 1989. Chemical and isotopic systematics of oceanic basalts: implications for mantle composition and processes. In: Saunders, A.D., Norry, M.J., (eds.). Magmatism in the Ocean Basins. Geological Society, London, Special Publications, 42, 313-345.

Söderlund, U., Patchett, P.J., Vervoort, J., Isachsen, C.E., 2004. The ^{176}Lu decay constant determined by Lu-Hf and U-Pb isotope systematics of Precambrian mafic intrusions. Earth and Planetary Science Letters, 219, 311-324.

Söderlund, U., Isachsen, C.E., Bylund, G., Heaman, L.M., Patchett, P.J., Vervoort, J.D., Andersson, U.B., 2005. U-Pb baddeleyite ages and Hf, Nd isotope chemistry constraining repeated mafic magmatism in the Fennoscandian Shield from 1.6 to 0.9Ga. Contributions to Mineralogy and Petrology, 150, 174-194.

Söderlund, U., Elming, S.Å., Ernst, R.E., Schissel, D., 2006. The central Scandinavian dolerite Group-Protracted hotspot activity or back-arc magmatism? Constraints from U-Pb baddeleyite geochronology and Hf isotopic data. Precambrian Research, 150, 136-152.

Talikka, M., Mänttäri, I., 2005. Pukala intrusion, its age and connection to hydrothermal alteration in Orivesi, southwestern Finland. Bulletin of the Geological Society of Finland, 77, 165-180.

Tatsumi, Y., Takahashi, T., 2006. Operation of subduction factory and production of andesite. Journal of Mineralogical and Petrological Sciences, 101, 145-153.

Taylor, S.R., McLennan, S.M., 1995. The geochemical evolution of the continental crust. Reviews of Geophysics, 33, 241-265.

Torvela, T., Ehlers, C., 2010. From ductile to brittle deformation: structural development and strain distribution along a crustal-scale shear zone in SW Finland. International Journal of Earth Sciences, 99, 1133-1152.

Torvela, T., Mänttäri, I., Hermansson, T., 2008. Timing of deformation phases within the South Finland shear zone, SW Finland. Precambrian Research, 160, 277-298.

Vaasjoki, M., Huhma, H., 1999. Lead and neodymium isotopic results from metabasalts of the Haveri Formation, southern Finland: Evidence for Palaeoproterozoic enriched mantle. Bulletin of the Geological Society of Finland, 71, 143-153.

Vaasjoki, M., Huhma, H., Lahtinen, R., Vestin, J., 2003. Sources of Svecofennian granitoids in the light of ion probe U-Pb measurements on their zircons. Precambrian Research, 121, 251-262.

Valbracht, P.J., Oen, I.S., Beunk, F.F., 1994. Sm-Nd isotope systematics of 1.9-1.8Ga granites from western Bergslagen, Sweden: inferences on a 2.1-2.0Ga crustal precursor. Chemical Geology, 112, 21-37.

Van Achterbergh, E., Ryan C., Jackson, S., Griffin W., 2001. Data reduction software for LA-ICP-MS, In: Sylverster, P., (ed.). Laser-Ablation ICPMS in the Earth Sciences–Principles and applications. Mineralogical Association of Canada short course series, 29, St John, Newfoundland, 239-243.

Vervoort, J.D., Patchett, P.J., 1996. Behavior of hafnium and neodymium isotopes in the crust: constraints from Precambrian crustally derived granites. Geochimica et Cosmochimica Acta, 60, 3717-3733.

Vervoort, J.D., Patchett, P.J., Soderlund, U., Baker, M., 2004. Isotopic composition of Yb and the determination of Lu concentrations and Lu/Hf ratios by isotope dilution using MC-ICPMS. Geochemistry Geophysics Geosystems, 5, 15pp.

Vuollo, J., Huhma, H., 2005. Paleoproterozoic mafic dikes in NE Finland. In: Lehtinen, M., Nurmi, P.A., Rämö, O.T. (eds.). Precambrian Geology of Finland–Key to the Evolution of the Fennoscandian Shield. Developments in Precambrian Geology, 14, 195-236.

Väisänen, M., Mänttäri, I., 2002. 1.90-1.88Ga arc and back-arc basin in the Orijärvi area, SW Finland. Bulletin of the Geological Society of Finland, 74, 185-214.

Väisänen, M., Kirkland, C.L., 2008. U-Th-Pb geochronology of igneous rocks in the Toija and Salittu Formations, Orijärvi area, southwestern Finland: Constraints on the age of volcanism and metamorphism. Bulletin of the Geological Society of Finland, 80, 73-87.

Väisänen, M., Mänttäri, I., Hölttä, P., 2002. Svecofennian magmatic and metamorphic evolution in southwestern Finland as revealed by U-Pb zircon SIMS geochronology. Precambrian Research, 116, 111-127.

Väisänen, M., Eklund, O., Lahaye, Y., O'Brien, H., Fröjdö, S., Högdahl, K., Lammi, M., 2012a. Intra-orogenic Svecofennian magmatism in SW Finland constrained by LA-MC-ICP-MS zircon dating and geochemistry. GFF, 134, 99-114.

Väisänen, M., Johansson, Å., Andersson, U.B., Eklund, O., Hölttä, P., 2012b. Palaeoproterozoic adakite- and TTG-like magmatism in the Svecofennian orogen, SW Finland. Geologica Acta, 10, 351-371.

Wasström, A., 1993. The Knaften granitoids of Västerbotten county, northern Sweden. In: Lundqvist, T., (ed.). Radiometric dating results. Sveriges geologiska undersökning. Serie C, 823, 60-64.

Wasström, A., 2005. Petrology of a 1.95Ga granite-granodiorite-tonalite-trondhjemite complex and associated extrusive rocks in the Knaften area, northern Sweden. GFF, 127, 67-82.

Wedepohl, K.H., 1995. The composition of the continental crust. Geochimica et Cosmochimica Acta, 59, 1217-1232.

Weihed, P., Arndt, N., Billström, K., Duchesne, J.-C., Eilu, P., Martinsson, O., Papunen, H., Lahtinen, R., 2005. Precambrian geodynamics and ore formation: the Fennoscandian Shield. Ore Geology Reviews, 27, 273-322.

Wehrmann, H., Hoernle, K., Garbe-Schönberg, D., Jacques, G., Mahlke, J., Schumann, K., 2014. Insights from trace element geochemistry as to the roles of subduction zone geometry and subduction input on the chemistry of arc magmas. International Journal of Earth Sciences, 103, 1929-1944.

Whitehouse, M.J., Kamber, B.S., Moorbath, S., 1999. Age significance of U-Th-Pb zircon data from early Archaean rocks of west Greenland–a reassessment based on combined ion-microprobe and imaging studies. Chemical Geology, 160, 201-224.

Wikström, A., Andersson, U.B., 2004. Geological features of the Småland-Värmland Belt along the Svecofennian margin, part I: from the Loftahammar to the Tiveden-Askersund areas. In: Högdahl, K., Andersson, U.B., Eklund, O., (eds.). The Transscandinavian Igneous Belt (TIB) in Sweden: A Review of Its Character. Geological Survey of Finland, Special Paper, 37, 22-39.

Wilson, M., Hamilton, P.J., Fallick, A.E., Aftalion, M., Michard, A., 1985. Granites and early Proterozoic crustal evolution in Sweden: evidence from Sm-Nd, U-Pb and O isotope systematics. Earth and Planetary Science Letters, 72, 376-388.

Winchester, J.A., Floyd, P.A., 1977. Geochemical discrimination of different magma series and their differentiation products using immobile elements. Chemical Geology, 20, 325-343.

Yang, J.H., Sun, J.F., Chen, F., Wilde, S.A., Wu, F.Y., 2007. Sources and petrogenesis of Late Triassic dolerite dikes in the Liaodong Peninsula: Implications for post-collisional lithosphere thinning of the eastern North China Craton. Journal of Petrology, 48, 1973-1997.

Manuscript received March 2017;
revision accepted August 2017;
published Online October 2017.

ELECTRONIC APPENDIX I

ANALYTICAL METHODS

Whole rock geochemistry

A total of 75 whole-rock samples were studied, of which 34 were from Orijärvi and 41 from Enklinge. The data include plutonic, dyke and volcanic rock samples. The Orijärvi and part of the Enklinge samples were analysed at Acme Analytical Laboratories Ltd. (Acme) in Vancouver, Canada (*cf.* Table I). The samples were pulverised in a mild steel swing mill and, after the $LiBO_2$ fusion and HNO_3 dilution, the major elements, Cr, and Sc were analysed by inductively coupled plasma-optical emission spectrometry (ICP-OES). The other trace elements were analysed by inductively coupled plasma-mass spectrometry (ICP-MS). The analytical precision is 1-5% for the major oxides and ±10% for the other elements. Part of the Enklinge samples were analysed at Activation Laboratories Ltd. (Actlabs), Ancaster, Canada, and part at Genalysis in Perth, Australia. At Actlabs the samples were pulverised in a mild steel swing mill. After the lithium metaborate/tetraborate fusion, the major elements were analysed by ICP-OES, and the trace elements by ICP-MS. The relative standard deviations for replicate analyses are ≤3% for major elements and ≤5% for trace elements. At Genalysis the samples were pulverised in a mild steel swing mill and, after lithium metaborate/tetraborate fusion the major elements, Cr, Ni, Sc and V were analysed by ICP-OES, and other trace elements by ICP-MS. The analytical precision is 1-5% for the major oxides and ±10% for the trace elements. The major and trace element data for the study areas are presented in Table I.

U-Pb zircon analyses

Two samples, one from each study area, were selected for U-Pb spot analyses on zircon in order to determine their crystallization ages and to perform Lu-Hf analyses on same zircon grains. The grains were separated using the standard procedure with crushing, panning, heavy liquid separation, magnetic separation and hand picking. The analytical spots were selected on the basis of BSE-images conducted using a LEO 1530 Gemini scanning electron microscope at Åbo Akademi University Finland (Orijärvi granodiorite) and a JEOL JSM-7100F FE-SEM at the Finnish Geosciences Research Laboratory at the Geological Survey of Finland in Espoo (Enklinge granodiorite).

The Orijärvi granodiorite U-Pb dating analyses were performed using a Nu Plasma AttoM single collector ICP-MS at the Geological Survey of Finland in Espoo connected to a Photon Machine Excite laser ablation system. Samples were ablated in He gas (gas flows = 0.4 and 0.1l/min) within a HelEx ablation cell (Müller *et al.*, 2009). The He aerosol was mixed with Ar (gas flow = 0.9l/min) prior to entry into the plasma. The gas mixture was optimized daily for maximum sensitivity. Typical ablation conditions were: beam diameter: 25µm, pulse frequency: 5Hz, beam energy density: 2J/cm^2. A single U-Pb measurement included a short pre-ablation, 15s of on-mass background measurement, followed by 30s of ablation with a stationary beam. ^{235}U was calculated from the signal at mass 238 using the natural $^{238}U/^{235}U$=137.88. Mass number 204 was used as a monitor for common ^{204}Pb. In an ICP-MS analysis, ^{204}Hg mainly originates from the He supply. The observed background counting-rate on mass 204 was 150-200cps, and has been stable at that level over the last two years. The contribution of ^{204}Hg from the plasma was eliminated by on-mass background measurement prior to each analysis. Age related common lead (Stacey and Kramers, 1975) correction was used when the analysis showed common lead contents significantly above the detection limit (*i.e.* >50cps). Signal strengths on mass 206 were typically 100,000cps, depending on the uranium content and age of the zircon.

Calibration standard GJ-1 (609±1Ma; Belousova *et al.*, 2006) and in-house standard A382 (1877±2Ma, Huhma *et al.*, 2012) were run at the beginning and end of each analytical session, and at regular intervals during sessions. Raw data were corrected for the background, laser induced elemental fractionation, mass discrimination and drift in ion counter gains, and reduced to U-Pb isotope ratios by calibration to concordant reference zircons, using the program Glitter (Van Achterbergh *et al.*, 2001). Further data reduction including common lead correction and error propagation was performed using an in-house Excel spreadsheet. Errors include measured within-run errors (SD) and quadratic addition of reproducibility of standard (SE). To minimize the effects of laser-induced elemental fractionation, the depth-to-diameter ratio of the ablation pit was kept low, and isotopically homogeneous segments of the time-resolved traces were calibrated against the corresponding time interval for each mass in the reference zircon.

The Enklinge granodiorite zircon U-Pb dating analyses were performed using a Nu Plasma HR multicollector ICP-MS at the Geological Survey of Finland in Espoo using a technique very similar to Rosa *et al.* (2009), except that a Photon Machine Analyte G2 laser ablation system was used. The analytical conditions were similar to the Nu

Plasma AttoM single collector ICP-MS described above, except: Ar gas flow rate was set to 0.8L/min, beam diameter was 20μm and beam energy density was 0.55J/cm^2. A single U-Pb measurement included 30s of on-mass background measurement, followed by 60s of ablation with a stationary beam. Masses 204, 206 and 207 were measured in secondary electron multipliers, and 238 in an extra high mass Faraday collector. The geometry of the collector block does not allow simultaneous measurement of ^{208}Pb and ^{232}Th. Ion counts were converted and reported as volts by the Nu Plasma time-resolved analysis software. The technique for calculating ^{235}U and monitoring common ^{204}Pb was similar to AttoM.

The same calibration procedure with the same zircon standards were used as described above but raw data were corrected using protocols adapted from Andersen *et al.*, (2004) and Jackson *et al.*, (2004). The calculations were performed off-line, using an interactive spreadsheet program written in Microsoft Excel/VBA by T. Andersen (Rosa *et al.*, 2009).

Plotting of the U-Pb isotopic data and age calculations were performed using the Isoplot/Ex3 program (Ludwig, 2003). All, expect one (calculated with 95% confidence level), ages were calculated with 2σ errors and without decay constants errors. Data-point error ellipses in the figures are at the 2σ level. The concordant age offset from ID-TIMS ages for several samples including zircon 91500 (1066Ma) and A382 (1877±2Ma; Patchett and Kouvo, 1986, and Huhma *et al.*, 2012) does not exceed 0.5%. The U-Pb isotopic data from the two analysed samples are presented in Table II.

Sm-Nd whole rock analyses

The Sm-Nd analyses were performed on nine samples, out of which four were from Orijärvi and five from Enklinge. The whole-rock powders of the investigated rocks have been analysed for their Sm and Nd contents, and Nd isotope compositions at the Laboratory for Isotope Geology of the Swedish Museum of Natural History. For the analyses, 150-200mg of rock powder was mixed with an appropriate amount of mixed ^{147}Sm-^{150}Nd spike, and dissolved in HF and HNO_3 (concentrated 10:1 mixture) in teflon capsules in an oven at 205°C for a few days. After evaporation, the samples were redissolved, first in 5ml 6M HCl at 205°C overnight, and then in 1ml 2.5M HCl at 60°C overnight. After centrifuging to obtain a clear solution, REE as a group was separated from the solution using standard cation exchange procedures with HCl and HNO_3 as media. The REE fractions were evaporated and redissolved in 0.05M HNO_3, and Sm and Nd separated from each other with HCl using the Ln-spec method (Pin and Zalduegui, 1997).

Samarium was analysed in static mode, and neodymium in multi-dynamic mode on a Finnigan MAT261 multicollector mass spectrometer, with corrections for isobaric interferences and fractionation as reported in the footnotes to Table 3. Results of repeated runs of the La Jolla Nd-standard are also reported there. Sm and Nd concentrations, and Nd isotope compositions were computed from the spiked analyses. T_{CHUR} Nd model ages have been calculated according to Jacobsen and Wasserburg (1984), and T_{DM} model ages according to the Depleted Mantle curve of DePaolo (1981). The Sm-Nd isotopic data from the nine samples are presented in Table III.

Lu-Hf zircon analyses

The in-situ zircon Lu-Hf isotope analyses were performed on the same or adjacent domains of the grains on which the U-Pb dating was done. The analyses were carried out using the Nu Plasma HR multicollector ICP-MS at the Geological Survey of Finland in Espoo using a technique very similar to Heinonen *et al.*, (2010) except that a Photon Machine Analyte G2 laser ablation system was used. The samples were ablated in He gas (gas flows=0.4 and 0.1L/min) within a HelEx ablation cell (Müller *et al.*, 2009). All analyses were made in static ablation mode using the following parameters: beam diameter: 50μm; pulse frequency: 5Hz; beam energy density: 3.4J/cm^2. Each ablation was preceded by a 30s on-mass background measurement. The MC-ICP-MS was equipped with 9 Faraday detectors and amplifiers with $10^{11}\Omega$ resistors. During the ablation, the data were collected in static mode (^{172}Yb, ^{175}Lu, ^{176}Hf-Yb-Lu, ^{177}Hf, ^{178}Hf, ^{179}Hf). The total Hf signal obtained for zircons with normal Hf concentration was 1.0-2.0V. Isotopic ratios were measured using the Nu Plasma time-resolved analysis software. The isotopic ratios were later calculated off-line using an Excel spreadsheet. The raw data were filtered at 2σ and corrected for mass discrimination using an exponential law. The mass discrimination factor for Hf was determined assuming ^{179}Hf/^{177}Hf=0.7325 (Patchett *et al.*, 1981). The mass discrimination factor for Yb was determined assuming ^{173}Yb/^{171}Yb=1.132685 (Chu *et al.*, 2002). A ^{176}Lu/^{175}Lu value of 0.02656 has been used for the correction of the ^{176}Lu interference on ^{176}Hf (Scherer *et al.*, 2001; Vervoort *et al.*, 2004). A value for the decay constant of ^{176}Lu of $1.867\times10^{-11}a^{-1}$ has been used in all calculations (Scherer *et al.*, 2001, 2007; Söderlund *et al.*, 2004).

For the calculation of ε_{Hf} values we use present-day chondritic ^{176}Hf/^{177}Hf=0.282785 and ^{176}Lu/^{177}Hf=0.0336 (Bouvier *et al.*, 2008). The zircon standard GJ-1 was run at frequent intervals for quality control. Multiple LA-MC-ICP-MS analyses, using the same instrumental parameters, of the reference zircon GJ-1 during the course of the present study yielded a ^{176}Hf/^{177}Hf of 0.28194±6 (1σ, n=26,

which is just within error to results obtained by solution MC-ICP-MS analyses for GJ1 (0.281998±7, Gerdes and Zeh, 2006; 0.282000±5, Morel *et al.*, 2008). Based on this result, analytical reproducibility is estimated to be in the range of ±1.6 to 2.2 ε-units. The Lu-Hf isotopic data from the two samples (the Orijärvi granodiorite and the Enklinge granodiorite) are presented in Table IV.

TABLE I. Geochemical analyses of the studied rocks

Sample	6-MJV-06	27-MJV-05	2-JPI-00	5-JPI-00	3-MJV-06	3-JPI-00	8-JPI-00	9-JPI-00	10-JPI-00	21-JPI-00	PENK-6	PENK-51	4-MJV-06	18-JPI-00
Locality	Enklinge	Enklinge	Enklinge	Enklinge	Enklinge	Enklinge	Enklinge	Enklinge	Enklinge	Enklinge	Enklinge	Enklinge	Enklinge	Enklinge
Rocktype	F. volcanics	F. volcanics	F. dyke	Ton dyke	Tonalite	Tonalite	Tonalite	Tonalite	Pl-por.	Tonalite	Tonalite	Tonalite	Pillow lava	M. vein
Classification	F. volcanics	F. volcanics	F. dyke	F. dyke	F. plutonic	F. plutonic	F. plutonic	F. plutonic	F. plutonic	F. plutonic	F. plutonic	F. plutonic	M. volcanics	M. dyke
Laboratory	Acme	Acme	Actlabs	Actlabs	Acme	Actlabs	Actlabs	Actlabs	Actlabs	Actlabs	Genanalysis	Genanalysis	Acme	Actlabs
N-Coord*	6704542	6703465	6708853	6708912	6704663	6708869	6708957	6709153	6709224	6707410	6708873	6708681	6703736	6709866
E-Coord*	155325	154258	157191	157193	156988	157192	157172	157076	157023	157584	155999	157008	155810	161565
SiO_2 (wt.%)	69.64	76.64	77.17	68.46	76.13	71.21	73.66	74.87	70.49	70.03	75.16	72.99	49.86	62.33
TiO_2 (wt.%)	0.63	0.17	0.055	0.32	0.12	0.287	0.146	0.194	0.413	0.421	0.259	0.400	1.41	0.632
Al_2O_3 (wt.%)	12.3	12.04	12.67	14.26	12.55	13.45	13.29	13.30	13.79	14.81	13.226	12.848	15.82	16.60
Fe_2O_3 (wt.%)	6.92	2.05	0.93	4. 32	1.88	3.94	1.77	2.42	4.15	2.89	3.002	5.004	14.04	6.51
MnO (wt.%)	0.08	0.02	0.009	0.076	0.02	0.051	0.027	0.03	0.053	0.029	n.a.	n.a.	0.24	0.127
MgO (wt.%)	0.93	0.85	0.18	138	0.58	1.26	0.37	0.4	0.78	0.94	0.796	1.791	5.04	1.6
CaO (wt.%)	1.45	1.24	2.55	383	1.02	3.35	1.15	2.14	3.5	4.05	3.358	2.659	8.49	4.4
Na_2O (wt.%)	3.09	3.16	4.34	3.86	4.46	3.23	3.66	3.86	3.92	3.88	3.620	3.100	3.91	3.51
K_2O (wt.%)	3.17	2.62	0.6	1.16	2.53	2.09	4.3	2.45	1.43	1.05	0.795	1.626	0.28	2.17
P_2O_5 (wt.%)	0.12	0.02	0.01	0. 06	0.03	0.05	0.04	0.05	0.09	0.09	0.041	0.060	0.15	0.39
LOI (wt.%)	1.5	1.1	0.41	0.84	0.6	0.92	0.55	0.5	0.69	0.45	n.a.	n.a.	0.7	1.82
Ba (ppm)	816.2	647.2	147	184	424	521	711	758	249	545	175	400	49.3	684
Rb (ppm)	70.5	60.8	17	45	59.9	57	114	78	50	30	20.5	70	2.7	107
Sr (ppm)	114	83.1	157	159	59	176	93	116	163	634	195	135	244	530
Ta (ppm)	0.9	1.3	0.6	0.5	0.9	0.7	1	0.7	0.6	0.3	0.5	0.68	0.2	1.1
Nb (ppm)	13.9	14.9	6	8	8.2	8	11	9	10	7	7.6	9.4	5	18
Hf (ppm)	10.3	8.6	1	3.7	5.1	3.9	3.5	4.1	4	4.3	3	4.6	3	5.4
Zr (ppm)	307	262.9	30	153	123.8	135	138	170	166	180	110	155	90	244
Y (ppm)	70.6	72.7	8	22	48.8	28	25	25	29	5	10.4	22	28.1	18
Th (ppm)	16.6	21.2	8.6	5.6	11.1	8.4	12.3	12.6	6.7	3.8	6.6	6.8	1.4	4
U (ppm)	4.9	6.3	2	1.8	3.5	3.3	4.6	4.7	2.3	1.4	2.45	2.65	0.9	2
Cr (ppm)[1]	b.d.l.	13.7	200	213	b.d.l.	211	228	223	239	191	140	155	27.4	123
Ni (ppm)	1.9	10	b.d.l.	b.d.l.	1	b.d.l.	b.d.l.	b.d.l.	b.d.l.	b.d.l.	6	11	5	b.d.l.
Pb (ppm)	1.6	2	9	7	2.2	7	11	7	5	16	10	6	5.6	11
La (ppm)	43.2	55	14.8	15.8	44.2	18.1	24	22.7	19.5	14.5	20.5	17	12.9	34.5
Ce (ppm)	93.7	110.4	25.8	30.9	90.4	36.7	45.5	45.9	39.4	22.8	37	37	30.4	74.5
Pr (ppm)	11.96	13.13	2.11	2.96	11.62	3.59	4.09	4.2	3.79	1.96	n.a.	n.a.	4.25	7.95
Nd (ppm)	46.1	52.9	8	13.4	42.3	16.3	17.5	17.6	17.3	7.9	11.4	15.5	18.7	35.2
Sm (ppm)	10.3	11.8	1.2	2.8	8.6	3.6	3.5	3.6	3.8	1.3	1.95	3.5	4.8	6
Eu (ppm)	1.77	1.12	0.36	0.61	0.45	0.6	0.44	0.56	0.79	0.98	0.6	0.8	1.4	1.71
Gd (ppm)	11.19	10.63	1	3.1	7.9	3.8	3.7	3.7	4.2	1	n.a.	n.a.	5.09	4.4
Tb (ppm)	1.91	1.98	0.2	0.5	1.34	0.7	0.6	0.6	0.7	0.2	n.a.	n.a.	0.84	0.6
Dy (ppm)	11.37	11.78	1	3.4	7.63	4.2	3.7	3.8	4.4	0.8	1.7	4.1	4.87	3.2
Ho (ppm)	2.17	2.34	0.2	0.7	1.46	0.9	0.8	0.8	0.9	0.2	n.a.	n.a.	0.95	0.6
Er (ppm)	6.51	7.4	0.7	2.2	4.11	2.8	2.4	2.5	2.8	0.5	0.94	2.3	2.49	1.5
Tm (ppm)	1.02	0.97	0.11	0.34	0.73	0.41	0.38	0.37	0.41	0.07	n.a.	n.a.	0.42	0.23
Yb (ppm)	6.58	7.23	0.8	2.4	4.45	2.7	2.7	2.5	2.8	0.5	0.94	2.2	2.47	1.4
Lu (ppm)	1.07	1.01	0.13	0.35	0.67	0.43	0.39	0.37	0.41	0.09	0.185	0.39	0.38	0.2
Eu/Eu*[2]	0.5	0.31	1	0.63	0.17	0.5	0.37	0.47	0.6	2.63	n.a.	n.a.	0.87	1.02

Geologica Acta, 16(1), 1-23, I-XIV (2018)
DOI: 10.1344/GeologicaActa2018.16.1.1

TABLE I. (Continued)

sample 65-MAV-02 shows high MgO and CaO

Sample	1-MJV-06	2-MJV-06	5-MJV-06	6-JPI-00	20-JPI-00	PENK-24	PENK-33	1-JPI-00	7-JPI-00	11-JPI-00	12-JPI-00	16-JPI-00	17-JPI-00	PENK-25
Locality	Enklinge	Enklinge	Enklinge	Enklinge	Enklinge	Enklinge	Enklinge	Enklinge	Enklinge	Enklinge	Enklinge	Enklinge	Enklinge	Enklinge
Rocktype	Gab dyke	Int. dyke	M. dyke	Gab dyke	M. dyke	Diorite	Diorite	Gabbro	Gabbro	Gabbro	Gabbro	Diorite	Diorite	Gabbro
Classification	M. dyke	M. dyke	M. dyke	M. dyke	M. dyke	M. plutonic	M. plutonic	M. plutonic	M. plutonic	M. plutonic	M. plutonic	M. plutonic	M. plutonic	M. plutonic
Laboratory	Acme	Acme	Acme	Actlabs	Actlabs	Genanalysis	Genanalysis	Actlabs	Actlabs	Actlabs	Actlabs	Actlabs	Actlabs	Genanalysis
N-Coord*	6708829	6708584	6703736	6708924	6707412	6708748	6708834	6708821	6708940	6709315	6708906	6706938	6708938	6708672
E-Coord*	156286	156389	155810	157191	157556	155931	156319	157181	157188	156940	156897	161948	161752	156022
SiO_2 (wt.%)	62.32	57.13	51.56	45.10	50.19	63.33	63.98	51.82	51.29	49.17	51.12	59.35	57.25	62.76
TiO_2 (wt.%)	0.49	0.64	1.05	1.392	0.976	0.517	0.550	0.493	0.838	0.536	0.946	0.745	0.776	0.500
Al_2O_3 (wt.%)	16.77	17.49	17.1	15.67	17.86	15.871	15.494	14.92	13.94	17.75	15.45	16.72	15.22	15.871
Fe_2O_3 (wt.%)	7.36	8.91	11.91	15. 08	9.45	7.149	7.006	9.63	10.61	10.84	12.24	8.76	9.61	7.006
MnO (wt.%)	0.1	0.16	0.19	0.251	0.173	n.a.	n.a.	0.192	0.174	0.238	0.19	0.135	0.163	n.a.
MgO (wt.%)	1.49	2.23	4.92	6.39	4.98	2.985	3.067	6.99	7.17	5.23	5.93	2.71	4.76	3.399
CaO (wt.%)	5.44	6.69	7.49	9.44	9.38	6.296	5.597	10.23	9.98	9.56	8.74	7.16	7.35	5.737
Na_2O (wt.%)	3.69	3.3	4.75	0.98	3.62	3.774	3.774	2.29	2.99	3.43	2.6	3.11	2.79	3.437
K_2O (wt.%)	0.9	1.48	0.28	2.65	0.93	0.723	1.156	1.03	0.89	0.64	0.62	0.78	1.09	1.927
P_2O_5 (wt.%)	0.14	0.1	0.09	0.12	0.26	0.069	0.078	0.02	0.11	0.08	0.15	0.12	0.12	0.069
LOI (wt.%)	1.3	1.7	0.6	1.49	0.85	n.a.	n.a.	1.33	0.93	1.02	0.74	0.49	1	n.a.
Ba (ppm)	169.2	246.7	55.3	327	237	145	240	124	144	93	106	159	173	420
Rb (ppm)	22.5	36.3	3	130	21	12	32	44	33	16	17	26	140	54
Sr (ppm)	314.6	305.7	287.5	108	624	185	190	147	168	243	221	261	220	215
Ta (ppm)	0.1	0.2	0.1	0.3	0.5	0.68	0.68	0.4	0.2	0.2	0.41	0.3	0.4	0.5
Nb (ppm)	3.7	3.3	1.7	5	9	11.6	12.5	6	3	3	7.4	5	6	9.8
Hf (ppm)	2.8	2.3	1.3	2.7	3	2.65	2.9	1.2	1.6	2.1	3.7	2.1	2.4	2.65
Zr (ppm)	84.8	64.5	40.2	99	123	84	98	39	60	78	59	87	82	90
Y (ppm)	21.1	19.6	14.2	44	25	54	43	20	24	16	30.1	14	19	49
Th (ppm)	1.1	1.1	1.3	2	1.4	4.7	4.5	1.5	1.6	2.4	1.78	2.2	1.8	3.1
U (ppm)	1.1	0.7	0.5	1	1	2.15	1.7	0.5	0.6	0.7	0.63	1	1	1.65
Cr (ppm)[1]	b.d.l.	b.d.l.	b.d.l.	98	135	170	270	150	244	75	245	137	230	200
Ni (ppm)	1.8	0.7	1.4	b.d.l.	28	21	23	b.d.l.	31	22	24	b.d.l.	30	39
Pb (ppm)	1.8	1.2	2.1	b.d.l.	13	6	4	b.d.l.	5	8	9	6	6	6
La (ppm)	8.4	6.3	5.3	7.1	19.7	16.5	14.5	12.1	7.6	6.5	14.2	7.7	10.4	14
Ce (ppm)	19.8	15	12.5	17.6	46.5	42	36	16.4	15.8	15.3	31.2	15.4	21.8	37
Pr (ppm)	2.92	2.36	1.79	2.13	5.44	n.a.	n.a.	2.3	1.75	1.59	4.78	1.67	2.46	n.a.
Nd (ppm)	12.3	10.6	8.1	12.2	26.9	24	17.5	10.8	9.2	8.1	22.1	8.4	12.3	22.5
Sm (ppm)	3.1	2.8	2.2	3.9	5.4	6.6	5	2.5	2.5	2.1	5.29	2.1	3	6.2
Eu (ppm)	0.93	0.89	0.74	1.38	1.58	1.04	1.02	0.88	0.8	0.74	1.27	0.85	0.91	0.96
Gd (ppm)	3.29	3.09	2.35	5.6	5	8.2	6	3.1	3.3	2.2	5.74	2.4	3.1	6.8
Tb (ppm)	0.59	0.61	0.43	1.1	0.8	n.a.	n.a.	0.6	0.6	0.4	1.02	0.4	0.6	n.a.
Dy (ppm)	3.32	3	2.52	7.4	4.5	10	7	3.7	3.8	2.5	6.13	2.6	3.3	8.4
Ho (ppm)	0.69	0.69	0.48	1.6	0.8	n.a.	n.a.	0.8	0.8	0.5	1.22	0.5	0.6	n.a.
Er (ppm)	1.99	1.81	1.31	5	2.5	5.6	4.2	2.3	2.5	1.6	3.81	1.5	1.9	4.9
Tm (ppm)	0.28	0.28	0.24	0.71	0.36	n.a.	n.a.	0.32	0.35	0.26	0.553	0.21	0.29	n.a.
Yb (ppm)	1.89	1.87	1.32	4.7	2.3	4.9	4.2	2.2	2.3	1.8	3.43	1.4	1.9	4.6
Lu (ppm)	0.29	0.33	0.18	0.7	0.33	0.84	0.74	0.31	0.34	0.3	0.474	0.2	0.29	0.74
Eu/Eu*[2]	0.89	0.93	1	0.9	0.93	0.43	0.57	0.97	0.85	1.05	0.7	1.16	0.91	0.45

Geologica Acta, 16(1), 1-23, I-XIV (2018)
DOI: 10.1344/GeologicaActa2018.16.1.1

TABLE I. (Continued)

Sample	PENK-32	PENK-43	PENK-45	15-JPI-00	19-JPI-00	PENK-46	PENK-47	PENK-3	PENK-37	13-JPI-00	26-MJV-05	14-JPI-00	PENK-26
Locality	Enklinge	Enklinge	Enklinge	Enklinge	Enklinge	Enklinge	Enklinge	Enklinge	Enklinge	Enklinge	Enklinge	Enklinge	Enklinge
Rocktype	Gabbro	Gabbro	Gabbro	Diorite	Gabbro	Gabbro	Gabbro	Amp. dyke	Gabbro	Hornbl	Gabbro	Gabbro	Gabbro
Classification	M. plutonic	M. plutonic	M. plutonic	M. plutonic	M. plutonic	M. plutonic	M. plutonic	Cumulate	Cumulate	Cumulate	Cumulate	Cumulate	M. plutonic
Laboratory	Genanalysis	Genanalysis	Genanalysis	Actlabs	Actlabs	Genanalysis	Genanalysis	Genanalysis	Genanalysis	Actlabs	Acme	Actlabs	Genanalysis
N-Coord*	6708799	6708569	6708594	6706982	6710627	6708342	6708360	6708897	6708354	6706947	6703410	6706987	6709023
E-Coord*	156344	156647	156569	161835	161290	157243	157260	155896	156661	161772	154232	161794	155906
SiO_2 (wt.%)	62.73	57.14	61.57	48.14	51.91	50.87	59.04	54.11	51.19	53.84	48.40	52.67	60.97
TiO_2 (wt.%)	0.350	0.634	0.392	0.591	0.915	3.169	1.401	0.867	0.317	0.632	0.91	0.567	0.417
Al_2O_3 (wt.%)	13.982	17.005	19.272	15.70	16.60	12.470	15.116	10.959	9.825	6.47	15.48	7.49	16.249
Fe_2O_3 (wt.%)	7.435	9.436	5.147	12.4	10.91	18.586	11.152	11.724	14.583	15.3	11.69	13.19	7.149
MnO (wt.%)	n.a.	n.a.	n.a.	0201	0.18	n.a.	n.a.	n.a.	n.a.	0.276	0.19	0.251	n.a.
MgO (wt.%)	5.472	4.643	1.658	819	5.07	5.803	2.736	12.270	14.259	11.71	8.54	12.18	4.062
CaO (wt.%)	6.436	8.395	6.156	10.1	7.85	8.675	6.296	8.675	9.794	9.78	10.2	9.59	7.276
Na_2O (wt.%)	3.235	3.033	6.066	1.38	2.67	1.685	3.168	1.820	1.321	0.73	1.91	1.05	3.774
K_2O (wt.%)	1.060	0.590	0.169	1.11	2.06	0.518	1.988	0.675	0.120	0.29	1.24	0.47	0.771
P_2O_5 (wt.%)	0.041	0.073	0.082	0.03	0.13	0.087	0.220	0.078	0.046	0.06	0.12	0.06	0.046
LOI (wt.%)	n.a.	n.a.	n.a.	1.42	1.31	n.a.	n.a.	n.a.	n.a.	1.08	1.1	1.5	n.a.
Ba (ppm)	220	112	210	99	357	72	360	62	24	31	71	105	135
Rb (ppm)	30	14.5	4	69	79	10.8	68	26.5	0.7	8	66.1	34	15
Sr (ppm)	165	200	290	182	302	90	205	140	19.5	33	207.2	47	190
Ta (ppm)	0.33	0.33	0.48	0.11	0.4	0.54	0.84	0.21	0.32	0.12	0.2	0.2	0.38
Nb (ppm)	6.6	5.6	8.4	3.4	6	8.4	13	3.4	5	3.3	2.4	2	5.8
Hf (ppm)	2	1.9	2.45	0.9	1.5	2.15	3.4	1.45	1.6	1.2	1.5	1	1.6
Zr (ppm)	66	56	92	40	46	66	118	46	66	41	44.8	47	45
Y (ppm)	19	18	21.5	8.3	15	35	40	15	15	14.9	20.1	13	11.2
Th (ppm)	2.2	2.55	3.7	0.7	1.2	1.45	7.4	0.56	1.8	2.08	1.2	0.9	2.4
U (ppm)	1.08	0.96	1.6	0.37	0.8	0.64	2.75	0.45	1.35	0.65	0.4	0.4	1.14
Cr (ppm)[1]	260	104	108	185	172	106	92	1120	1200	391	307.9	475	125
Ni (ppm)	56	20	8	24	29	15	1	195	190	40	132	82	17
Pb (ppm)	4	4	12	b.d.l.	7	n.a.	n.a.	6	4	b.d.l.	2.3	b.d.l.	4
La (ppm)	12	9.4	14.5	3.6	7.7	7.8	22.5	3.5	4.6	3.54	7.1	4.6	11.4
Ce (ppm)	29	22.5	30	7.83	16.9	20	48	10	13.5	8.3	12.7	10.2	23
Pr (ppm)	n.a.	n.a.	n.a.	1.09	1.87	n.a.	n.a.	n.a.	n.a.	1.26	1.75	1.1	n.a.
Nd (ppm)	13	10	12.5	4.97	9.2	12	23.5	7.4	8.4	6.3	8.7	5.9	7.4
Sm (ppm)	2.85	2.5	2.85	1.29	2.2	3.7	5.4	2.3	2.2	1.76	2.5	1.6	1.65
Eu (ppm)	0.9	0.8	0.82	0.524	0.93	1.25	1.75	0.84	1.14	0.513	0.83	0.5	0.7
Gd (ppm)	3.1	2.9	3.2	1.52	2.4	4.7	6.4	2.55	2.4	2.19	2.94	2.1	1.8
Tb (ppm)	n.a.	n.a.	n.a.	0.29	0.4	n.a.	n.a.	n.a.	n.a.	0.44	0.58	0.4	n.a.
Dy (ppm)	3.4	3.3	3.7	1.78	2.5	6.4	7.2	2.65	2.5	2.7	3.58	2.2	2
Ho (ppm)	n.a.	n.a.	n.a.	0.37	0.5	n.a.	n.a.	n.a.	n.a.	0.56	0.73	0.5	n.a.
Er (ppm)	1.95	1.9	2.1	1.12	1.5	3.8	3.9	1.4	1.45	1.64	2.36	1.3	1.2
Tm (ppm)	n.a.	n.a.	n.a.	0.165	0.22	n.a.	n.a.	n.a.	n.a.	0.244	0.27	0.19	n.a.
Yb (ppm)	2.05	1.75	1.9	1.06	1.5	3.6	3.5	1.25	1.3	1.54	1.85	1.2	1.12
Lu (ppm)	0.35	0.31	0.33	0.153	0.24	0.6	0.6	0.215	0.24	0.22	0.3	0.17	0.195
Eu/Eu*[2]	0.93	0.91	0.83	1.14	1.24	0.92	0.91	1.06	1.52	0.8	0.94	0.83	1.24

Geologica Acta, 16(1), 1-23, I-XIV (2018)
DOI: 10.1344/GeologicaActa2018.16.1.1

TABLE I. (Continued)

Sample	46.2-MAV-02	101-MAV-02	22-MJV-06	45-MAV-02	TKJ-13-10-4	12.2-MAV-02	11-MAV-02	50-MAV-02	30-MJV-06	33-MJV-06	29a-MJV-06	37.2-MAV-02	68-MAV-02
Locality	Orijärvi	Orijärvi	Orijärvi	Orijärvi	Orijärvi	Orijärvi	Orijärvi	Orijärvi	Orijärvi	Orijärvi	Orijärvi	Orijärvi	Orijärvi
Rocktype	UM. rock	Gabbro	Gabbro	Gabbro	Anorth	Tonalite	Tonalite	Grdr	Tonalite	Tonalite	Tonalite	Grdr	Tonalite
Classification	Lay Intr.	Lay Intr.	Lay Intr.	Lay Intr.	Lay intr.	F. plutonic	F. plutonic	F. plutonic	F. plutonic	F. plutonic	F. plutonic	F. plutonic	F. plutonic
Laboratory	Acme	Acme	Acme	Acme	Acme	Acme	Acme	Acme	Acme	Acme	Acme	Acme	Acme
N-Coord*	6676911	6676993	6676944	6676936	6676884	6673082	6675331	6677231	6673403	6674647	6673955	6671660	6674174
E-Coord*	302029	301696	302002	302159	302032	288694	284740	306119	302079	301158	296673	300329	299848
SiO_2 (wt.%)	38.79	43.79	45.14	43.31	54.10	77.85	71.44	67.77	70.69	68.30	73.48	71.34	68.19
TiO_2 (wt.%)	3.21	2.15	4.45	2.97	0.75	0.2	0.34	0.51	0.29	0.30	0.18	0.31	0.37
Al_2O_3 (wt.%)	14.01	16.84	13.85	15.06	25.05	11. 93	13.93	14.79	14.05	14.55	13.1	14.09	14.42
Fe_2O_3 (wt.%)	26.3	14.95	16.23	20. 3	2.57	2.14	4.09	4.08	4.36	5.15	2.89	3.17	5.23
MnO (wt.%)	0.43	0.18	0.25	033	0.05	0.03	0.07	0.05	0.07	0.08	0.03	0.04	0.08
MgO (wt.%)	7.63	6.71	6.13	447	0.77	0.28	0.75	1.98	0.86	1.18	0.44	0.62	1.35
CaO (wt.%)	6.91	11.96	9.87	907	9.09	1.83	2.83	4.39	3.06	3.87	2.25	2.26	3.97
Na_2O (wt.%)	1.51	1.58	2.36	2.7	5.47	4.74	2.8	3.59	3.61	3.24	3.84	3.6	3.5
K_2O (wt.%)	0.28	0.36	0.52	0.23	0.79	0.24	2.74	1.29	2.04	1.98	1.48	3.63	1.91
P_2O_5 (wt.%)	0.19	0.13	0.15	1.51	0.28	0.01	0.05	0.15	0.07	0.06	0.05	0.06	0.07
LOI (wt.%)	n.a.	n.a.	0.9	na.	n.a.	n.a.	n.a.	n.a.	0.9	1.1	2.1	n.a.	n.a.
Ba (ppm)	87	75	118.4	114	174	155	863	568	725.4	414.4	624.2	1160	638
Rb (ppm)	8.1	6.3	9.1	4	11.5	7.7	65.2	31.2	53.7	53.1	31.3	81.7	58.3
Sr (ppm)	107.3	359.2	353.1	520.7	782.3	133.8	250.6	851.1	163.3	156.6	143.2	321.2	184.4
Ta (ppm)	0.1	0.1	0.3	0.2	0.2	0.8	0.7	0.4	0.8	0.6	0.7	0.8	0.5
Nb (ppm)	1.7	0.7	2.9	2.4	2.9	12.1	10	6.3	8.3	6	7	8.4	6.7
Hf (ppm)	0.6	0.5	1.2	0.8	b.d.l.	6.1	4.5	3	4.2	3.6	4.1	4.2	3.2
Zr (ppm)	18.2	15	28.6	27.8	17.4	191.5	150.4	99.5	134.8	114.6	110.3	154.5	105.7
Y (ppm)	7	10.7	11.6	28.8	8.5	31.9	26.4	5.1	23.3	22	15	14.1	17.7
Th (ppm)	0.3	0.2	2.1	1	0.7	11.9	10.6	4.3	7.8	7.3	14.8	10.3	12
U (ppm)	0.2	0.1	0.6	0.3	0.3	4.3	5.9	1.8	4.6	2.7	4.3	3	2.4
Cr (ppm)[1]	6.84	88.95	b.d.l.	7	n.a.	7	34.21	41.05	b.d.l.	b.d.l.	b.d.l.	34.21	7
Ni (ppm)	0.1	35.6	11.7	0.1	n.a.	1.7	2.2	14.2	1	4.7	1	1.9	1.7
Pb (ppm)	0.7	2.4	259	0.6	n.a.	35.1	110.8	9.7	4.2	7.2	5.6	15.9	4
La (ppm)	3.2	2.9	5.7	10.4	7	33.8	27.5	21.1	18.6	27.9	24.6	38	24.2
Ce (ppm)	7.9	7.4	12.8	26.2	15.5	68.8	56.3	40.2	36.3	55.5	44.5	69.5	46.6
Pr (ppm)	1.08	1.07	1.89	4.19	1.79	7.65	6.38	4.36	4.09	6.04	4.56	7.35	5.08
Nd (ppm)	5.2	5.3	7.9	23.8	8.2	29.6	25.9	17.6	17.6	21.4	17	25.6	17.9
Sm (ppm)	1.2	1.5	1.9	6.3	2	5.2	5.2	2.4	3.5	4	2.5	3.9	3.4
Eu (ppm)	1.14	0.84	0.93	2.95	2.15	0.91	0.95	0.73	0.63	0.55	0.55	1.03	0.76
Gd (ppm)	1.3	2.08	2.28	6.94	1.75	5.18	3.98	1.58	3.74	3.7	2.18	2.88	2.78
Tb (ppm)	0.2	0.35	0.35	1.05	0.27	0.84	0.71	0.21	0.69	0.7	0.43	0.46	0.46
Dy (ppm)	1.36	1.89	2.31	5.93	1.64	5.22	4.07	1.07	3.75	3.89	2.29	2.5	2.67
Ho (ppm)	0.25	0.4	0.41	1.03	0.3	1.11	0.88	0.17	0.75	0.73	0.48	0.46	0.56
Er (ppm)	0.65	1.03	1.11	2.59	0.82	3.25	2.78	0.46	2.2	2.12	1.47	1.31	1.7
Tm (ppm)	0.09	0.16	0.17	0.33	0.08	0.49	0.41	0.06	0.36	0.32	0.22	0.19	0.28
Yb (ppm)	0.62	0.89	0.94	1.82	0.61	3.26	2.92	0.5	2.05	2	1.72	1.44	1.79
Lu (ppm)	0.08	0.12	0.16	0.24	0.08	0.51	0.35	0.06	0.31	0.33	0.24	0.19	0.31
Eu/Eu*[2]	2.79	1.45	1.37	1.36	3.51	0.54	0.64	1.15	0.53	0.44	0.72	0.94	0.76

Geologica Acta, 16(1), 1-23, I-XIV (2018)
DOI: 10.1344/GeologicaActa2018.16.1.1

TABLE I. (Continued)

Sample	58-MAV-02	64-MAV-02	23-MJV-06	27-MJV-06	2-MAV-02	32.2-MJV-06	12.1-MAV-02	49-MJV-07	31-MJV-06	86-MAV-02	53-MAV-02	34-MAV-02	65-MAV-02
Locality	Orijärvi	Orijärvi	Orijärvi	Orijärvi	Orijärvi	Orijärvi	Orijärvi	Orijärvi	Orijärvi	Orijärvi	Orijärvi	Orijärvi	Orijärvi
Rocktype	Tonalite	Qz por.	Rhyolite	Tonalite	Tonalite	Int. dyke	Diorite	Diorite	Diorite	Diorite	Diorite	Diorite	Gabbro
Classification	F. plutonic	F. plutonic	F. volcanics	F. plutonic	F. plutonic	M. dyke	M. plutonic	M. plutonic	M. plutonic	M. plutonic	M. plutonic	M. plutonic	M. plutonic
Laboratory	Acme	Acme	Acme	Acme	Acme	Acme	Acme	Acme	Acme	Acme	Acme	Acme	Acme
N-Coord*	6679435	6677900	6681303	6673554	6675251	6673778	6673082	6679712	6677166	6675357	6679623	6672373	6671810
E-Coord*	309335	300116	306149	288840	291339	306210	288694	306540	306067	308145	304540	303684	295895
SiO_2 (wt.%)	67.15	72.96	83.55	70.32	71.50	61.13	58.75	56.42	61.36	54.21	55.06	50.70	45.76
TiO_2 (wt.%)	0.35	0.17	0.13	0.35	0.32	0.87	0.51	1.13	0.69	1.35	0.70	1.21	0.24
Al_2O_3 (wt.%)	14.57	12.63	8.13	14.00	13.32	16. 66	15.12	14.1	16.72	15.81	14.94	16.05	14.89
Fe_2O_3 (wt.%)	5.94	2.07	1.29	4.41	3.82	6.47	8.88	10.15	5.65	10.94	9.28	9.82	12.23
MnO (wt.%)	0.1	0.02	0.02	0.06	0.05	0.08	0.17	0.15	0.07	0.14	0.14	0.14	0.18
MgO (wt.%)	1.74	0.93	0.41	103	0.72	3.02	4.06	4.39	3.14	3.72	5.78	6.46	10.83
CaO (wt.%)	4.33	0.89	3.82	342	2.47	5.92	7.35	7.11	5.84	7.37	8.93	10.48	12.92
Na_2O (wt.%)	3.46	1.44	0.81	3.38	3.31	3.39	2.1	3.23	3.54	3.41	2.57	2.72	0.92
K_2O (wt.%)	1.4	7.7	0.38	1.6	3.4	1.3	1.3	1.77	1.23	1.42	1.11	1.06	0.23
P_2O_5 (wt.%)	0.05	0.02	0.04	0.09	0.06	0.27	0.15	0.235	0.22	0.35	0.11	0.37	0.03
LOI (wt.%)	n.a.	n.a.	1.3	1.3	n.a.	0.8	n.a.	1.1	1.4	n.a.	n.a.	n.a.	n.a.
Ba (ppm)	453	1437	45.6	586	923	414.9	398	443	518.6	828	496	506	28
Rb (ppm)	34.4	91	10.4	42.8	74	28.6	38.3	49.9	25.6	30.8	26.8	15.1	6.9
Sr (ppm)	171	32.4	73.3	286.3	247.8	796.7	294.6	358.3	894.4	472.3	205.7	621.3	155.4
Ta (ppm)	0.5	0.7	0.5	0.9	0.6	0.6	0.6	0.8	0.5	0.6	0.4	0.6	0.1
Nb (ppm)	6.8	5.8	5.3	8.8	8.8	8.2	9.4	16.8	6.5	12.9	6.1	11.5	0.8
Hf (ppm)	3.8	3	3	5.5	4.5	6.1	2.3	3.4	3.3	4.2	2.5	2.9	0.5
Zr (ppm)	113.5	84.2	101	159	143.6	209.8	70	117.5	110.3	160.8	80.7	107.6	10.1
Y (ppm)	20.3	11.3	12.9	20.6	22.7	8.2	17.5	27.5	6	26.3	24.6	20.3	7.7
Th (ppm)	7.4	11.3	9.9	8	11.5	6.7	6.3	6.5	7	2.4	3.1	2.4	0.7
U (ppm)	2.6	3.2	4	4.3	2.3	1.8	2.6	2.1	1.5	0.9	1.4	1.2	0.4
Cr (ppm)[1]	13.68	13.68	13.7	b.d.l.	34.21	13.7	41.05	88.9	41.1	7	191.58	164.21	171.05
Ni (ppm)	3.5	1.2	2.2	3.5	4.1	16.4	13.6	27.5	24.5	5.7	36.2	37.5	19.9
Pb (ppm)	7.5	6.8	10.9	4.1	2.8	3	8.7	4.8	3.2	4.3	2	12.6	3
La (ppm)	24.5	20.8	18.9	21.7	15.8	28.6	17.3	26.4	35.5	26.1	13.8	25.9	3.2
Ce (ppm)	46	36	38.4	44.3	33.6	59.4	37.6	56.6	68.2	63.5	29.1	56.8	8.2
Pr (ppm)	5.65	3.72	4.34	5.1	4.13	6.42	4.67	7.63	6.52	7.87	3.37	6.88	1.2
Nd (ppm)	22.8	13.5	14.1	21	18	25	20.1	29.5	22.9	30	15.5	27.5	5.7
Sm (ppm)	4	2.3	2.4	3.9	4.2	3.4	4	5.59	2.8	5.6	3	4.8	1.6
Eu (ppm)	0.83	0.33	0.58	0.76	0.89	0.93	1.02	1.19	0.8	1.54	0.81	1.39	0.44
Gd (ppm)	3.21	1.54	2.07	3.57	3.7	2.71	3.61	5.12	1.76	4.94	3.5	3.9	1.45
Tb (ppm)	0.59	0.28	0.38	0.63	0.58	0.37	0.5	0.86	0.26	0.72	0.64	0.62	0.25
Dy (ppm)	3.46	1.68	1.98	3.13	3.62	1.48	3.05	5.15	1.14	4.4	3.99	3.74	1.43
Ho (ppm)	0.67	0.33	0.31	0.62	0.71	0.28	0.58	1	0.16	0.87	0.82	0.74	0.28
Er (ppm)	2.09	1.14	1.05	1.96	2.33	0.75	1.74	2.83	0.51	2.45	2.56	2	0.82
Tm (ppm)	0.34	0.19	0.21	0.32	0.34	0.11	0.26	0.45	0.08	0.41	0.39	0.31	0.11
Yb (ppm)	2.1	1.35	1.36	2.07	2.46	0.75	1.78	2.65	0.51	2.49	2.63	1.78	0.73
Lu (ppm)	0.29	0.2	0.21	0.3	0.37	0.1	0.27	0.42	0.07	0.37	0.38	0.29	0.1
Eu/Eu*[2]	0.71	0.54	0.8	0.62	0.69	0.94	0.82	0.68	1.1	0.9	0.76	0.98	0.88

Geologica Acta, 16(1), 1-23, I-XIV (2018)
DOI: 10.1344/GeologicaActa2018.16.1.1

TABLE I. (Continued)

Sample	57-MAV-02	28-MJV-06	37.1-MAV-02	24-MJV-06	35.2-MJV-06	34-MJV-06
Locality	Orijärvi	Orijärvi	Orijärvi	Orijärvi	Orijärvi	Orijärvi
Rocktype	Tonalite	Tonalite	Tonalite	Basalt	M. dyke	Int. dyke
Classification	F. plutonic	F. plutonic	F. plutonic	M. volcanics	M. dyke	M. dyke
Laboratory	Acme	Acme	Acme	Acme	Acme	Acme
N-Coord*	6678805	6672386	6671660	6681109	6679309	6672715
E-Coord*	311739	295841	300329	306080	312230	296591
SiO_2 (wt.%)	69.85	65.74	65.00	51.52	46.80	59.57
TiO_2 (wt.%)	0.33	0.53	0.65	0.56	0.77	0.69
Al_2O_3 (wt.%)	13.36	14.49	15.85	16.84	16.69	16.16
Fe_2O_3 (wt.%)	5.38	7.78	5.61	10.04	10.74	9.42
MnO (wt.%)	0.08	0.11	0.09	0.14	0.2	0.15
MgO (wt.%)	2.18	1.4	145	7.32	8.23	1.84
CaO (wt.%)	1.91	5.19	449	7.73	11.85	6.26
Na_2O (wt.%)	3.59	3.01	3.99	3.28	2.3	3.58
K_2O (wt.%)	2.19	0.65	1.89	0.58	0.9	0.94
P_2O_5 (wt.%)	0.07	0.16	0.18	0.09	0.26	0.21
LOI (wt.%)	n.a.	0.9	n.a.	1.7	1	1
Ba (ppm)	452	272.2	1008	155.1	102.3	276.8
Rb (ppm)	117.2	16.5	61.6	11.8	11.3	23.1
Sr (ppm)	132.8	240.6	580.9	156.1	418.9	372
Ta (ppm)	0.4	0.4	0.6	0.3	0.3	0.3
Nb (ppm)	7	6.5	12.3	3.6	5.2	3.6
Hf (ppm)	4.4	5.8	5.9	2.1	2.2	2.3
Zr (ppm)	134.8	172.5	231.6	56.4	65.2	63.4
Y (ppm)	22.7	26.4	19.7	22.2	19.8	20.9
Th (ppm)	5.6	5.4	4.2	3.6	5.5	2.2
U (ppm)	2.4	2.6	2.6	1.3	2	1.1
Cr (ppm)[1]	13.68	b.d.l.	7	17.1	164.2	b.d.l.
Ni (ppm)	1.4	2.5	4.2	11.2	36	1.9
Pb (ppm)	14.1	1.1	3.2	11.6	4	3.4
La (ppm)	18.3	25.2	33.9	14	24	3.8
Ce (ppm)	39.1	52.2	65.5	29.7	55.2	16.2
Pr (ppm)	4.7	6.61	7.42	3.9	6.91	1.98
Nd (ppm)	20.4	25.7	30.5	15.3	29.8	11.5
Sm (ppm)	3.9	4.8	5.3	3.6	5.7	3.3
Eu (ppm)	0.97	1.23	1.35	1.21	1.52	1.11
Gd (ppm)	3.44	4.69	4.45	3.77	4.5	3.56
Tb (ppm)	0.61	0.83	0.63	0.62	0.67	0.66
Dy (ppm)	3.91	4.02	3.74	3.26	3.46	3.48
Ho (ppm)	0.7	0.86	0.63	0.63	0.65	0.75
Er (ppm)	2.44	2.46	1.9	1.92	1.81	2.19
Tm (ppm)	0.32	0.41	0.27	0.3	0.24	0.3
Yb (ppm)	2.36	2.37	1.94	1.84	1.48	1.95
Lu (ppm)	0.32	0.39	0.27	0.3	0.23	0.31
Eu/Eu*[2]	0.81	0.79	0.85	1	0.92	0.99

*Coordinates in EUREF-FIN system. 1) Calculated after Cr_2O_3. 2) Normalizing values after Boynton (1984). b.d.l.=below detection limit; n.a.=not analysed; F=Felsic, Int=Intermediate, M=Mafic, UM=Ultra mafic, Ton=Tonalite, Pl-por=Plagioclase porphyrite, Gab=Gabbro, Anorth=Anorthosite, Lay intr=Layered intrusion, Grdr=Granodiorite, Qz-por=Quartz porphyry, Hornbl=Hornblendite.

Geologica Acta, 16(1), 1-23, I-XIV (2018)
DOI: 10.1344/GeologicaActa2018.16.1.1

TABLE II. Zircon U-Pb isotope data for the Orijärvi and Enklinge granodiorites

Sample	ppm			^{206}Pbc (%)	Ratios*						ρ*	Discordance central (%)*	Ages						Comment
	U	Th	Pb		^{207}Pb/^{206}Pb*	1σ	^{207}Pb/^{235}U*	1σ	^{206}Pb/^{238}U*	1σ			^{207}Pb/^{206}Pb	1σ	^{207}Pb/^{235}U	1σ	^{206}Pb/^{238}U	1σ	
Orijärvi granodiorite (29a-MJV-06) [1]																			
Origrano-38	202	46	71	0.01	0.11550	0.00052	5.43080	0.11097	0.34102	0.00689	0.99	0	1888	8	1890	17	1892	33	igneous
Origrano-42	168	36	59	0.01	0.11527	0.00055	5.45769	0.11183	0.34341	0.00694	0.98	1	1884	9	1894	17	1903	33	igneous
Origrano-44	264	62	94	0.01	0.11544	0.00049	5.45642	0.11127	0.34282	0.00692	0.99	1	1887	8	1894	17	1900	33	igneous
Origrano-49	191	38	68	0.01	0.11505	0.00054	5.47274	0.11199	0.34501	0.00697	0.98	2	1881	8	1896	17	1911	33	igneous
Origrano-8	646	173	237	0.00	0.11558	0.00053	5.67099	0.11597	0.35586	0.00719	0.99	4	1889	8	1927	18	1963	34	igneous
Origrano-9	200	56	71	0.01	0.11648	0.00057	5.41303	0.11102	0.33705	0.00681	0.98	-2	1903	9	1887	17	1872	33	igneous
Origrano-1	516	130	186	0.00	0.11642	0.00045	5.61536	0.11464	0.34983	0.00710	0.99	2	1902	7	1918	17	1934	34	igneous
Origrano-15	414	93	145	0.01	0.11582	0.00048	5.46810	0.11194	0.34241	0.00696	0.99	0	1893	7	1896	17	1898	33	igneous
Origrano-14	497	125	161	0.00	0.11604	0.00055	5.26107	0.10826	0.32882	0.00669	0.98	-3	1896	8	1863	17	1833	32	igneous
Origrano-22	329	68	103	0.01	0.11455	0.00054	5.04970	0.10387	0.31971	0.00650	0.98	-5	1873	8	1828	17	1788	32	igneous
Origrano-64	271	79	90	0.01	0.11586	0.00050	5.14753	0.10549	0.32222	0.00655	0.99	-5	1893	8	1844	17	1801	32	igneous
Origrano-46	400	91	123	0.01	0.11336	0.00044	4.54882	0.09284	0.29102	0.00591	0.99	-11	1854	7	1740	17	1647	29	igneous
Enklinge granodiorite (3-MJV-06) [2, 3]																			
3-MJV-06-60a	209	-	73	0.16	0.11017	0.00057	5.25884	0.26359	0.34620	0.01726	1.00	7	1802	9	1862	43	1916	83	metamorphic
3-MJV-06-60b	461	-	133	0.10	0.11064	0.00060	4.46766	0.22396	0.29286	0.01460	0.99	-10	1810	9	1725	42	1656	73	metamorphic
3-MJV-06-48	371	-	55	0.00	0.11115	0.00065	2.36621	0.11049	0.15439	0.00715	0.99	-53	1818	10	1232	33	926	40	metamorphic
3-MJV-06-10a	312	-	60	0.26	0.11184	0.00060	3.03148	0.13638	0.19659	0.00878	0.99	-40	1830	10	1416	34	1157	47	metamorphic
3-MJV-06-28	219	-	68	0.06	0.11225	0.00059	4.87619	0.11972	0.31506	0.00755	0.98	-4	1836	9	1798	21	1766	37	metamorphic
3-MJV-06-20	256	-	86	0.14	0.11241	0.00055	5.13501	0.25630	0.33130	0.01645	1.00	0	1839	9	1842	42	1845	80	metamorphic
3-MJV-06-10b	236	-	62	0.00	0.11266	0.00056	4.11216	0.18544	0.26473	0.01187	0.99	-20	1843	8	1657	37	1514	60	metamorphic
3-MJV-06-121a	588	-	190	0.11	0.11283	0.00056	5.13083	0.23942	0.32980	0.01530	0.99	-1	1846	9	1841	40	1837	74	metamorphic
3-MJV-06-9a	347	-	121	0.02	0.11296	0.00084	5.37979	0.18983	0.34541	0.01192	0.98	4	1848	13	1882	30	1913	57	metamorphic
3-MJV-06-78	314	-	95	0.38	0.11296	0.00073	4.70238	0.25821	0.30192	0.01646	0.99	-9	1848	11	1768	46	1701	82	metamorphic
3-MJV-06-90b	687	-	221	0.49	0.11352	0.00061	5.23407	0.21793	0.33440	0.01381	0.99	0	1856	9	1858	35	1860	67	metamorphic
3-MJV-06-21	262	-	168	0.10	0.11366	0.00053	4.79558	0.23525	0.30599	0.01494	1.00	-8	1859	8	1784	41	1721	74	metamorphic
3-MJV-06-59a	331	-	85	0.23	0.11370	0.00056	5.82061	0.26799	0.37128	0.01699	0.99	11	1859	9	1949	40	2035	80	metamorphic
3-MJV-06-3	468	-	123	0.12	0.11346	0.00060	5.73436	0.26604	0.36657	0.01689	0.99	10	1856	9	1937	40	2013	80	metamorphic
3-MJV-06-152	524	-	101	0.01	0.11461	0.00054	3.66326	0.14286	0.23181	0.00897	0.99	-31	1874	8	1563	31	1344	47	igneous
3-MJV-06-9b	285	-	113	0.00	0.11445	0.00058	5.43922	0.25762	0.34469	0.01623	0.99	2	1871	9	1891	41	1909	78	igneous
3-MJV-06-18	458	-	115	0.06	0.11466	0.00055	5.47107	0.24298	0.34606	0.01528	0.99	3	1875	8	1896	38	1916	73	igneous
3-MJV-06-35	367	-	161	0.03	0.11467	0.00055	5.29898	0.14505	0.33517	0.00903	0.98	-1	1875	8	1869	23	1863	44	igneous
3-MJV-06-36	1072	-	121	0.06	0.11497	0.00055	5.64585	0.14742	0.35616	0.00914	0.98	5	1879	8	1923	23	1964	43	igneous
3-MJV-06-37	374	-	77	0.07	0.11489	0.00063	5.68591	0.29411	0.35894	0.01846	0.99	6	1878	10	1929	45	1977	88	igneous
3-MJV-06-61	380	-	282	0.07	0.11539	0.00057	5.61169	0.25322	0.35272	0.01582	0.99	4	1886	8	1918	39	1948	75	igneous
3-MJV-06-121b	717	-	135	0.00	0.11497	0.00054	5.50026	0.20479	0.34698	0.01282	0.99	3	1879	8	1901	32	1920	61	igneous
3-MJV-06-195	1049	-	376	0.00	0.11566	0.00061	5.70335	0.19479	0.35763	0.01207	0.99	5	1890	9	1932	30	1971	57	igneous
3-MJV-06-181	90	-	235	0.00	0.11644	0.00061	5.49400	0.20018	0.34221	0.01234	0.99	0	1902	9	1900	31	1897	59	igneous
3-MJV-06-29b	367	-	137	0.26	0.11526	0.00061	5.93969	0.25812	0.37376	0.01612	0.99	10	1884	9	1967	38	2047	76	igneous
3-MJV-06-81	221	-	133	0.07	0.11568	0.00065	6.07912	0.24831	0.38115	0.01542	0.99	12	1890	10	1987	36	2082	72	igneous
3-MJV-06-45	210	-	350	0.01	0.11474	0.00056	5.99992	0.17144	0.37925	0.01068	0.99	12	1876	8	1976	25	2073	50	igneous
3-MJV-06-46	770	-	80	0.14	0.11482	0.00056	5.99935	0.22464	0.37897	0.01407	0.99	12	1877	9	1976	33	2071	66	igneous
3-MJV-06-59b	304	-	29	0.00	0.11461	0.00060	6.06966	0.25660	0.38410	0.01611	0.99	14	1874	9	1986	37	2095	75	igneous
3-MJV-06-65b	296	-	114	0.00	0.11967	0.00103	6.39431	0.30575	0.38752	0.01823	0.98	10	1951	15	2031	42	2111	85	inherited

Geologica Acta, 16(1), 1-23, I-XIV (2018)
DOI: 10.1344/GeologicaActa2018.16.1.1

TABLE II. (Continued)

Sample	ppm			^{206}Pbc (%)	Ratios*						ρ*	Discordance central (%)*	Ages						Comment
	U	Th	Pb		^{207}Pb/^{206}Pb*	1σ	^{207}Pb/^{235}U*	1σ	^{206}Pb/^{238}U*	1σ			^{207}Pb/^{206}Pb	1σ	^{207}Pb/^{235}U	1σ	^{206}Pb/^{238}U	1σ	
3-MJV-06-106	559	-	127	0.00	0.11975	0.00140	4.17742	0.19116	0.25300	0.01119	0.97	-29	1953	20	1670	37	1454	58	inherited
3-MJV-06-4	352	-	90	0.00	0.11977	0.00078	4.10897	0.20904	0.24883	0.01256	0.99	-30	1953	11	1656	42	1432	65	inherited
3-MJV-06-90	324	-	98	0.00	0.12172	0.00094	5.27486	0.22521	0.31430	0.01320	0.98	-13	1982	13	1865	36	1762	65	inherited
3-MJV-06-38	248	-	70	0.00	0.12194	0.00079	4.71069	0.22737	0.28018	0.01340	0.99	-22	1985	12	1769	40	1592	67	inherited
3-MJV-06-65a	496	-	183	0.00	0.12207	0.00139	6.49231	0.24482	0.38573	0.01387	0.95	7	1987	19	2045	33	2103	65	inherited
3-MJV-06-39b	323	-	120	0.00	0.12285	0.00082	6.30050	0.28779	0.37195	0.01681	0.99	2	1998	12	2019	40	2039	79	inherited
3-MJV-06-90c	318	-	89	0.00	0.12644	0.00097	5.02026	0.21927	0.28796	0.01238	0.99	-23	2049	13	1823	37	1631	62	inherited
3-MJV-06-101	324	-	104	0.00	0.12726	0.00085	5.89596	0.24865	0.33601	0.01399	0.99	-11	2060	12	1961	37	1867	68	inherited
3-MJV-06-19	178	-	32	0.00	0.13051	0.00156	3.25458	0.19802	0.18086	0.01079	0.98	-53	2105	20	1470	47	1072	59	inherited
3-MJV-06-47	437	-	166	0.00	0.13331	0.00186	7.10770	0.26888	0.38668	0.01359	0.93	-2	2142	24	2125	34	2107	63	inherited
3-MJV-06-52	379	-	128	0.00	0.13468	0.00127	6.41676	0.26599	0.34555	0.01395	0.97	-13	2160	16	2035	36	1913	67	inherited
3-MJV-06-39a	202	-	56	0.00	0.14159	0.00141	5.50812	0.24112	0.28215	0.01203	0.97	-32	2247	17	1902	38	1602	60	inherited

* Errors are 1-sigma absolute; ρ=Error correlation between ^{206}Pb/^{238}U and ^{207}Pb/^{235}U, normal discordance are showed by negative number.
1) The Orijärvi granodiorite U–Pb dating analyses were performed using a Nu Plasma AttoM single collector ICP-MS with Photon Machine Excite laser ablation system.
2) The Enklinge granodiorite U–Pb dating analyses were performed using a Nu Plasma HR multicollector ICP-MS with Photon Machine Analyte G2 laser microprobe.
3) Tom Andersen is greatly acknowledged for providing the program used for data reduction of the Enklinge granodiorite.

Geologica Acta, 16(1), 1-23, I-XIV (2018)
DOI: 10.1344/GeologicaActa2018.16.1.1

TABLE III. Sm-Nd isotope data from Orijärvi and Enklinge

Sample	Rock type	Locality	Sm (ppm) [1]	Nd (ppm) [1]	$^{147}Sm/^{144}Nd$ [1]	$^{143}Nd/^{144}Nd \pm 2\sigma_m$ [2] (measured)	ε_{Nd} [3] (present)	ε_{Nd} [3] (initial)	T_{CHUR} [4] (Ga)	T_{DM} [5] (Ga)
22-MJV-06	Gabbro	Orijärvi	1.83	6.09	0.1818	0.512554 ± 12	- 1.6	+ 2.0 (1892)	0.87	2.35
23-MJV-06	Rhyolite	Orijärvi	2.16	11.9	0.1099	0.511537 ± 11	- 21.5	- 0.4 (1892)	1.93	2.21
29a-MJV-06	Granodiorite	Orijärvi	2.86	16.3	0.1052	0.511506 ± 10	- 22.1	+ 0.1 (1892)	1.87	2.15
36-MJV-06	Basalt	Orijärvi	13.6	62.1	0.1323	0.511890 ± 2	-14.6	+ 1.1 (1892)	1.77	2.15
1-MJV-06	Gabbro dyke	Enklinge	3.14	12.0	0.1588	0.512267 ± 15	- 7.2	+ 1.9 (1882)	1.49	2.15
3-MJV-06	Granodiorite	Enklinge	7.43	35.5	0.1264	0.511825 ± 13	-15.9	+ 1.1 (1882)	1.76	2.12
4-MJV-06	Basalt	Enklinge	4.21	16.3	0.1560	0.512233 ± 15	- 7.9	+ 1.9 (1882)	1.52	2.13
5-MJV-06	Basalt dyke	Enklinge	1.82	7.24	0.1521	0.512233 ± 33	- 7.9	+ 2.9 (1882)	1.39	2.00
6-MJV-06	Rhyolite	Enklinge	9.84	43.5	0.1367	0.511958 ± 16	- 13.3	+ 1.2 (1882)	1.73	2.14
BCR-2	Basalt standard	Columbia river	6.65	28.9	0.1391	0.512624 ± 3	-0.3		0.04	0.87

1) Sm and Nd contents and $^{147}Sm/^{144}Nd$ ratio from isotope dilution analysis with combined ^{147}Sm-^{150}Nd tracer. Estimated analytical uncertainty of $^{147}Sm/^{144}Nd$ ratio is ±0.5 %.

2) $^{143}Nd/^{144}Nd$ ratios calculated from ID run, corrected for Sm interference and normalized to $^{146}Nd/^{144}Nd$=0.7219. Two runs of the La Jolla Nd-standard during the measurement periods gave a a $^{143}Nd/^{144}Nd$ ratio of 0.511857±15 ($2\sigma_m$) and 0.511847±6 ($2\sigma_m$), respectively. Error given as 2 standard deviations of the mean from the mass spectrometer run in the last digits. All analyses done at the Finnigan MAT261 mass spectrometer, except sample 36-MJV-06 and the BCR-2 standard, which were analysed at the Triton mass spectrometer.

3) Present-day and initial ε_{Nd} values (at the given age), according to Jacobsen and Wasserburg (1984): present-day chondritic $^{147}Sm/^{144}Nd$ ratio 0.1967, present-day chondritic $^{143}Nd/^{144}Nd$ ratio of 0.512638.

4) Model age calculated relative to the chondritic uniform reservoir (CHUR) of Jacobsen and Wasserburg (1984).

5) Model age calculated relative to the depleted mantle curve (DM) of DePaolo (1981).

Geologica Acta, 16(1), 1-23, I-XIV (2018)
DOI: 10.1344/GeologicaActa2018.16.1.1

TABLE IV. Zircon Lu-Hf isotope data for the Orijärvi and Enklinge granodiorite

Sample	$^{176}Hf/^{177}Hf$	2σ	$^{178}Hf/^{177}Hf$	2σ	$^{176}Lu/^{177}Hf$	2σ	$^{176}Yb/^{177}Hf$	2σ	$^{176}Hf/^{177}Hf_i$	2σ	εHf_i [1]	2σ	Age (Ga)
Orijärvi granodiorite													
ORIGRANO-64	0.28165	0.00002	1.46735	0.00003	0.00109	0.00001	0.03624	0.00034	0.281607	0.000022	1.1	0.8	1.892
ORIGRANO-44c	0.28165	0.00002	1.46733	0.00003	0.00091	0.00002	0.03252	0.00090	0.281613	0.000023	1.3	0.8	1.892
ORIGRANO-37b	0.28161	0.00002	1.46731	0.00002	0.00106	0.00001	0.03650	0.00039	0.281569	0.000023	-0.3	0.3	1.892
ORIGRANO-48a	0.28154	0.00002	1.46728	0.00002	0.00075	0.00000	0.02504	0.00014	0.281515	0.000023	-2.2	0.8	1.892
ORIGRANO-61	0.28161	0.00002	1.46729	0.00003	0.00102	0.00001	0.03914	0.00039	0.281578	0.000023	0.0	0.8	1.892
ORIGRANO-40	0.28159	0.00003	1.46730	0.00002	0.00136	0.00001	0.04600	0.00016	0.281537	0.000028	-1.4	1.0	1.892
ORIGRANO-19	0.28163	0.00002	1.46733	0.00003	0.00152	0.00003	0.05847	0.00137	0.281580	0.000024	0.1	0.9	1.892
ORIGRANO-39	0.28167	0.00002	1.46730	0.00002	0.00119	0.00001	0.04144	0.00067	0.281627	0.000024	1.8	0.9	1.892
ORIGRANO-36c	0.28158	0.00002	1.46727	0.00003	0.00096	0.00000	0.03454	0.00019	0.281548	0.000025	-1.0	0.9	1.892
ORIGRANO-54b	0.28155	0.00002	1.46731	0.00003	0.00098	0.00001	0.03477	0.00061	0.281514	0.000025	-2.2	0.9	1.892
ORIGRANO-16	0.28154	0.00003	1.46727	0.00003	0.00107	0.00001	0.03738	0.00059	0.281497	0.000026	-2.8	0.9	1.892
ORIGRANO-21	0.28148	0.00003	1.46729	0.00002	0.00096	0.00000	0.03239	0.00013	0.281449	0.000026	-4.5	0.9	1.892
ORIGRANO-34c	0.28162	0.00003	1.46729	0.00003	0.00081	0.00000	0.02748	0.00016	0.281590	0.000026	0.5	0.9	1.892
ORIGRANO-59	0.28156	0.00003	1.46732	0.00003	0.00113	0.00002	0.04377	0.00081	0.281522	0.000026	-2.0	0.9	1.892
ORIGRANO-51	0.28154	0.00003	1.46735	0.00002	0.00075	0.00002	0.02822	0.00087	0.281517	0.000027	-2.1	1.0	1.892
ORIGRANO-34a	0.28165	0.00003	1.46729	0.00003	0.00115	0.00001	0.04046	0.00019	0.281604	0.000027	1.0	1.0	1.892
ORIGRANO-43	0.28162	0.00003	1.46727	0.00002	0.00135	0.00002	0.05065	0.00054	0.281570	0.000028	-0.2	0.5	1.892
ORIGRANO-34b	0.28157	0.00003	1.46736	0.00003	0.00074	0.00001	0.02481	0.00032	0.281545	0.000028	-1.1	1.0	1.892
ORIGRANO-37a	0.28158	0.00003	1.46730	0.00003	0.00122	0.00003	0.04348	0.00089	0.281539	0.000028	-1.4	1.0	1.892
ORIGRANO-48b	0.28161	0.00003	1.46728	0.00003	0.00194	0.00002	0.07373	0.00108	0.281544	0.000028	-1.2	1.0	1.892
ORIGRANO-32	0.28156	0.00003	1.46727	0.00003	0.00109	0.00001	0.03921	0.00039	0.281524	0.000029	-1.9	1.0	1.892
ORIGRANO-15	0.28169	0.00003	1.46733	0.00003	0.00122	0.00002	0.04194	0.00055	0.281641	0.000029	2.3	1.0	1.892
ORIGRANO-54a	0.28159	0.00003	1.46726	0.00002	0.00100	0.00002	0.03651	0.00070	0.281550	0.000030	-1.0	0.9	1.892
ORIGRANO-1	0.28163	0.00003	1.46727	0.00003	0.00146	0.00002	0.04905	0.00053	0.281574	0.000032	-0.1	0.9	1.892
ORIGRANO-36b	0.28162	0.00003	1.46734	0.00003	0.00135	0.00002	0.04544	0.00076	0.281569	0.000033	-0.3	0.6	1.892
ORIGRANO-23	0.28158	0.00004	1.46726	0.00003	0.00094	0.00000	0.03232	0.00025	0.281547	0.000038	-1.1	0.8	1.892
ORIGRANO-47b	0.28172	0.00004	1.46728	0.00003	0.00422	0.00015	0.17728	0.00629	0.281570	0.000042	-0.2	1.0	1.892
ORIGRANO-22	0.28159	0.00003	1.46731	0.00003	0.00078	0.00000	0.02692	0.00015	0.281565	0.000029	-0.4	0.2	1.892
ORIGRANO-47a	0.28157	0.00003	1.46720	0.00002	0.00216	0.00004	0.08700	0.00169	0.281495	0.000030	-2.9	1.1	1.892
ORIGRANO-29	0.28169	0.00003	1.46732	0.00004	0.00118	0.00001	0.04531	0.00067	0.281650	0.000034	2.6	1.2	1.892
ORIGRANO-45a	0.28148	0.00003	1.46734	0.00003	0.00088	0.00000	0.03121	0.00023	0.281443	0.000030	-4.7	1.1	1.892
ORIGRANO-24	0.28153	0.00003	1.46728	0.00003	0.00119	0.00003	0.04290	0.00108	0.281492	0.000033	-3.0	1.2	1.892
ORIGRANO-27	0.28170	0.00004	1.46724	0.00003	0.00200	0.00004	0.07800	0.00134	0.281632	0.000036	2.0	1.3	1.892
ORIGRANO-50	0.28152	0.00004	1.46734	0.00003	0.00160	0.00001	0.06156	0.00043	0.281466	0.000043	-3.9	1.5	1.892
ORIGRANO-63	0.28151	0.00004	1.46728	0.00003	0.00116	0.00002	0.03976	0.00116	0.281473	0.000042	-3.7	1.5	1.892
ORIGRANO-6	0.28158	0.00005	1.46734	0.00004	0.00212	0.00004	0.08390	0.00287	0.281506	0.000050	-2.5	1.8	1.892
ORIGRANO-45b	0.28148	0.00005	1.46735	0.00004	0.00090	0.00001	0.03217	0.00030	0.281452	0.000053	-4.4	1.9	1.892
Enklinge granodiorite													
Enklinge magmatic													
3-MJV-06-3	0.28164	0.00005	1.46735	0.00003	0.00280	0.00003	0.10963	0.00167	0.281543	0.000047	-1.4	1.2	1.882
3-MJV-06-18	0.28170	0.00005	1.46735	0.00003	0.00220	0.00002	0.08736	0.00043	0.281617	0.000046	1.2	1.6	1.882
3-MJV-06-29	0.28178	0.00003	1.46739	0.00003	0.00193	0.00005	0.08101	0.00226	0.281707	0.000035	4.4	1.2	1.882
3-MJV-06-46	0.28172	0.00004	1.46742	0.00003	0.00315	0.00002	0.12840	0.00176	0.281608	0.000044	0.9	1.6	1.882
3-MJV-06-94	0.28163	0.00005	1.46736	0.00004	0.00219	0.00004	0.08727	0.00142	0.281550	0.000046	-1.2	0.8	1.882

Geologica Acta, 16(1), 1-23, I-XIV (2018)
DOI: 10.1344/GeologicaActa2018.16.1.1

TABLE IV. (Continued)

Sample	$^{176}Hf/^{177}Hf$	2σ	$^{178}Hf/^{177}Hf$	2σ	$^{176}Lu/^{177}Hf$	2σ	$^{176}Yb/^{177}Hf$	2σ	$^{176}Hf/^{177}Hf_i$	2σ	εHf_i [1]	2σ	Age (Ga)
3-MJV-06-210	0.28165	0.00005	1.46738	0.00003	0.00225	0.00002	0.09217	0.00112	0.281574	0.000046	-0.3	1.0	1.882
3-MJV-06-195	0.28169	0.00003	1.46732	0.00002	0.00232	0.00006	0.09049	0.00296	0.281608	0.000034	0.9	1.2	1.882
3-MJV-06-35	0.28169	0.00004	1.46738	0.00003	0.00413	0.00005	0.18094	0.00244	0.281541	0.000039	-1.5	1.4	1.882
3-MJV-06-59	0.28163	0.00008	1.46750	0.00003	0.00227	0.00004	0.08542	0.00176	0.281546	0.000079	-1.3	0.2	1.882
3-MJV-06-81	0.28157	0.00004	1.46742	0.00003	0.00207	0.00003	0.07842	0.00044	0.281499	0.000044	-3.0	1.5	1.882
3-MJV-06-152	0.28169	0.00003	1.46738	0.00002	0.00165	0.00001	0.06338	0.00045	0.281630	0.000029	1.7	1.0	1.882
Enklinge inherited													
3-MJV-06-65b	0.28172	0.00003	1.46740	0.00003	0.00237	0.00002	0.09022	0.00118	0.281637	0.000033	3.5	1.2	1.951
3-MJV-06-4	0.28175	0.00003	1.46736	0.00003	0.00294	0.00003	0.12776	0.00172	0.281640	0.000032	3.7	1.1	1.953
3-MJV-06-101	0.28170	0.00004	1.46731	0.00002	0.00195	0.00001	0.07306	0.00088	0.281622	0.000038	5.5	1.4	2.060
3-MJV-06-47	0.28174	0.00003	1.46739	0.00002	0.00318	0.00003	0.13976	0.00127	0.281608	0.000034	6.9	1.2	2.142
3-MJV-06-39	0.28165	0.00006	1.46736	0.00004	0.00208	0.00003	0.08172	0.00062	0.281559	0.000056	7.6	2.0	2.247
Enklinge metamorphic													
3-MJV-06-60a	0.28173	0.00003	1.46736	0.00002	0.00220	0.00003	0.09269	0.00139	0.281658	0.000035	0.8	1.2	1.802
3-MJV-06-60b	0.28168	0.00003	1.46733	0.00003	0.00177	0.00003	0.07396	0.00202	0.281619	0.000027	-0.4	0.2	1.810
3-MJV-06-10a	0.28159	0.00003	1.46742	0.00003	0.00250	0.00005	0.10365	0.00347	0.281501	0.000031	-4.1	1.1	1.830
3-MJV-06-121a	0.28171	0.00003	1.46735	0.00003	0.00236	0.00005	0.09578	0.00186	0.281626	0.000032	0.7	1.1	1.846
3-MJV-06-90b	0.28174	0.00003	1.46739	0.00002	0.00255	0.00002	0.10112	0.00054	0.281647	0.000032	1.6	1.1	1.856

1) Calculated according to a λ of $1.867 \cdot 10^{-11} a^{-1}$ (Scherer *et al.* 2001) and the present-day chondritic values of $^{176}Lu/^{177}Hf$=0.0336 and $^{176}Hf/^{177}Hf$=0.282785 (Bouvier *et al.* 2008).
External error based on the SD (n=26) of zircon standard GJ1 run during the analyses is estimated to be in the range of ±1.6 to 2.2 ε-units.

Geologica Acta, 16(1), 1-23, I-XIV (2018)
DOI: 10.1344/GeologicaActa2018.16.1.1